Cement and Concrete Research 124 (2019) 105806

Contents lists available at ScienceDirect

Cement and Concrete Research

journal homepage: www.elsevier.com/locate/cemconres

Advances in characterizing and understanding the microstructure of cementitious materials

Paulo J.M. Monteiro[a,*], Guoqing Geng[b], Delphine Marchon[a], Jiaqi Li[a], Prasanth Alapati[c], Kimberly E. Kurtis[c], Mohammad Javad Abdolhosseini Qomi[d]

[a] Department of Civil and Environmental Engineering, University of California, Berkeley, CA, United States
[b] Paul Scherrer Institute, 5232 Villigen PSI, Switzerland
[c] School of Civil and Environmental Engineering, Georgia Institute of Technology, Atlanta, GA 30332, United States
[d] Department of Civil and Environmental Engineering, University of California, Irvine, CA, United States

A B S T R A C T

Progress in microstructural characterization methods is summarized. Special attention is given to advanced probes, such as X-ray imaging and spectroscopy, ^{1}H NMR relaxometry, in-situ and high-pressure X-ray diffraction, and digital holographic microscopy. Microtomography has become a mature technique and nanotography has improved its spatial resolution significantly, particularly with the use of ptychography. The review also discusses the effect of plasticizers on the microstructure of concrete and presents a critical analysis of how organic admixtures affects the hydrates obtained from pure synthesis in saturated solutions and from more realistic hydrating systems. The addition of nanomaterials into cementitious systems modifies the microstructure of the matrix so a summary of recent research is presented. It is important to integrate the impressive progress in the characterization of the micro(nano)structure with efforts developing realistic models. Therefore, the present work gives a short but critical presentation of physical chemistry approaches that aim to link the chemical composition, texture, and microstructure of the cement hydrates.

1. Introduction

New knowledge and improvements in understanding the microstructure of cement-based materials, particularly those insights gained after the last International Congress on the Chemistry of Cement (ICCC) in 2015, are the focus of this review. Because of their importance in facilitating the acquisition of new knowledge, this review starts with a presentation of the advances in direct and indirect imaging methods applied to cements and concrete. Examples of insights gained through their application to probe the structure of hydrated cementitious material are discussed. Emerging methods and their pioneering applications for characterization of hydrated cementitious materials will also be analyzed. Prior reviews have been published in the past decade [1–5]; those along with two recent books describing the methods to measure the concrete microstructure are recommended for those interested in obtaining a deeper knowledge in the field [6,7].

Organic compounds influence the mineral phases [8–12] and have a significant effect on the microstructure of the cementitious matrix. Chemical admixtures are essential for the manufacture of sustainable concrete with improved properties [12–16] and for the creation of new building technologies [17–20]. The increasing complexity of the concrete mixture design, the interactions of the various types of admixtures with the mixture constituents, and the stringent requirements for the concrete performance require a deep understanding of the interactions between the cement and the chemical admixtures [8,20]. Concrete admixtures have a significant influence on the solid-liquid interface, where the cement hydration reactions initiate and control the resulting microstructure; this includes the dissolution of the anhydrous phases and the nucleation and growth of the hydrates. This review discusses the influence of organic admixtures on the microstructure of concrete and summarizes recent research examining the precipitation of silicate and aluminate hydrates and the modification brought by the presence of polycarboxylate ether (PCEs) plasticizing admixtures. Specifically, the review differentiates the influence of organic admixtures on hydrates obtained from pure synthesis in saturated solutions and from the more realistic hydrating systems composed of pure phases and model cements.

Interest in using nanomaterials (nanoparticles and nano-reinforcement) for cementitious materials continues to increase [21]. They have the potential to reduce the cement content in concrete without compromising its performance, to impart new functionality (e.g., sensing or photocatalytic capabilities), and to enhance concrete's physical and mechanical properties. This review discusses recent progress in the understanding the underlying microstructural features of nanomodified cementitious materials and their influence on physical and mechanical properties. The topic of nanomodification of cement matrix was not

* Corresponding author.
E-mail address: monteiro@ce.berkeley.edu (P.J.M. Monteiro).

https://doi.org/10.1016/j.cemconres.2019.105806
Received 26 February 2019; Received in revised form 1 July 2019; Accepted 1 July 2019

reviewed in prior ICCC.

Inspired by breakthrough successes obtained through micromechanics-facilitated design of concrete, including strain-hardening and bendable cementitious composites [22,23], researchers are dedicating a tremendous effort to develop new concepts of nanomechanics to increase the strength density beyond that of ultra-high-performance concrete and to manufacture concrete with significantly improved durability. The most promising path seems to be via understanding and manipulating the molecular building block of calcium-silicate-hydrate (C-S-H) [24–28]. The use of molecular physics approaches to explore the nanoscale composition-structure-property relationships highlighted the role of defect attributes [29], densification [30] and network isostaticity [31,32], which are now regarded as new dimensions in concrete nanoengineering. However, unlike in oxide glasses and ceramics, such scientific discoveries have gained little to no traction in concrete practice. It appears that the major obstacle to materialize such fundamental breakthroughs lies within C-S-H's multiscale porous structure [33,34]. In other words, concrete nanoengineering proves practically futile until researchers solve the relationship between the chemical composition and textural attributes of cement hydrates at the mesoscale and discover heuristic approaches to economically manipulate the structure of cement hydrates at this length scale. In this portion of the review, experimental advances in the micro(nano) structure of concrete are integrated with recent progress in mesoscale simulations toward addressing the present knowledge gap.

2. Microscale experimental probes

It is common to classify methodologies for microstructural characterization as *direct* or *indirect* methods. The former directly images two-dimensional (2D) and/or three-dimensional (3D) morphology, whereas the latter measures the response of the material under certain stimulation, which can then be translated into structural information via model interpretation. Here, advances in commonly employed techniques (e.g., SEM, XRD) as well as some emerging methods, are reviewed and examples of their pioneering applications for characterization of hydrated cementitious materials are presented.

2.1. Direct methods

2.1.1. Electron microscopy

Scanning Electron Microscopy (***SEM***): A SEM image is obtained from the secondary electron (SE) or backscattered electron (BSE) signal produced by the sample volume under the scanning of a focused electron beam. Although a large number of SEM SE images of cementitious material have been generated in the past, often these lack detailed quantitative information. In the past five years, the remarkable increase in spatial resolution in modern microscopes has tremendously facilitated quantitative morphological studies, particularly of early hydration products, such as calcium silicate hydrates (C-S-H) [35–37]. For example, the number of C-S-H nucleation cites per unit area on the surface of C_3S particle [35] (Fig. 1a) or on a substrate (e.g. calcite) [36,37] (Fig. 1b) can be directly counted using SE imges of sufficient resolution. Further image analysis can provide statistical estimation of the size of the C-S-H particles and consequently the measurement of the total volume of C-S-H as a function of hydration or growing time [36,37]. Such data contribute to elucidating early hydration kinetics, which previously have often been beyond the capability of bulk method such as quantitative XRD analysis.

BSE imaging, when combined with EDS, provides quantitative and spatial information, powerful for relating composition and structure. While the methodology has been established for decades [38], some notable improvements have occurred in the recent years. Apart from the conventional grayscale segmentation algorithm, extra image masks from elemental mapping are shown to be highly useful in the quantitative study of systems containing slag [39] and fly ash [40]. In particular, the Mg and O mapping can efficiently highlight unreacted slag and fly ash, respectively. In addition, by properly segmenting the elemental composition on a ternary diagram, it is possible to differentiate SCMs that are of different chemical compositions [40,41]. Note that this analysis usually requires large quantities of BSE images and EDS elemental mapping, which is possible only when using modern SDD detectors [6]. For example, BSE images of unhydrated portland cement grains and the resulting hydrated microstructure, (Fig. 2, (a) and (b)), when overlain with false color compositional maps obtained by EDS, facilitate identification and distinction of different phases present in these complex materials.

Even without a quantitative approach, advances in higher-resolution microscopy can readily provide useful information that was previously unattainable. For example, the filler effect of supplementary cementitious materials (SCMs) can be robustly determined by examining surface nucleation and growth of C-S-H, occurring on cement grains and SCM particles [42]. A topographic study of early C-S-H formation has provided evidence to validate the conceptualized morphology of the basic C-S-H structural units (i.e., fine fibers and thin sheets), as well as their assemblage as influenced by various curing conditions [43]. With qualitative observation, caution must be taken to ensure observations are representative, including examining a sufficient number of structures or regions of interest.

3D imaging is now possible when SEM is combined with a Focused Ion Beam (FIB). Relevant work are often reported for clay systems [44] but seldom for cement-based systems. A recent work utilized SEM-FIB to study a $\sim 100\,\mu m^3$ volume of a mature high performance concrete, at a voxel resolution of 6–10 nm [45]. This method provides 3D morphological information down to the smallest capillary pore. The sampling size and resolution are comparable to the best X-ray nanotomographic imaging reported so far (as will be reviewed later). More SEM 3D imaging research is expected to be reported in the next few years.

Recommendations for SEM experimental protocols have also been recently reported. A supercritical drying method of exchanging pore solution with isopropanol and afterwards trifluoromethane, was recently recommended to preserve the cement-based microstructure [46]. For EDS measurements, recommendations include [47]: a) using optimized voltage (~15 kV) and beam current (~1 nA), b) fixing the total number of counts instead of counting time for quantitative comparison, c) calibration the minor elements with standards. The intermixing of phases is a major limitation to SEM-EDS, but it may be improved by the manual selection of the measurement location under a sufficient magnification ($> 4000\times$). The reader is referred to a recently published handbook for a comprehensive guide of studying cement-based material using SEM [6].

Transmission Electron Microscopy (***TEM***): Compared with SEM, TEM is less commonly used for characterization of cement-based materials as it demands extensive experimental efforts in preparing and locating representative sampling regions, and in minimizing the rapid beam damage to the delicate nanostructure of hydration products. Nonetheless, TEM is the only method capable of directly probing the single-nanometer structure, critical for generating new insights the nanoscale origin of the meso- and micro- morphology of hydration products. Recent TEM studies have been reported for the cementitious matrix [48–50], lab-synthesized C-(A-)S-H [51,52], systems incorporating SCMs such as fly ash [53–56], blast furnace slag [57,58] and silica fume [59]. TEM can be coupled with EELS and it can also be performed with EDX and, since the sampling regions are typically a few hundred nanometer thin, it is much easier to relate nanoscale featueres to compositional variations in TEM-EDX study, and to avoid phase-intermixing. Apart from hydrated systems, TEM was also used to probe surface defects on anhydrous C_3S before and after annealing, and these features are reported to be important for the induction period of C_3S hydration [60].

In terms of quantitative structural study, TEM allows the direct measurement of the size of fibrillary C-(A-)S-H [62]. The interlayer

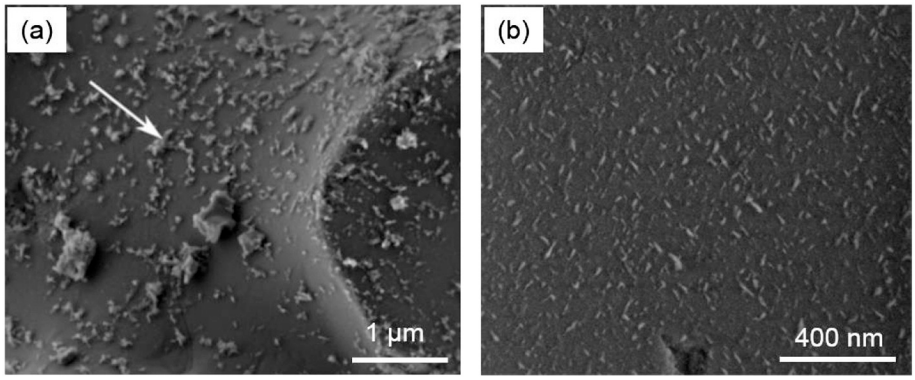

Fig. 1. SEM images of surface nucleated C-S-H: (a) on a C_3S particle surface after 2 h hydration [35] (white arrow indicating C-S-H), and (b) on a calcite substrate surface [9].

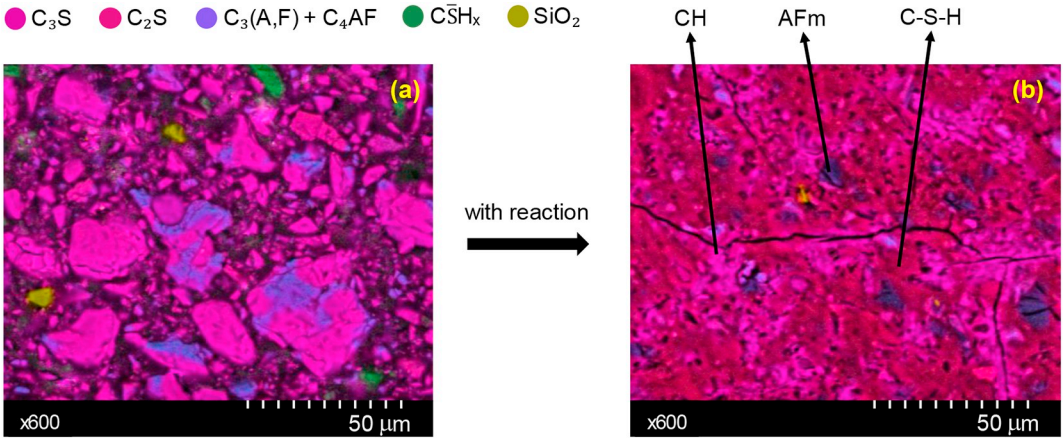

Fig. 2. Micrographs of ASTM C150 Type I/II OPC, at 600× magnification, show (a) unhydrated cement grains where phase compositions are elucidated and (b) the resulting hydrated cement paste at 56 days, with w/c of 0.45.

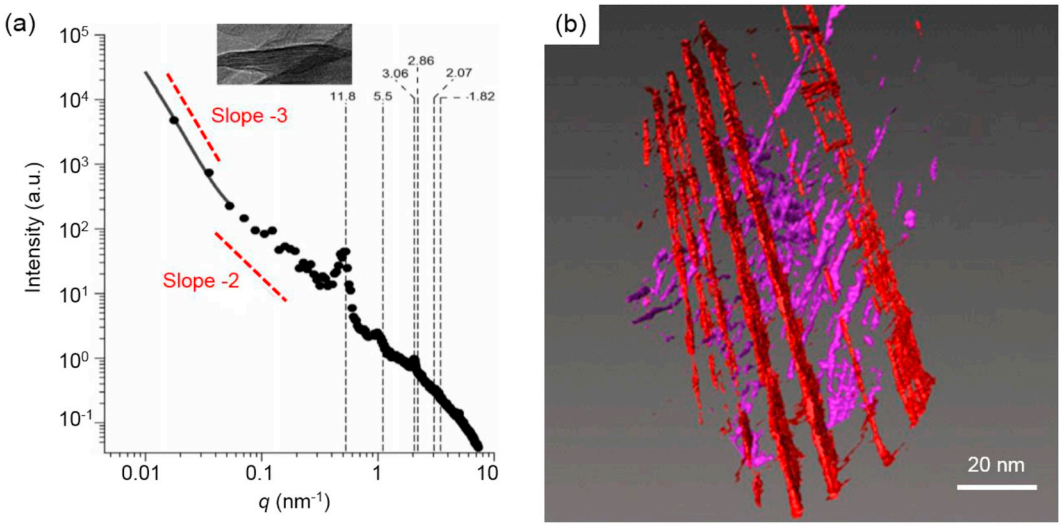

Fig. 3. a) Small angle scattering curve of type-I C-S-H calculated from TEM image [61], b) 3D image of C-S-H obtained from TEM tomography [61].

spacing of C-(A-)S-H can also be directly measured from TEM images, although more accurate measurement is readily obtained from XRD. Theoretical calculation of small angle scattering (SAS) curve provides an alternative way to quantify morphological information from TEM images [63]. Recent experiments have confirmed that the method is a reliable complement to the high-q (i.e., scattering vector) end of the small-angle-scattering (SAS) measurements using an X-ray or neutron source [61,62]. An example of the approach is shown in Fig. 3(a). However, it should be noted that even though the calculated SAS is a quantitative representation of the TEM morphology, it still cannot be directly used as input for further modeling unless the SAS data are properly interpreted by a structural model, for example a fractal assembly of basic C-S-H units of certain geometry.

Three-dimensional TEM-based tomography of a relatively large area

with spatial resolution better than ~1 nm has the potential to provide a key to understanding the mesoscale structure of the cementitious matrix. As discussed in Section 5, the mesostructure is believed to be responsible for multiple macroscale concrete behaviors, such as shrinkage, creep, medium transport and load-induced crack initiation. Pioneering work has demonstrated that such TEM tomography is technically feasible [61,64], overcoming a limitation of TEM – its inability to distinguish among heavily overlapped structural morphologies. An example is shown in Fig. 3(b), where two overlapped C-S-H layer structures were successfully resolved. While these are significant advances, further improvements are needed to develop a robust protocol for TEM tomographic study of cementitious material.

2.1.2. X-ray imaging

Micro and Nano X-ray Computed Tomography (µXCT***and nXCT)*** are widely available both in laboratories and in synchrotron-radiation facilities. With the equipment improvements over the 30 years of XCT studies on cement-based materials, researchers are now able to conduct robust lab-based µXCT with sufficient temporal resolution (a few minutes per sample) and spatial resolution (0.5–1 µm). Many µXCT studies have been reported in the past five years, including on cementitious material subjected to elevated temperature [65], leaching [66], alkali-silica-reaction [67], and corrosion of reinforcement [68], as well as studies on cementitious matrix containing air entraining voids [69,70], recycled aggregates [71], SCMs [72] and fibers [73]. By combining XCT experiments with uniaxial loading, in situ crack evolution with increasing loads has been studied [74]. µXCT has also been used to study water distribution, where the X-ray attenuation of concrete pore solution is enhanced with cesium chloride [75].

Over the past five years, a remarkable improvement in nXCT resolution has occurred, using synchrotron X-ray facilities [76–78]. For example, partially hydrated cement grains, affixed on a tungsten needle tip, were imaged at a series of rotation angles from -90° to 90° by condensed X-ray beam in a transmission mode are reconstructed, resolving features at resolution of ~20 nm. For example, Fig. 4(a) is an nXCT image of hydrated C_3A particles. The 20-nm voxel resolution enables directly observation of the heterogeneous surface dissolution. Similar investigations were reported for hydrated C_3S and fly ash particles [77,78], where the attenuation difference was used to track the density and packing density of hydration products as a function of hydration time. Soft X-ray nXCT has also been used to obtain high-resolution 3D images, as demonstrated in the work of Brisard et al. [79] and Jackson et al. [80] to image C-S-H and Al-tobermorite clusters, respectively.

Phase segmentation is often a challenge in the quantification of the XCT images. In most XCT experiments, the transmission signal is used to generate a tomograph with attenuation contrast. Volumes with similar chemical compositions and densities have similar values of attenuation and are thus not well-differentiated in the reconstructed image. Satisfactory segmentation is usually obtained for voids (cracks and pores), organic fibers, hydration products, aggregates, anhydrous phases and steel reinforcement bars/fibers. However, it is difficult to differentiate among the various hydration products, or to distinguish empty cracks and pores from those that are fully or partially filled with fluid. A combination of X-ray absorption spectra can aid phase-identification [76,77], but with limited spatial resolution. Contrary to transmitted X-rays, the scattered x-ray signal can provide improved contrast between phases of similar attenuation. In particular, recent publications have demonstrated that the SAS signal is sensitive to sub-pixel or sub-voxel structural features or changes, such as the change due to water content [81–83]. This SAS signal can be measured by a Talbot-Lau interferometry through “X-ray Phase Contrast Imaging” (XPCI). As shown in Fig. 4(b), phase contrast imaging can differentiate wet and dry regions, which was not possible with attenuation contrast imaging [81]. Using a lab-scale XPCI setup, temporal and quantitative information of the water displacement was obtained in an early age cementitious material [82].

X-ray ptychography is a novel synchrotron imaging method that provides 2D and 3D images with both superb resolution and unique contrast between phases. Benefiting from the non-destructive manner of sample interrogation and fast data acquisition, groundbreaking work examining cement reactions at the nanoscale has demonstrated the advantage of this technique [76,84–87].

Refraction and attenuation simultaneously occur when X-ray passes through matter. They are measured by the complex refractory index $n = 1 - \delta + i \cdot \beta$, where δ is the decrement of the real part of refractory index from unity and β is the attenuation. To measure both δ and β, it is necessary to obtain both amplitude and phase of the X-ray that is refracted by the object, however a detector only measures the amplitude. In ptychographic (meaning ‘to fold’ in Greek) imaging, the incident beam spot illuminates the sample in a spatial step size that is much smaller than the spot size. As a result, the overlap between adjacent illumination spots provide sufficient over-determination to solve both the amplitude and phase of the object. Recently developed iterative algorithms enables such rapid and robust calculations. Ptychography does not require a high-quality lens, yet readily provides a resolution beyond the limit of direct X-ray imaging. However, it requires a high coherence of the incident X-ray, typically only available at synchrotron

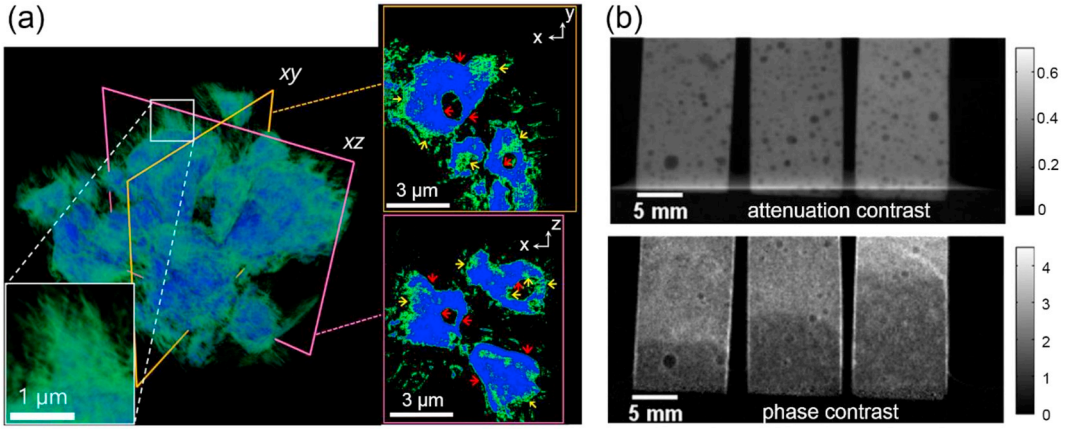

Fig. 4. (a) Nano-tomography of hydrated C_3A particles, where the hydration product (ettringite) and anhydrous C_3A are colored with green and blue, respectively; yellow and red arrows in the cross-section indicate highly reacted and nearly-unreacted surface regions, respectively. Images are adopted from [76]. (b) Comparison of attenuation contrast (top) and phase contrast (bottom) tomographic images of concrete subjected to water ingress following heat treatment. The dry and wet regions cannot be distinguished by their attenuation signal, whereas they are readily differentiated by the phase signal. Images are adopted from [81]. (For interpretation of the references to color in this figure legend, the reader is referred to the web version of this article.)

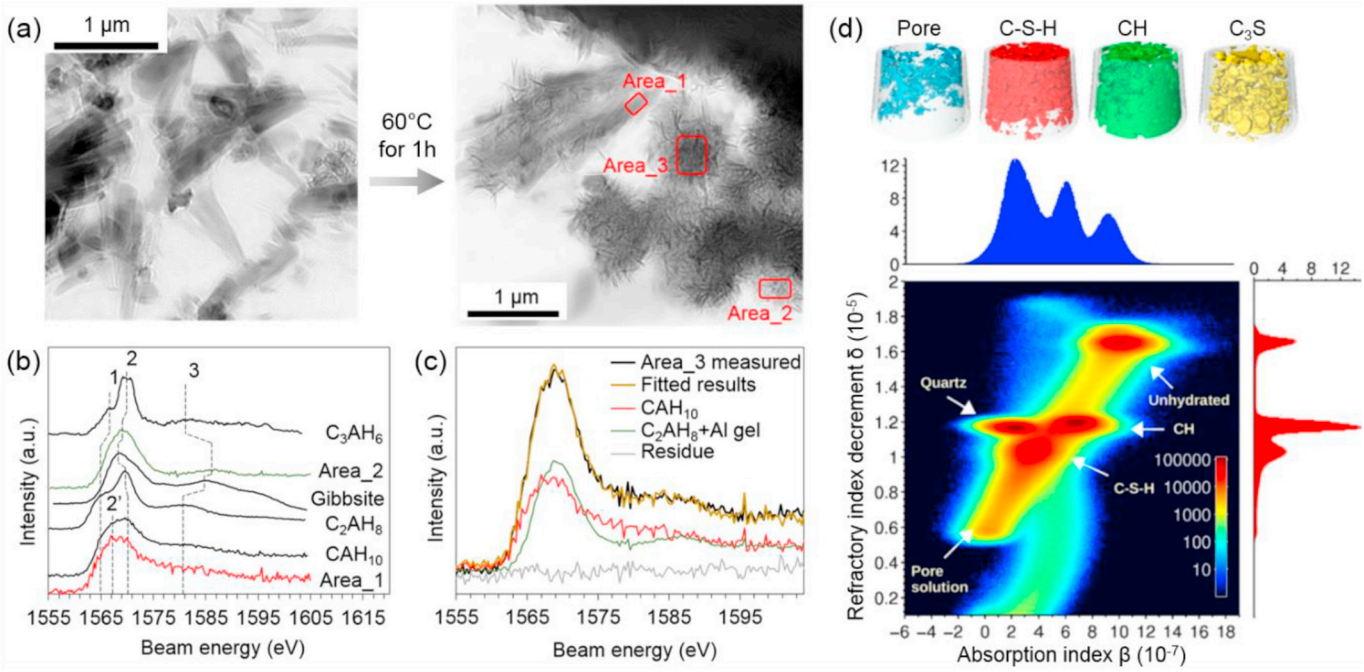

Fig. 5. Examples of X-ray ptychography imaging: (a) 2D nano-morphological change of CAH_{10} after exposure to a 60 °C water bath for 1 h, to facilitate conversion; (b) and (c) Al *K*-edge XANES spectra of selective areas and reference pure phases; images adopted from [84]. (d) 3D reconstruction of a partially hydrated C_3S particle in a quartz capillary tube; images adopted from [86].

facilities, such as in a Scanning Transmission X-ray Microscopy (STXM) beamline [88].

Fig. 5(a) is an example of ptychographic study of CAH_{10} conversion at elevated temperature, conducted at beamline 5.3.3.1 of Advanced Light Source in Berkeley, California [84]. Sharp contrast highlights the 2D morphology of the conversion product needles at ~10 nm resolution. Coupling with X-ray Absorption Near Edge Structure (XANES) study at Al *K*-edge, crystals of different morphology are differentiated by comparing the micro-XAS spectra with the spectra of reference crystal phases (Fig. 5(b) and (c)). A similar study was conducted on the hydration of C_3A in the presence of gypsum. The ptychographic images allows tracking of the radius of ettringite needles as a function of hydration time, water-to-solid ratio and growth locations, i.e., on a surface or in confined regions, including between adjacent C_3A particles [76].

Fig. 5(d) shows a ptychographic tomography study of partly hydrated C_3S particles packed in a quartz capillary tube, conducted at cSAXS beamline at the Swiss Light Source in Villigen, Switzerland [86]. Projection images of both δ and β contrast were independently used for tomographic reconstruction. On the combined 2D histogram (Fig. 5(d) bottom), distribution peaks are rather isolated and therefore allow a more efficient material phase segmentation (Fig. 5(d) top) compared with conventional X-ray tomography using attenuation contrast. In addition, the δ value of each voxel is linked to its mass density ρ (Eq. (1)), which can be used to track the sub-voxel density changes in C-S-H at different locations and at different hydration age.

$$\rho = \frac{1}{N_A}\frac{2\pi\delta A}{Zr_0\lambda^2} \quad (1)$$

where N_A is Avogadro's number, A is the molar mass, Z is the total number of electrons in the formula unit, r_0 is the classical electron radius and λ is the X-ray wavelength.

X-ray ptychography can be particularly useful for cement chemistry studies for the following reasons: a) it utilizes X-ray beam of lower energy compared with electron microscope, therefore induces limited morphological damage to the object even after long-term observation, b) in situ experiments are possible using properly-designed reaction cells, c) chemical information (e.g., XANES spectra) can be measured with remarkable spatial resolution, opening the possibility to directly observe the nanoscale mechanism of multi-phase cement hydration. Unfortunately, presently X-ray ptychography is only available in a few synchrotron facilities.

2.1.3. Digital holographic microscopy (DHM)

Introduced in the mid-2000s, to enhance electron microscopy, digital holographic microscopy (DHM) is most commonly used with light microscopy [89]. With DHM, the light wave front information originating from an object is collected as a hologram (rather than as a project image), and the hologram is then processed to yield the object's 3D morphology. The horizontal resolution is diffraction-limited whereas the vertical (depth) resolution reaches a remarkable 0.5 nm when used in reflection mode [90]. Only recently has DHM been applied to cementitious materials. The technique has been used to investigate the surface dissolution of C_3A [90], calcite [91] and gypsum [92], and showed the following advantages: a) fast image acquisition, b) in-situ observation in aqueous conditions, and c) quantitative information of the surface retreat. Fig. 6(a) shows a sequence of images of gypsum dissolution in deionized water where different surface retreat regions (smooth, wide pits, narrow pits and cleavage steps) were identified and their retreat rates quantified [92]. DHM measurements provide quantitative information of the surface dissolution rate and surface heterogeneity of cement-based minerals, which can be used to validate existing hydration models.

2.1.4. Neutron imaging

Neutron imaging is widely used to study the internal structure of solids. An earlier review of its application in geomaterials and other porous engineering materials is available [93]. The coarser resolution of neutron imaging (~100 μm) is not comparable with X-ray and electron imaging. However, because of the strong attenuation of water to neutrons, moisture distribution inside concrete specimens can be readily identified from either a 2D neutron transmission radiography or 3D neutron tomography. New studies reported a) quantification of water redistribution in mortar containing shrinkage-reducing admixture and lightweight aggregate [94], b) real-time measurements of

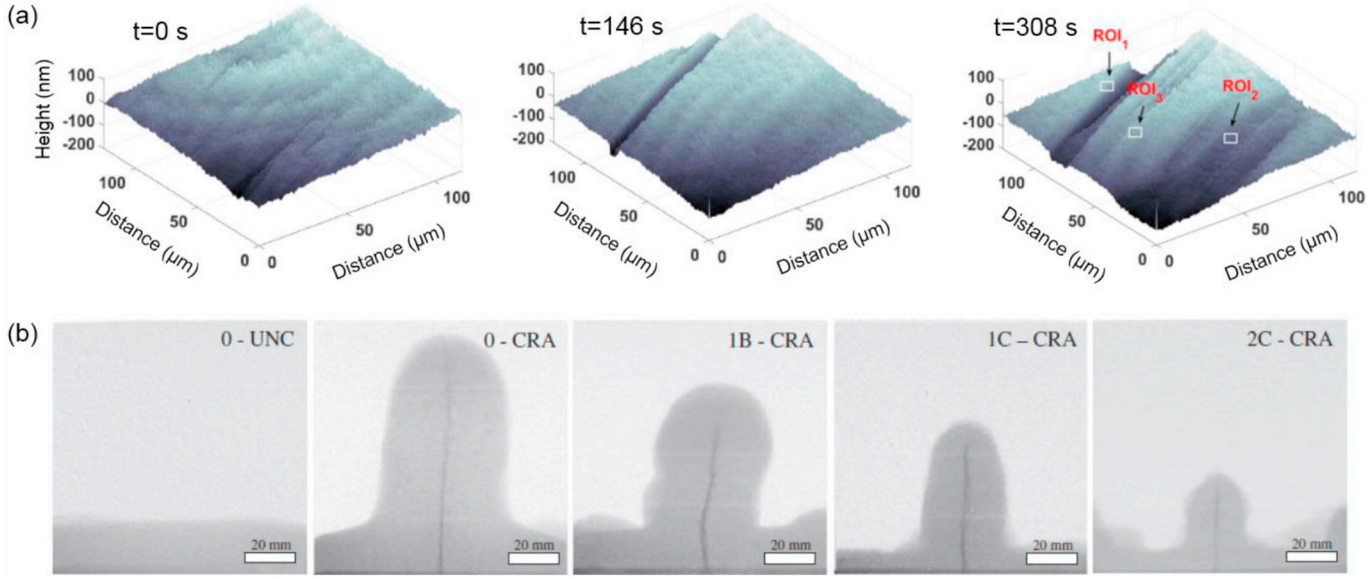

Fig. 6. Example of imaging results obtained using (a) DHM, (b) Neutron radiography, and (c) ERT. (a) Surface topography of a gypsum grain measured by DHM showing development of etch pits; images adopted from [92]. (b) Neutron radiography conducted after 4 h contact with water for non-cracked specimen without SAP addition (0-UNC) and cracked samples without SAP addition (0-CRA), with 1% SAP B (1B-CRA), 1% SAP C (1C-CRA) and 2% SAP C (2C-CRA); images adopted from [96].

moisture profiles in high-performance concrete exposed to high temperatures [95], and c) visualization of water penetration in cementitious materials with superabsorbent polymers (SAP) [96]. Fig. 6(b) shows radiographic images of moisture distribution in pre-cracked mortar specimens in contact with water for 4 h [96]. Inhibited moisture diffusion was observed in specimens containing superabsorbent polymers, since SAP swells in humid environment and can seal pre-existing cracks.

2.2. Indirect methods

2.2.1. In situ X-ray Diffraction (XRD) correlated with isothermal calorimetry

While XRD has been used for over a century to characterize both anhydrous and hydrated cementitious materials, recent advancements in detector technologies - allowing a full scan (from 5 to 70° 2θ) to be performed in < 7 min on a single sample, with a good peak data resolution – provide new opportunities to relate microstructure formation to ongoing hydration reactions. Time-resolved, in situ XRD can be performed on hydrating samples that are cast in the sample holders [97–101]. Evaporation and carbonation can be avoided by covering the exposed sample surface with a low-permeability thin film of known diffraction pattern, such as polyethylene terephthalate (i.e., PET or 'Mylar') or Kapton film. Fig. 7 shows diffraction patterns, obtained hourly for a sealed hydrating OPC paste sample up to 24 h of hydration. The peak heights measured from this diffraction patterns can be plotted as time series data and compared to isothermal calorimetry results to relate changes in relative amounts of reactants and products with heat evolution. An example is shown in Fig. 8 where increasing peak heights (obtained from Fig. 7) of the early hydration products ettringite and portlandite, are contrasted with the depletion of cementitious alite and belite phases. This semi-quantitative method allows having an indication of the phases assemblage and its general evolution during the hydration [99]. However, for a reliable quantification of the phases, in-situ XRD coupled with a Rietveld refinement analysis using an external standard [102] can be preferred and were recently used to better understand the evolution of the chemical balance in the first hours of hydration as well as the effect of admixtures [97,98,100,101,103].

The peak normalization method can also be used to understand the influence of citric acid dosage [104] in retarding the hydration kinetics and ettringite crystallization in calcium sulfoaluminate (CSA) paste mixtures, thereby increasing the time to set, as shown Fig. 9. However, care should be taken when comparing XRD obtained from two different samples. A layer of water may form between the sample and the protective film, which changes the absorption of the X-ray and therefore causes possible errors in the peak analysis [105]. Samples with bleeding tendency, as it is often the case for samples with superplasticizers, may also present higher peaks for portlandite and, in some cases, for ettringite, which leads to their overestimation. Preferential direction of grain growth may also be created, which can result in inaccurate quantification of phase content. This can often be avoided by complementing with additional XRD tests on finely ground powders or by using other characterization methods such as thermogravimetric analysis (TGA). For example, Fig. 10(a) shows the influence of PCE on reaction kinetics and phase development in a hydrating CSA paste mixture. For the mixture with PCE addition, the peak height of the ettringite phase is about twice the peak height of the ettringite phases in the mixture without PCE. However, the peak heights of the hydrating ye'elimite phase, which is mainly responsible for the formation of ettringite, is similar after 6.5 h of hydration in both the mixtures with and without PCE addition. From the TGA (Fig. 10(b)) performed at 6.5 h of hydration on both the mixtures with and without PCE addition, an insignificant difference in ettringite phase is found between both the mixtures. Upon SEM investigation of the ettringite phase morphology in both of those mixtures (shown in Fig. 10 (c) and (d)), the ettringite needles in mixture without PCE were longer and exhibit preferential direction of growth, whereas, with PCE addition, the ettringite needles were short, well-packed and do not seem to exhibit any preferential direction of grain growth (refer to Section 3.1.2 for more details). For additional information of XRD technique and sample preparation procedures, the readers are referred to guidebooks on microstructure characterization of cementitious systems [102].

2.2.2. Small angle X-ray & neutron scattering (SAXS and SANS)

When an incident beam passes through a material, the scattered X-ray or neutron measured at low scattering angle carries the structural information of the material at nanoscale (from 1 to 100 nm). The raw small angle scattering (SAS) data is in the form of intensity vs. the scattering

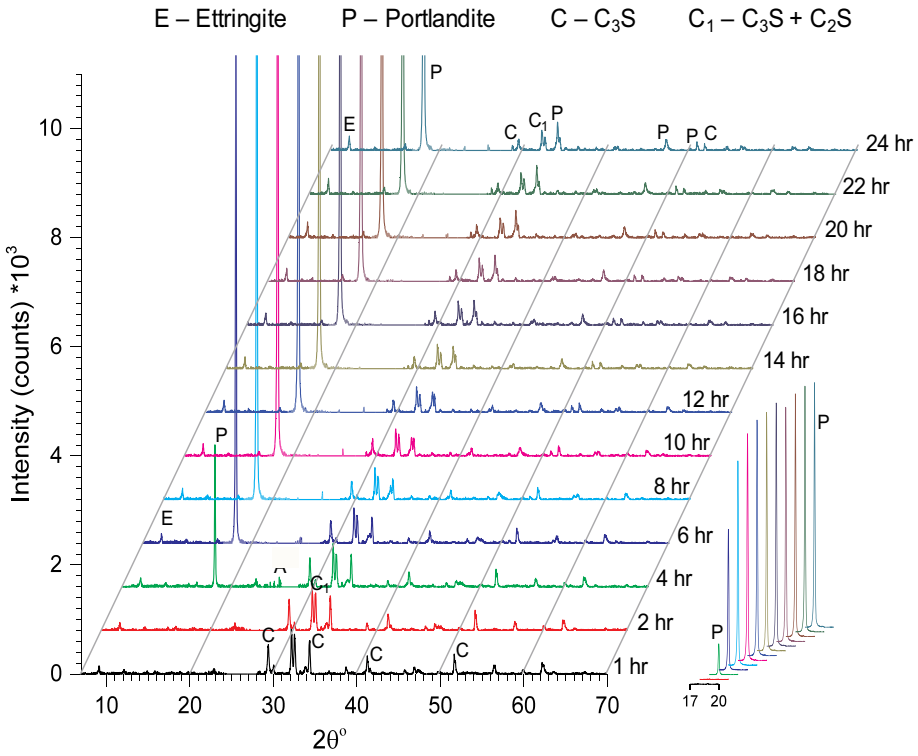

Fig. 7. XRD of hydrating OPC paste mixture at every hour until 24 h of hydration time.

vector Q, where $Q = \frac{4\pi \sin\theta}{\lambda}$; θ and λ are the scattering angle and the beam wavelength, respectively. The interested reader can find a detailed description of the mathematical foundation in [106–108]. SAXS and SANS have been applied to cementitious system for nearly 20 years. One of its major contributions was to show the globular nature of C-S-H at the mesoscale [75]. SAXS and SANS have been applied on cementitious system for nearly 20 years. Recently, researchers have refined the globular model of C-S-H to an alternated layer-packing of calcium silicate and water, resulting in a modified mathematic expression of the scattering intensity [109,110]. Such a model allows fitting both the thickness of water and the calcium silicate layer of the C-S-H lamellar structure, using the SANS data with extended Q range from 0.015 to 1.0 $Å^{-1}$ [75,76]. Apart from the C-S-H samples, SAXS was recently used to study the nano-morphology of magnesium-silicate-hydrate (M-S-H) [111]. The diameter of M-S-H nano globules can be fitted by adopting a spherical shape for basic M-S-H solid units. The hydration of C_3A in the presence of gypsum was recently studied by in-situ SAXS experiment (Fig. 11(a) [76]). By adopting a needle (cylindrical) shape for the ettringite crystals, their average radius was tracked as a function of hydration time. The fitted geometry is comparable to the results obtained by direct image analysis, as shown in Fig. 11(b). This study demonstrated the possibility of conducting in-situ SAXS experiment for a fast-evolving cementitious-system, so that the certain nano-morphological information can be obtained in a minute-based rate.

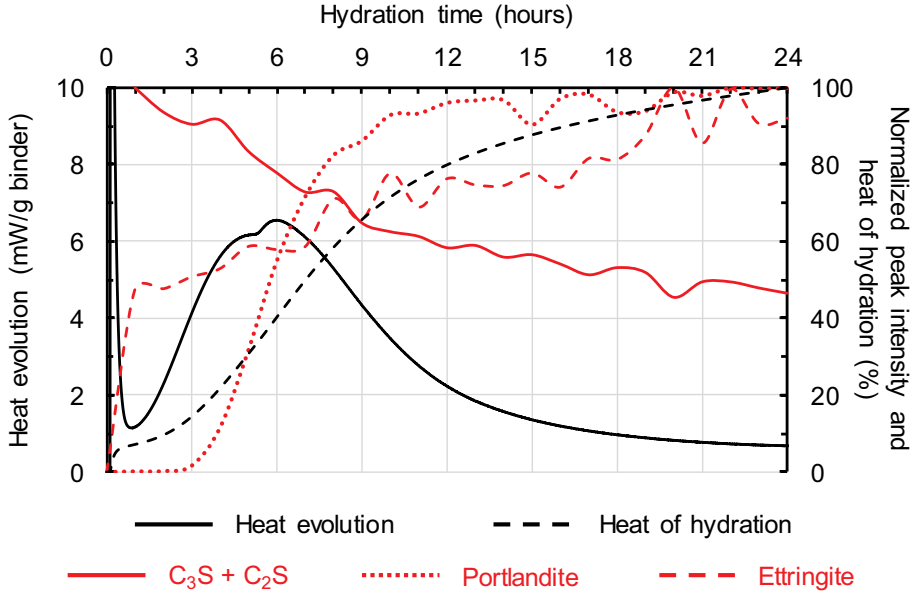

Fig. 8. Comparing early age heat evolution and heat of hydration with phase development in Portland cement paste.

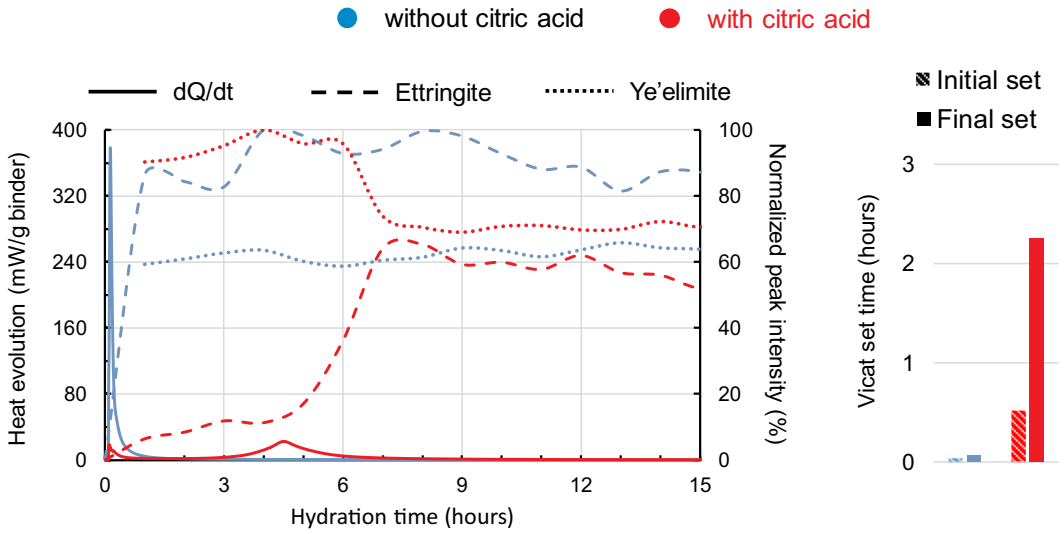

Fig. 9. Influence of set modifier (citric acid) on early age heat evolution, phase development, and setting time of CSA cement pastes.

2.2.3. ^{1}H NMR Relaxometry

The multiscale pore structure of cementitious material is often characterized by the different physical states of water in pores of various sizes. The hydrogen nuclei in water act as sub-atomic magnets which respond to an applied magnetic field. After coherent precession excitation, the excited nuclei gradually relax to lose their coherence. In a cementitious system, the dominating mechanism of such relaxation is the fast interaction between exited hydrogen nuclei with the pore surface. Hydrogen nuclei relax faster in smaller pores where the surface-to-volume ratio is larger. Based on this 'fast exchange model', the time constant of the relaxation, also termed as T_2, is used to calculate the pore size according to Eq. (2), where S/V is the specific surface area of the pore and λ is a calibrated empirical parameter.

$$\frac{1}{T_2} = \frac{S}{V} \times \lambda \tag{2}$$

Readers are referred to [113] for the detailed theory of the existing models and a comprehensive review of ^{1}H NMR Relaxometry

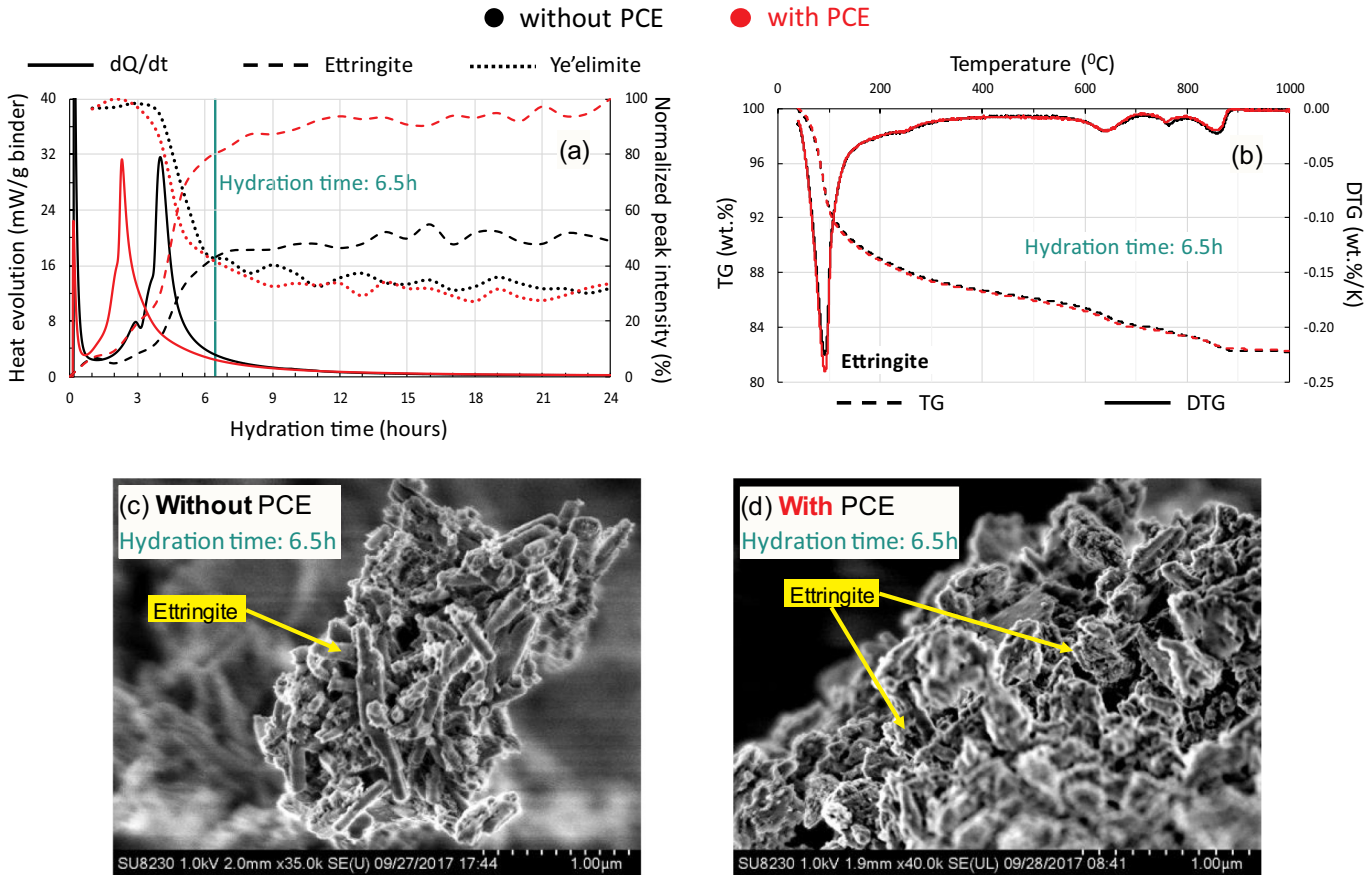

Fig. 10. Influence of PCE on (a) hydration kinetics, (b) phase development and (c, d) phase morphology in CSA paste mixtures.

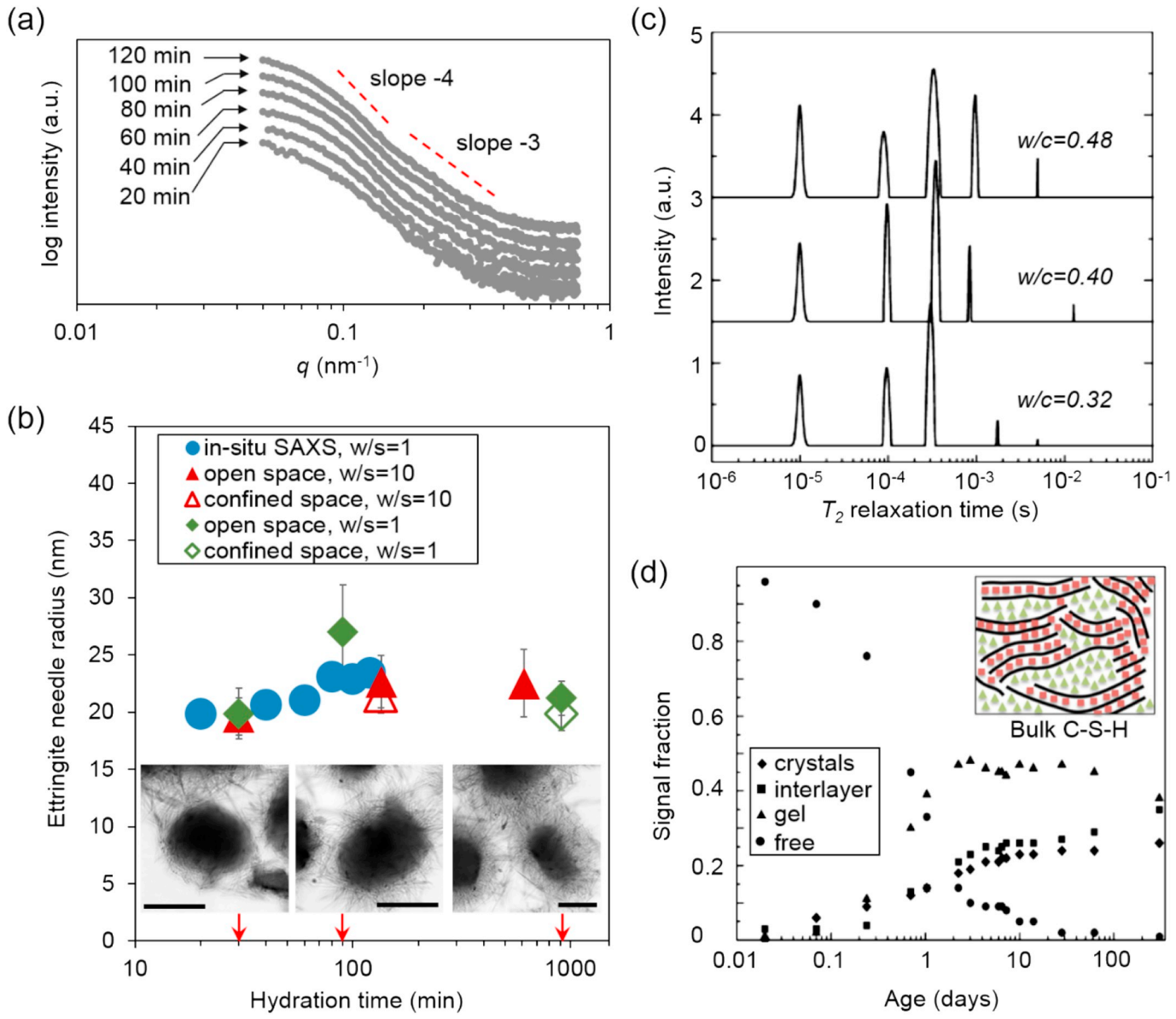

Fig. 11. (a) and (b) in-situ SAXS study [76], (c) and (d) in-situ ^{1}H NMR Relaxometry study [112]. (a) SAXS results of ettringite from the in-situ measurement of hydrated C_3A in the presence of gypsum (w/s = 1, C_3A/gypsum = 2.5). (b) Evolution of ettringite needle radius both from fitting the SAXS data and from direct image analysis. (c) The T_2 distribution of white cement pastes at 10 days hydration. (d) Evolution of the fractions of different signals in a white cement paste (w/c = 0.4) as a function of hydration time.

applications for cement-based materials.

In the past 5 years, ^{1}H NMR Relaxometry has been used to study several fundamental cement-chemistry topics. Fig. 11(c) shows the T_2 distribution of white cement paste cured for 10 days hydration, where five principal components are observed. In an increasing order of T_2 peak positions, they are assigned to chemical water in CH (and ettringite), interlayer pore water, gel pore water, free water in the interhydrate space, and in the capillary pores [112]. By casting the cement paste into glass NMR tubes, the fractions of different pore spaces can be tracked in situ as a function of hydration time, see Fig. 11(d). Coupled with the mass fraction of CH and ettringite measured by XRD and TGA, the solid density (exclusive of gel water) and bulk density (inclusive of gel water) of C-S-H can be calculated, as well as its specific surface area. A similar study was conducted on white cement hydration system containing silica fume [114], and on the early hydration of alite and OPC [115]. The release of water by organic internal curing agents, also in white cement, has also been recorded with ^{1}H NMR, and the rate of moisture migration related to the composition and structure of the agent [116].

Using an NMR temperature control module, researchers have studied the change of water state within the cementitious pore space due to temperature changes. The results indicate that the fraction of gel water increases but the fraction of interlayer water decreases when temperature increases from 20 °C to 38 °C [117]. A change of the pore size distribution was also observed in specimens undergoing drying-wetting cycles [118]. Researchers have also used ^{1}H NMR Relaxometry measurements to calibrate the internal relative humidity of a cementitious matrix self-cured in a seald container [119], and to assess the accuracy of mercury intrusion porosimetry [120]. To summarize, ^{1}H NMR Relaxometry has been tuned into be a robust method to measure pore structure and water binding state over a large spatial scale in a remarkable non-destructive manner.

2.2.4. *Texture of the hydration products*

The orientation distribution of grains in polycrystalline materials, often referred to as “texture”, is extensively studied by metallurgists

and geologists [121]. When a single grain exhibits non-isotropy for certain physical properties, the texture of the matrix will greatly determine the bulk property. The orientation distribution of crystals can be measured by evaluating the variation of intensity along the azimuthal angle of the Debye rings obtained from synchrotron X-ray diffraction measurements [122]. The cementitious matrix contains crystalline and nanocrystalline phases, and their orientations have always been assumed to be random in existing multiscale models of concrete. An early investigations indicated that CH prefers to align its *c*-axis perpendicular to the cement-aggregate interface [123,124]. In a microXRD texture study conducted on ettringite precipitated during sulfate attack [125], the *c*-axis of the trigonal crystallites are found to be preferentially oriented perpendicular to the fracture surfaces. By averaging single-crystal elastic properties over the orientation distribution, it is possible to estimate the elastic anisotropy of ettringite aggregates.

Previously, texture analysis of C-(A-)S-H has not been reported, largely due to its poorly crystallized nature making it poorly suited for conventional XRD conditions. However, recently Geng et al. [93], using a synchrotron-based High-Pressure XRD setup in a radial diffraction geometry, were able to characterize the texture of C-(A-)S-H as a function of applied external compression. The experimental geometry allowed the determination of the orientation of the C-(A-)S-H layers by analyzing the intensity distribution of the (002) diffraction ring at different azimuthal angles. As shown in Fig. 12(a), when loaded under hydrostatic stresses, the (002) ring had a uniformly distributed intensity. However, when the stress tensor contained deviatoric components, the intensity concentrated at the horizontal direction. The results indicate that the ordinarily randomly oriented C-(A-)S-H nanocrystals tend to align themselves perpendicular to the applied uniaxial compression with soft lateral confinement, as shown in Fig. 12(b). Deviatoric stress is the driving force to develop such a texture, as texture does not form when C-(A-)S-H is loaded by hydrostatic force (Fig. 12(a)). Such a texture may largely alter the macro-property of C-(A-)S-H matrix especially when its atomistic scale property is anisotropic.

3. Effects of superplasticizers on the microstructure

Comb-shaped polycarboxylate ether (PCE) superplasticizers (Fig. 13) are among the most widely used concrete dispersants and can strongly impact the microstructure of hydrating cement in different ways [126–129]. Through their adsorption on cement particle surfaces,

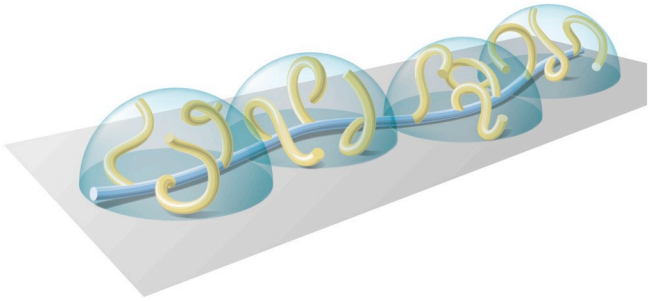

Fig. 13. Schematic representation of a PCE molecule with its backbone adsorbed on the surface of a cement particle and its side chains occupying a volume around the backbone. This figure shows the blob model describing the polymer as self-excluding chain of half spheres [142].
Adapted from [132].

thanks to their charged backbones, they can alter the dissolution of the anhydrous phases, which is believed to be at the origin of the cement hydration retardation, and modify the structure and morphology of the hydration products, which may impact the equilibrium between the main phases [8,103,130–134]. Their side chains induce steric repulsion between cement particles, changing the precipitation location of the hydrates and therefore the spatial distribution of the cement phases [135]. The adsorption affinity of the polymer influences its interaction with different cement phases, which is highly dependent on the surface chemistry of the phases and on the PCEs own molecular structure [129,136,137]. The latter is very versatile and can be easily modified to reach the desired adsorption and rheological properties [15,126,127,130,135,138–141]. This implies, for example, that modifying the chemistry and structure of PCEs – e.g., the monomers composing both the backbone and the side chains, the bonds between them, the length of the backbone, the number, length and distribution of side chains, and the charge density– microstructure can be influenced and potentially tailored.

3.1. Ideal systems

3.1.1. Silicates

The way the chemical admixtures can modify the morphology of C-S-H has great importance, as it influences the final properties. As will be

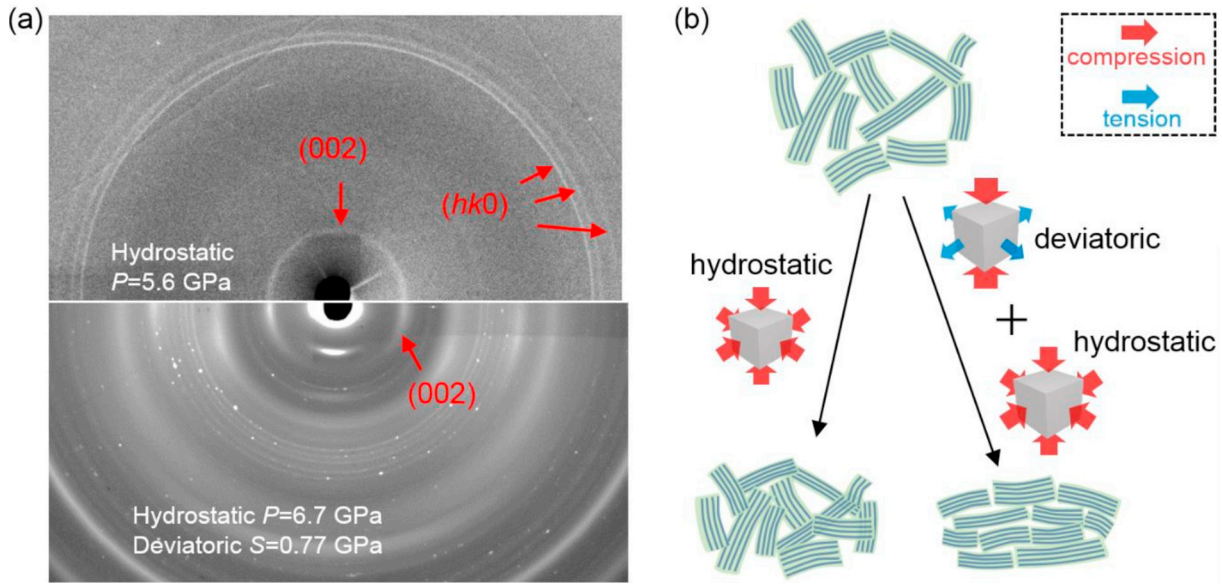

Fig. 12. Texture study of C-A-S-H under different stress condition: (a) 2D diffraction images of C-A-S-H loaded without (top) and with (bottom) deviatoric stress; (b) a schematic illustration of C-A-S-H developing preferred orientation under different loading condition [93].

discussed in Section 4, the synthesis of C-S-H seeds in presence of PCEs can be use as accelerating admixtures [143–146]. PCEs molecules, used to stabilize and disperse the seeds in solution during their synthesis, significantly influence the C-S-H morphology by causing the precipitation of smaller particles and by modifying the assemblage of the platelets [145]. The structure of the agglomeration of these modified particles and the surface created depend on the molecular structure and charge density of the polymer [145,147]. These modifications have a great practical significance because the efficiency of the seeds depends on the structure formed, on the density of the aggregates, and on the surface available for further hydration [147].

The modifications in the morphology of the hydrated particles are relatively easy to observe and to measure. However, such observations only reflect the changes caused by the presence of the chemical admixtures and do not inform about the exact process on how molecules interfere with the precipitation of the particles. While there are several models to explain the C-S-H nucleation and growth process, a consensus has not yet been reached [49,146,148–153]. The exact role of the addition of admixtures in the different steps of these processes must be dependent on the real process of C-S-H precipitation and consequently still remains unclear.

Recent studies showed evidences of a non-classical precipitation of C-S-H with a transition from globular or spheroidal nanoparticles, defined as amorphous precursors, to the more characteristic C-S-H nanofoils (Fig. 14) [154,155]. The presence of PCEs delays this conversion, probably by forming a layer around the precursors that stabilizes the metastable particles and prevent them from converting to the more stable foil-like structure [155]. The kinetics of the conversion depends on the molecular structure of the polymer, with a longer delay for the highly charged molecule. These results confirm the stabilization of precursors with linear polycarboxylates, already observed during the formation of $CaCO_3$ that was previously used as a model system for cement hydrates [156]. For the $CaCO_3$ precipitation, the growth, size and morphology of the crystals also depend on the structure of the polymer and its charge density [157,158].

Recent research has focused on the characterization of the molecular bonds between the polymer and the C-S-H surface [159–161]. Orozco et al. [159] studied PCEs composed of carboxylate and silanol groups that are known to increase the adsorption in extreme environment where normally PCEs fail to adsorb [138,162–164]. The use of integrated advanced characterization technics, such as synchrotron X-ray radiation and NMR, showed that the adsorption of the carboxylate groups on Ca-ions changed the order of symmetry of the ion and that the silanol groups form covalent bond with the silicon at the surface. Furthermore, a small basal spacing increase was observed, which, according to the authors, is not due to intercalation of PCEs, but probably caused by a change of stacking order of C-S-H layers caused by the dispersion effect of the polymer and/or a shift of Ca complexing on the surface that leads to more water in the interspace. A higher degree of polymerization and hence a greater average length of the silicate chains are observed for PCEs with silanol groups and for more common PCEs with carboxylate functions [159,165].

The effects of other chemical bonds, such as hydrogen bonds, between the C-S-H surface and polymers have been measured. These chemical bonds together with the carboxylate functions make the interaction between the polymer and C-S-H stronger [160]. This led to the development of a composite C-S-H/polymer capable of withstanding flexural stresses of several hundreds of MPa by combining the stiffness of the C-S-H and elasticity of the polymers along with its ability to dissipate energy [161]. Although the quantity of organic admixture

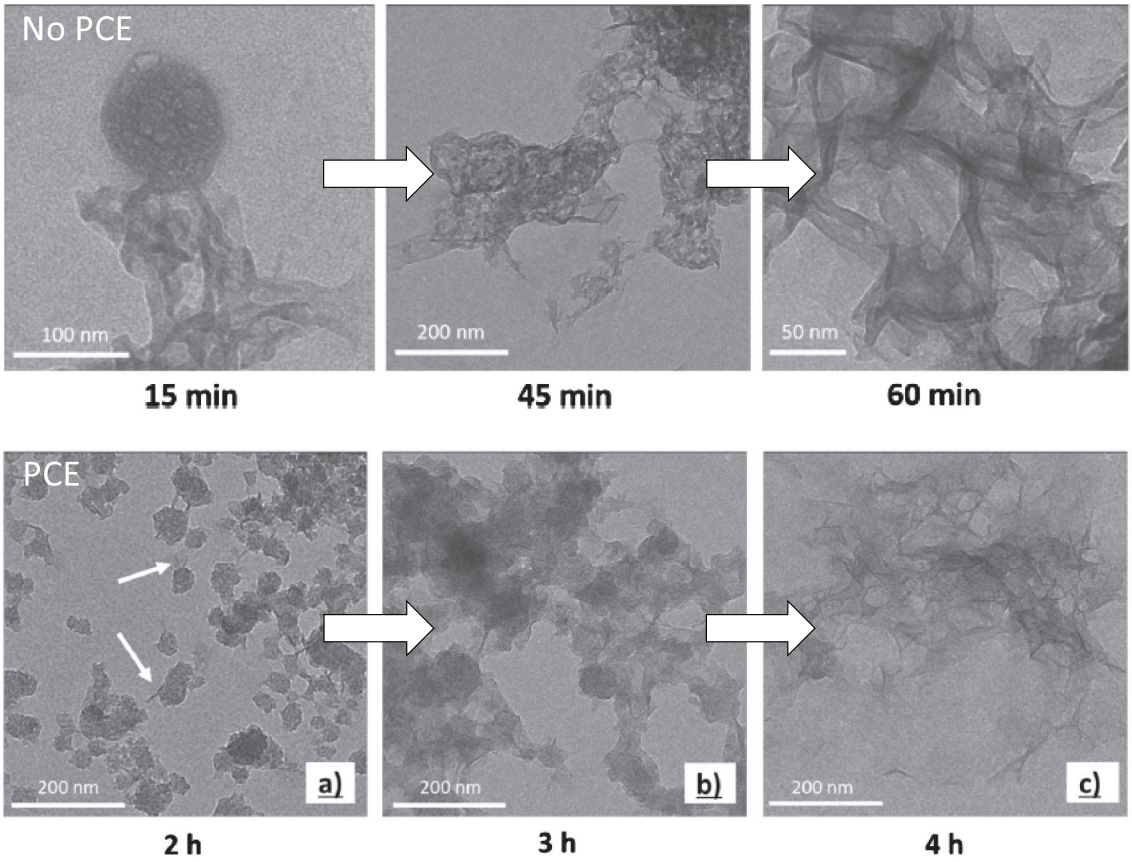

Fig. 14. TEM images of C-S-H precipitated without PCE (above) and with a highly charged PCE (below). The conversion from globules to nanofoils in the system without PCE is completed after 60 min. In presence of PCE, the globules are smaller and more dispersed, and the conversion is completed only after some hours. Reproduced and adapted from [155].

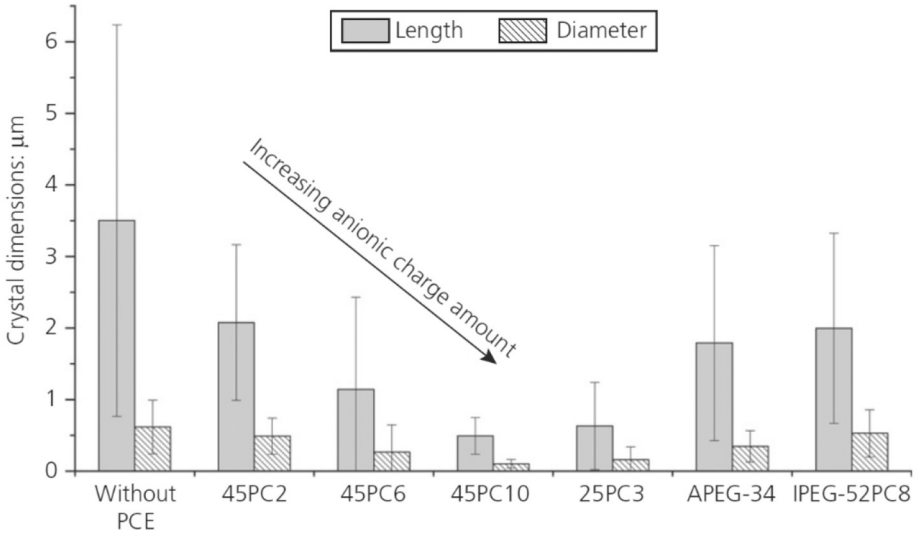

Fig. 15. Average length and diameter of ettringite crystals obtained from calcium hydroxide and aluminum sulfate solutions after 10s of reaction without polymer and with different types of PCEs [179].

needed for creating this material is higher than the dosage of PCEs used in practice, the results show that the behavior of cementitious materials with better mechanical properties could begin at the nanoscale.

Studies on the effect of chemical admixtures on C-S-H are numerous. However, to the best of our knowledge, few studies focused on the influence of the admixtures on the portlandite precipitation [166–168]. For example, sucrose, that is known to have a strong affinity for portlandite and to inhibit its precipitation, strongly modifies the morphology of its crystals [167]. PCEs seem to affect more the size by creating smaller crystals than the morphology. It is clear that more research is needed to determine the influence of admixtures on the precipitation of portlandite as it represents an important factor in the overall hydration kinetics of C_3S [169].

3.1.2. Aluminates

3.1.2.1. AFm precipitation. Anionic PCEs have a higher affinity for aluminate than silicate surfaces, due to their positively charged surface. PCEs with high charge density are particularly known to intercalate between the cationic layered structure of calcium aluminate hydrates (or AFm) to form a so-called organomineral phase (OMP) or a hybrid layered double hydroxide (LDH) structure [170]. This intercalation has been observed during the synthesis of hydrocalumite in presence of PCEs [171–175] and in realistic systems using hydrating calcium aluminate cements both with high polymer concentration and with more practical dosages [173]. SEM and TEM analysis confirmed the formation of intercalates composed of nano-sized foils. XRD, SAXS and NMR TRAPDOR measurements provided a better characterization of the interlayer chemistry and distance between the layers. The latter is greater in presence of PCEs and also depends on the molecular structure and polydispersity of the polymer and its steric characteristics. The composite structure was rationalized by using a model of adsorption conformation of comb copolymers derived from scaling laws using the structural parameters of a molecule [171]. This allowed to describe the intercalated polymers as bilayers of hemispheric cores with sizes dependent on the molecular parameters of the polymer, similar to what is described in Fig. 13. Changes in stacking orders of the composite particles were also observed but, as mentioned by the authors, it could be an artefact of the sample preparation that led to the alignment of the particles.

In practice, the intercalation of the molecules in LDH structures means that a part of the polymer is lost and therefore is not used for the dispersion. Because the intercalation depends on the molecular structure and on the aluminates and sulfates content, changes in the rheological behavior will occur depending on the charge density of the polymer and its affinity for intercalation and the type of cement. Understanding such interaction at a molecular scale is needed to develop new superplasticizers able to avoid such incompatibilities with cement [170].

3.1.2.2. Ettringite precipitation. The strong change in ettringite precipitation caused by the presence of superplasticizers is also one of the main reasons for incompatibilities between admixtures and cement [133]. Several studies focused on the spontaneous precipitation of ettringite from calcium hydroxide and aluminum sulfate solutions in presence of various chemical admixtures [176,177], including PCE with different molecular structures [178,179]. Cody et al. [177] performed a careful and systematic analysis of the ettringite precipitation with a high number of admixtures from inorganic salts, small organic compounds to larger organic molecules. In the case of superplasticizers, except for naphthalene sulfonates that seem to lead to larger crystals [176], the presence of dispersants generally leads to a larger number of smaller crystals, indicating a favored nucleation of ettringite crystals linked to a growth inhibiting effect [178,179]. Besides the change in size, the crystals have also different morphologies and aspect ratios depending on the type of molecule, from generally finer needles for PCEs to thick prisms for naphthalene sulfonates as shown by Shi et al. [176]. This may be due to differences in adsorption and affinity of the molecules for the various faces or edges of the crystal structure, which prevents further growth in different directions.

Changes in crystals size, morphology and aspect ratio were also observed for PCEs molecules with different structural architecture after 10 s of crystallization (Fig. 15) [179]. The effects varied with the chemistry and the charges density of the molecules, with a stronger impact for the most anionic molecule. In practice, the influence on the number of crystals, their size and dimensions lead to a higher specific surface of the aluminates surface and a higher and faster consumption of the ettringite components, such as sulfate and water. Because the interaction between PCEs and ettringite precipitation occurs during the first minutes of hydration, the main consequences of the modification brought by the polymer have a negative influence on the rheological properties of the concrete and perturb the hydration kinetics [19,132,180–182]. So far, the exact mechanism for the enhanced nucleation of ettringite has not been explained neither quantified with respect to the molecular structure of PCEs. Once the mechanism is fully understood, it will be possible to control this strong incompatibility

between cement and PCEs. Such control will be particularly useful for applications that need an early stiffening and structural build-up, such as for 3D printing [18,19].

3.1.3. Challenges and limitations of the ideal systems

Regarding the changes in ettringite precipitation, presently there is no clear understanding if the modifications are related to alterations in the way the nuclei are formed with complexed molecules or if the modifications are associated to the adsorption of the molecules on the already formed nuclei, leading to a different growth mechanism. Explaining this at the nanoscale remains one of the most important challenge in admixtures technology. Combining advanced techniques, such as NMR, SAXS or cryo-TEM, that have been useful in the development of new insight for the C-S-H precipitation [154,155], has the potential to increase the understanding of the action of PCEs on ettringite nucleation and growth. This challenge is however not trivial because ettringite precipitation is fast and, if not well controlled, can be altered by the precipitation of other phases, such as AFm or calcium sulfates.

The complexation ability of the molecules plays a critical role in any perturbation of hydrates precipitation. For example, through Ca-ions titration, polyacrylate chains, similar to the backbone of most of the commercial comb-shaped copolymers, have shown a strong ability to modify the way the ions are consumed for C-S-H precipitation: from a nucleation with one step of Ca-ions consumption without organic admixtures to a several steps process with an initial complexation period at higher supersaturation in presence of the polymer [183]. Such modified uptake of calcium ion during C-S-H formation could be another evidence of the stabilization of precursors by the polymer observed by Schönlein and Plank [155].

Finally, the hydrates morphologies described above for either C-S-H or ettringite are observed after their synthesis from saturated solutions. The impact of admixtures on the hydrates formation may differ in real cementitious systems as every aspect of hydrates precipitation is dependent on the solution composition and ionic strength, the type and composition of the anhydrous phases as well as their dissolution characteristics, the solid to liquid ratio, etc. Some of these aspects are discussed in the next section.

3.2. Cementitious systems

3.2.1. Pure C_3S phases

Although focusing only on one phase neglects the equilibrium between the main phases of cement, it is also useful to analyze in details the impact of polymers solely on C_3S, as it is the main component of cement. In recent studies, new insights in the influence of PCEs on C_3S hydration were gained [132,134,166,184–192].

A direct experimental evidence showed that silicate dissolution is reduced by the presence of PCEs [132]. The fact that low dosages of polymer may effectively block the dissolution of a reactive phase may be understood from the perspective of blocking reactive surface areas on the surface, that are generally etch pits, or modifying the kinetics and the way they expand (Fig. 16a) [132,193]. As a confirmation, the exact same rate of reaction, and therefore retardation, was observed between a C_3S with PCEs and the same C_3S but annealed to remove defects on the surface (Fig. 16b) [132].

In the pore solution of a C_3S paste, sedimentation coefficient analysis performed by ultracentrifugation showed evidences of nanoscale clusters composed of polymers and C-S-H, probably formed due to the complexation between the anionic functional groups of the polymer and Ca-ions [187]. This phenomenon, combined to the dispersion effect of the PCE, may explain the transition from heterogeneous to homogeneous nucleation, that was highlighted by nucleation and growth models [194]. Micro-tomography performed on cement pastes also indicated changes in spatial distribution between the anhydrous phases and C-S-H [195].

Questions about the real influence of the PCEs on the chemical composition of C-S-H, such as the Ca/Si ratio, and the development of the C-S-H platelets in real systems still remain. By following the phase assemblage evolution with X-ray diffraction and estimating the mass balance of Ca-ions between the different phases, it was found that in C_3S pastes the evolution of the Ca/Si ratio of C-S-H is different from a reference paste to a system with polymers [188,196]. To validate the results, the heat release was back calculated from the phase quantification with commonly used stoichiometry of C_3S hydration reaction and fitted to the actual calorimetric curves. While, for the system without polymer, the fitting was straightforward, with polymer the fitting was possible only by taking into account a possible change in entropy of C-S-H reaction as well as taking into account the water content with respect to the changes of Ca/Si ratio, all these aspects followed the commonly used C-S-H models [188]. This discrepancy, corrected with thermodynamic considerations of C-S-H formation, may indicate a structural change in C-S-H particles assembly as well as a variation of the Ca/Si ratio, which are both mentioned in pure synthesis of C-S-H with PCEs [145,159] but never for C-S-H in C_3S pastes.

3.2.2. Cement models

In recent studies, different strategies were used to monitor and characterize ettringite precipitation in a more realistic hydrating systems [132,176,197]. Using C_3A and gypsum reacting for 28 days at a water to binder ratio of 0.29, Shi et al. [176] observed differences in the morphology of ettringite reacting in presence of different types of superplasticizers: a) large rods for the reference sample; b) needle-like crystals for samples containing PCEs; and c) shorter, thicker, and flatter crystals for samples containing naphthalene sulfonate. The same trend was observed for ettringite synthesized from saturated solutions. However, a direct comparison between both systems, in solution and in hydrating paste, for each individual admixture, shows strong differences in the morphology of the ettringite crystals. This is not surprising as the kinetics of ettringite precipitation are very different; from a very

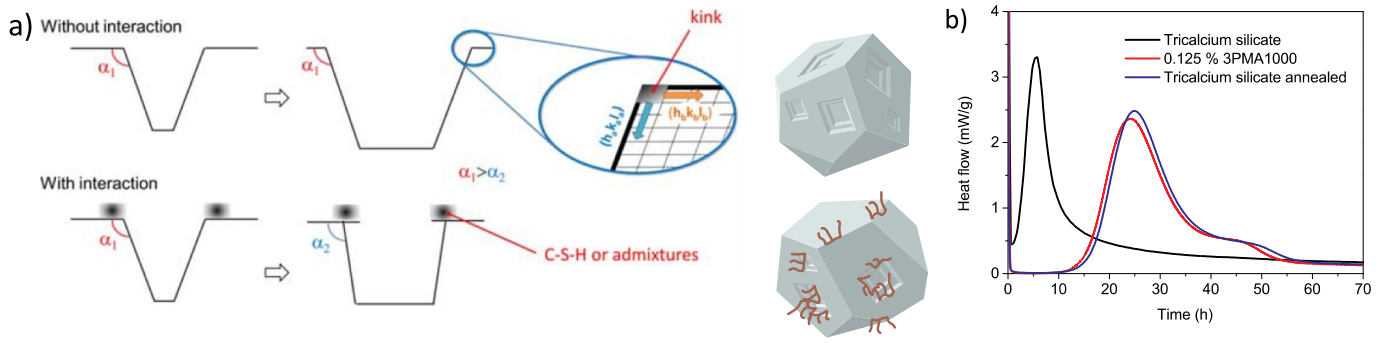

Fig. 16. a) Schematic representation of growth of etch pits in the absence and presence of PCEs adsorbed on the surface of tricalcium silicate close to the etch-pit, b) heat flows of a pure tricalcium silicate without and with PCE, and after annealing. Reproduced and adapted from [132,193].

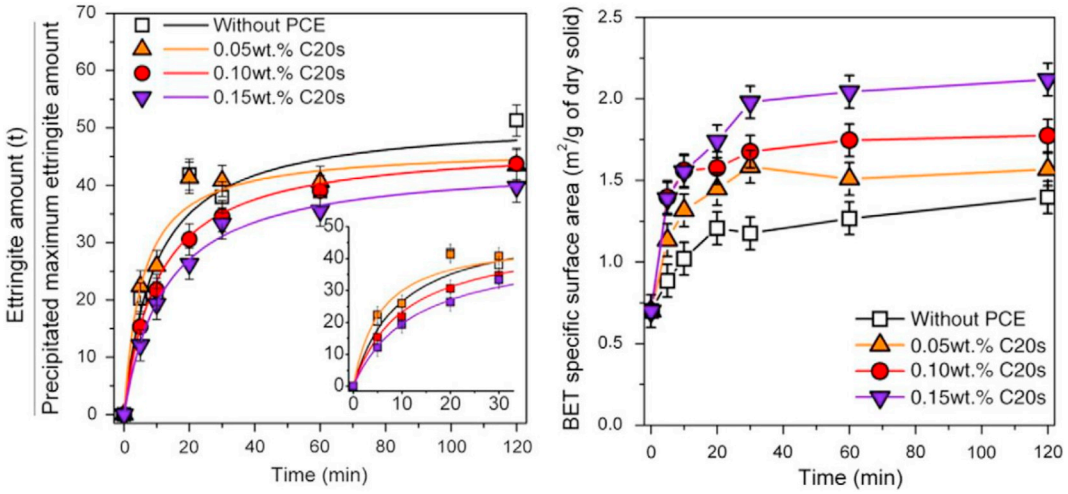

Fig. 17. Evolution of the amount of ettringite precipitated (left) and the corresponding evolution of the BET specific surface area (right) for a paste without admixture and with different dosages of the same PCE. Reproduced from [197].

fast nucleation and growth in a large volume of supersaturated solution, to a nucleation controlled by the dissolution of the anhydrous particles at low water content. Note that the dissolution of the reactants may as well be influenced by the adsorption of the admixtures [198]. In the same study, d-spacing analysis and bonding states measured by XRD and XPS respectively also indicated structural and chemical changes varying from one superplasticizer to the another [176]. This can imply different stability of the crystals depending on the organic molecule used.

To better represent fresh cement paste in term of specific surface development and therefore workability, Dalas et al. [197] used a mixture of C_3A (16% w/w), calcium sulfate (4% w/w) and calcium carbonate (80% w/w) in a synthetic pore solution saturated with respect to $Ca(OH)_2$ and containing sulfate. Calcium carbonate was used to mimic the presence of silicates without having to deal with their hydration. The influence of PCEs dosage and molecular structure on ettringite precipitation in the first minutes of hydration was monitored using in-situ NMR relaxometry, BET and DSC. The results indicated that the presence of the polymers did not modify the progress of hydration but led to slightly lower amounts of ettringite. This effect is stronger for the highly charged PCEs and for higher dosages (Fig. 17 left). However, despite the fact that the amount of ettringite did not seem to be strongly influenced by the polymers, BET measurements revealed a strong increase in specific surface area, indicating the formation of smaller crystals (Fig. 17 right). This is in accordance with other studies that showed a strong increase in specific surface area and/or the presence of sub-micron particles in the pore solution [199]. Some hypotheses were developed to explain this favored ettringite nucleation: a) adsorption on ettringite crystals which slows down their growth and favors their nucleation, as proposed for ettringite synthesized in supersaturated solution, and b) a favored homogenous nucleation due to the complexion ability of the polymer, its dispersion property and/or its adsorption on anhydrous surface making heterogeneous nucleation less favorable.

More recently, a study focused on the hydration retardation caused by PCEs used a customized clinker composed of 80% (w/w) of C_3S and 20% (w/w) of C_3A mixed with hemihydrate [132,189]. In a realistic and representative manner, this model cement takes a step forward in simplifying the cement chemistry and the hydration reactions. Also, in this system, the presence of PCE resulted in a strong increase of the specific surface area from the very beginning of hydration. However, unlike the system of Dalas et al. [197], a higher amount of ettringite was observed. SEM pictures confirmed the presence of a large number of small particles as well (Fig. 18).

In this study, using a very high aluminate content had several advantages: a) it enhanced the strong interaction between ettringite precipitation and PCEs to highlight the negative influence of the polymer on the equilibrium of the main phases, namely a very strong acceleration of the sulfate depletion point and, consequently, a strong delay of silicate hydration and b) it highlighted the buffering effect of ettringite with respect to silicate hydration. Up to a certain dosage of polymer, c*, the increase in ettringite surface seems to uptake all the PCE molecules dosed in the system, due to their higher affinity for aluminate surface, leaving the silicate surface free to react normally (zone I in Fig. 19). It was found that the surface occupied by all the PCE molecules at c*, which is PCE molecular structure dependent and above which hydration retardation starts, corresponds perfectly to the total surface created in the system and assumed to be ettringite's (zone II). In other words, first, at this critical dosage, all the surface of ettringite formed is completely covered by all the polymer in the system, and second the extent of created surface at this dosage is dependent on the molecular structure. Above this dosage, the excess of ettringite created is not high enough to adsorb all the polymer, which allows PCE molecules to adsorb on the silicate phase, slowing down its dissolution and retarding the hydration of the cement model (zone III). After a second critical dosage c**, the strong increase of specific surface area of ettringite is large enough to finally lead to a very early sulfate depletion point. The behavior of the system after this point is similar to an undersulfated cement that suffers of a flash set and a strong delay of hydration (zone IV) [8,12,132]. Although this last behavior is enhanced here because of the high dosage of polymer and too high content of aluminate compared to an ordinary Portland cement, it cannot be completely neglect as low-CO_2 cements usually contain Al-rich materials. Furthermore, the buffering effect of ettringite visible at low dosages illustrates why cements with high content of C_3A show a lower sensitivity to hydration retardation by PCEs but a higher perturbation of the aluminate/sulfate balance [136].

It is clear from the specific surface area analysis, which shows for the first time an indirect quantification of one aspect of the strong PCEs and ettringite interaction, that the enhanced precipitation is closely dependent on the molecular structure of the polymer. However, as mentioned earlier, understanding the way the polymer affects the ettringite precipitation and how this is linked to the molecular structure remains a challenging topic in concrete admixtures technology.

At this point, it would be worth mentioning that studying aluminate and sulfate hydration reactions at very early ages for characterizing ettringite precipitation requires careful sample preparation and measurement protocols [200–202]. Too extreme conditions for stopping hydration and drying the sample can cause the dehydration of ettringite

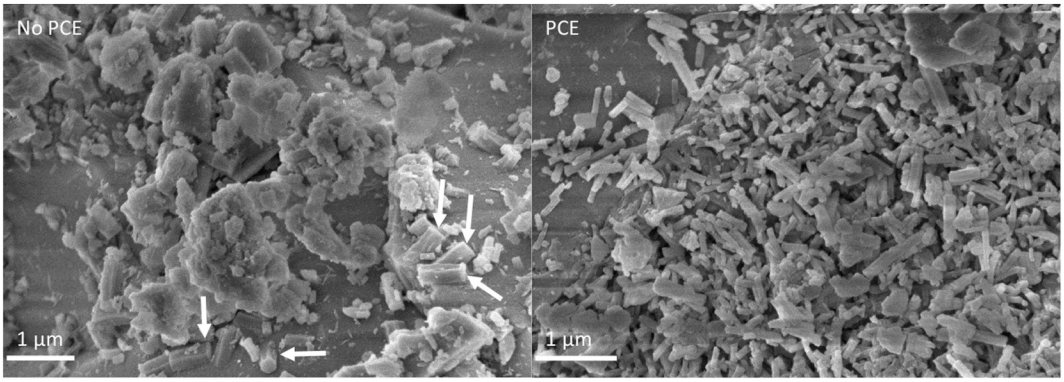

Fig. 18. SEM images of the model cement composed of 80% (w/w) of C_3S and 20% (w/w) of C_3A mixed with hemihydrate without polymer (left) and with polymer (right) stopped after 2 h of hydration. The arrows highlight ettringite crystals in the system without polymer while ettringite crystals are more numerous and smaller in the system with polymer [189].

or the decomposition of gypsum to hemi-hydrate or anhydrite. This generally leads to higher values of specific surface and modification of the crystalline structure that can produce misleading results.

4. The effect of nanoparticles on the microstructure

The most favorable nanoparticles used in cement are nano SiO_2, Al_2O_3, Fe_2O_3, TiO_2, and $CaCO_3$, although studies of cements containing nano ZrO_2 and ZnO_2 have been also reported in the past decade. Such nanoparticles are broadly available, effortlessly manufactured, and economical. A practical range of nanoparticle addition is 0.5–10 wt% depending on the surface area of the particles and their compositions. An overdose of nanoparticles or improper dispersion treatments results in their agglomeration, reduced workability of the pastes, unexpected additional defects in microstructure, and generation of misleading results. Taking nano $CaCO_3$ as an example, Kawashima et al. compared the efficiency of different dispersion methods and different surfactants and found that polycarboxylate superplasticizer is a promising candidate for dispersing nanoparticles [203]. In addition to the agreement on high dispersion efficiency of PCE-based surfactants, a recent review concluded that a combination of dispersion methods can stabilize a desired state of dispersion [204]. With a proper dose to cement content, almost all nanoparticles exhibit filler effect-refinement of the pore structure and denser microstructure of the matrix. Based on their roles or mechanisms in the cement hydration, the nanoparticles can be divided into four groups:

Group I: nanoparticles in this group, such as ZrO_2 and CuO, mainly contribute to filler effects during the early hydration of cement. The understanding of the mechanisms of microstructure modification

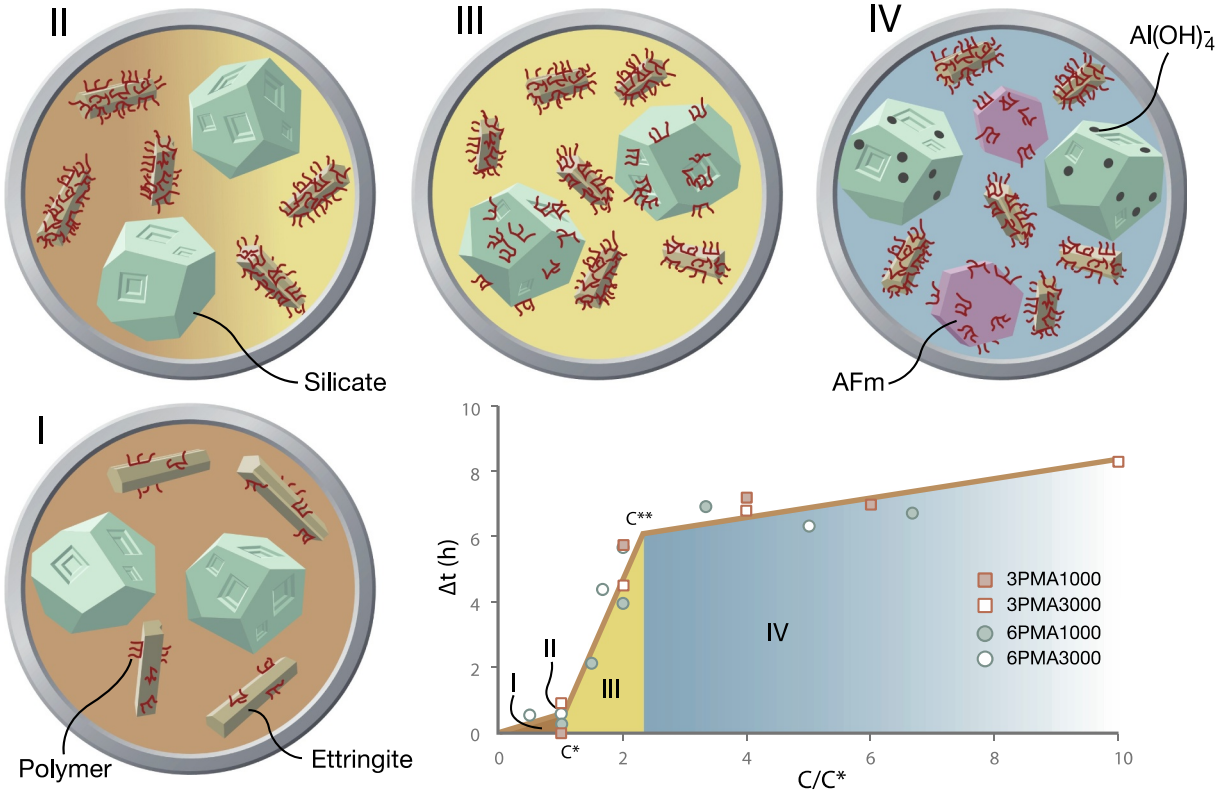

Fig. 19. Retardation of a model cement composed of 80% (w/w) of C_3S and 20% (w/w) of C_3A mixed with hemihydrate with the direct addition of different PCEs and the schematic representation of the buffering effect of ettringite. Reproduced from [132].

using these nanofillers has been well developed in the past 4–5 years. Numerous studies have shown that such nanoparticles provide additional heterogeneous nucleation sites for C-S-H and relative more space due to the diluted cement content. Berodier and Scrivener [205] suggested that shearing increased by the addition of fillers generates more nucleation sites on the cement boundaries. Thus, the addition of these nanoparticles can enhance the compressive strength due to the accelerated growth of hydration product in the pores and enhanced filling of voids between clinker grains.

Group II: nano pozzolanas in his group mainly includes nano-silica and calcined nano-clay. It is generally understood that nano-silica mimics the role of silica fume in the hydration of cement, but with much higher pozzolanic reactivity and fills finer voids. In addition to filler effects, nano-silica accelerates the strength gain of concrete and generates more C-S-H due to its pozzolanic reaction with "Ca $(OH)_2$-rich" pore solution. Unlike nano-clays, which mainly behave as nanofillers or nano-reinforcement in cementitious materials, calcined nano-clay (amorphous aluminosilicate) exhibits much higher pozzolanic reactivity. A large number of recent studies has investigated the influence of calcined nano-clay on the microstructure of hardened cement, although the size and specific surface area of the so-called "calcined nano-clay" were not well characterized in some of the studies. A recent research showed that in addition to lower residual portlandite content, hydrated cement containing calcined nano montmorillonite exhibits finer pore-size and ~2% lower total porosity compared to hydrated cement containing nano montmorillonite [206]; therefore, higher compressive strengths were achieved in cement paste with calcined nano montmorillonite than with nano-montmorillonite. Note that, this study may have overlooked the difference in surface area between the calcined and non-calcined nanoclay. As calcined nanoclay is also aluminate rich, the addition of calcined nanoclay may also influence the reactivity of aluminate-rich phases during the deceleration period as reported in the studies of micro calcined clay; although such studies are still rarely reported.

Group III: only includes nano alumina. Several publications have pointed out that nano alumina enhances hydration kinetics during the dormant and acceleration periods, refines the microstructure of paste matrix at different ranges of pore-size, and enhances the mechanical properties [207–210]. The suggested role of nano alumina in cement hydration is similar to other nanofillers. On the contrary, a decreased compressive strength of cement with nano alumina at 1d was reported by Barbhuiya et al. [211], suggesting retardation in early hydration of cement or a less refined pore structure of cementitious materials. There remain debates on the mechanism of the modification of cement hydration by nano alumina. A calorimetry study by Land and Stephan [212] reported the retardation of white cement hydration with nano alumina from dormant to deceleration periods. The deviation in early hydration behavior was explained by the different surface structures of the nano alumina produced by different processes (grinding versus bottom-up process). Similar to nano silica, they also observed the accelerated formation of monosulfate in the presence of nano alumina during the deceleration period. It is not yet clear how nano alumina contributes to the formation of monosulfate at earlier times. It was not possible to determine whether aluminates of nano alumina also contribute to the reaction during the deceleration period. It was also not clear whether nano alumina is highly pozzolanically reactive, as the incorporation of aluminum in C-S-H due to the presence of nano alumina has not been well examined.

Group IV: includes nano $CaCO_3$ and C-S-H seeds. Although $CaCO_3$ is not a pozzolan, the slight dissolution of calcite and, possibly, the arrangement of calcium atoms on the grain boundaries of calcite accelerates the nucleation of C-S-H. A preferred growth template for C-S-H on limestone filler was unveiled by Berodier and Scrivener [205]. Both experimental evidence and thermodynamic modeling have shown that calcite reacts with Al-rich phases, leading to the formation of monocarbonate and/or hemicarbonate, and indirectly stabilizing ettringite. These reactions also lead to a decreased porosity of cement pastes at an early age [213]. Therefore, nano $CaCO_3$ with much higher surface area compared to limestone powder has been suggested to exhibit clear influences on the early hydration of PC and on the microstructure of hardened pastes. Greater influence of nano $CaCO_3$ addition on the refinement of microstructure and hydration rate of PC-fly ash or PC-slag was observed at early and late ages [214–217]. The positive contribution of nano $CaCO_3$ in these ternary hydration systems can be explained by the above-mentioned interaction between calcite and Al-rich phases, as well as the filler effects.

C-S-H seeds have been observed to be an ideal template for C-S-H nucleation and further growth of hydration product, and this nucleation-growth mechanism is suggested to be the main reason for accelerated hydration in the studies of calorimetry and mechanical properties. There has been intensive research to study the nucleation and microstructure of hydrated cement with C-S-H nano seeds. Apart from conventional methodologies (MIP, SEM, ^{1}H NMR) for determining the microstructure of cementitious materials with the addition of nanoparticles, synchrotron-based X-ray tomography was also recently employed to investigate the nucleation of C-S-H during cement hydration in the presence of C-S-H seed [218]. The most common C-S-H seeds are synthetic semicrystalline C-S-H by either pozzolanic reaction or direct precipitation method, followed by C-S-H gel synthesized by sol-gel method. A recent review on nucleation seeding with C-S-H by John et al. [146] summarizes the different synthesis methods for semicrystalline C-S-H and C-S-H gel and the difference in the compositions and crystallinity of the products. For direct synthesis of C-S-H from silica-lime reaction, precise control on Ca/Si ratio of C-S-H products is difficult in the absence of mechanochemical treatment. As suggested in Section 3.1.1, in the presence of PCE, the size and shape of C-S-H seed can be controlled, which are crucial to the nucleation and growth of hydration products and the microstructure of cement pastes. For example, Sun et al. used semicrystalline C-S-H/PCE nanocomposite to modify the microstructure and early hydration of cement. In addition to the accelerated early hydration of cement and an increased 1d strength, porosity of cement paste at 3d was decreased from 33% to 26% with 0.6 wt% CSH/PCE, and the amount of large capillary pores was reduced [219]. Bost et al. [220] compared the acceleration effects of different accelerators on cement hydration up to 90 h using isothermal calorimetry. They demonstrated that X-Seed (a commercial C-S-H seed product by BASF) exhibited the strongest acceleration effect compared to other nanoparticles (e.g., nano $CaCO_3$, silica, TiO_2, and Fe_2O_3) and conventional salt accelerators (e.g., $CaCl_2$ and calcium nitrate). By adjusting pH of C-S-H/PCE nanocomposites, the smallest C-S-H seeds, namely the highest number of seeds, with an equal weight exhibited the strongest seeding effect during the early hydration of cement [221]. Another study by Land and Stephan [222] developed a factorial design of experimental setup to optimize the parameters for the syntheses of C-S-H seeds using mechanochemical and sol-gel methods. The sol-gel C-S-H with smaller size presented a more pronounced seeding effect than mechanochemical C-S-H. Mechanochemical C-S-H seeds with Ca/Si of 2 were suggested to present stronger nucleation effect than seeds at Ca/Si of 0.4. The influence of the Ca/Si ratio existing in the C-S-H seeds on the cement hydration and on the resulting microstructure is still not very understood as Si-precursor, which also influences early hydration, remains in seed products at Ca/Si of 0.4.

Although the acceleration of early hydration and enhancement in the microstructure of cement pastes with the addition of C-S-H seeds have been well accepted, inconsistent results in terms of long-term compressive strength have been reported. Compared to unseeded pastes, 14% reduction in 28d strength of pastes with 2 wt% addition of C-S-H seed was found by Owens et al. [223], whereas Kong et al. [224]

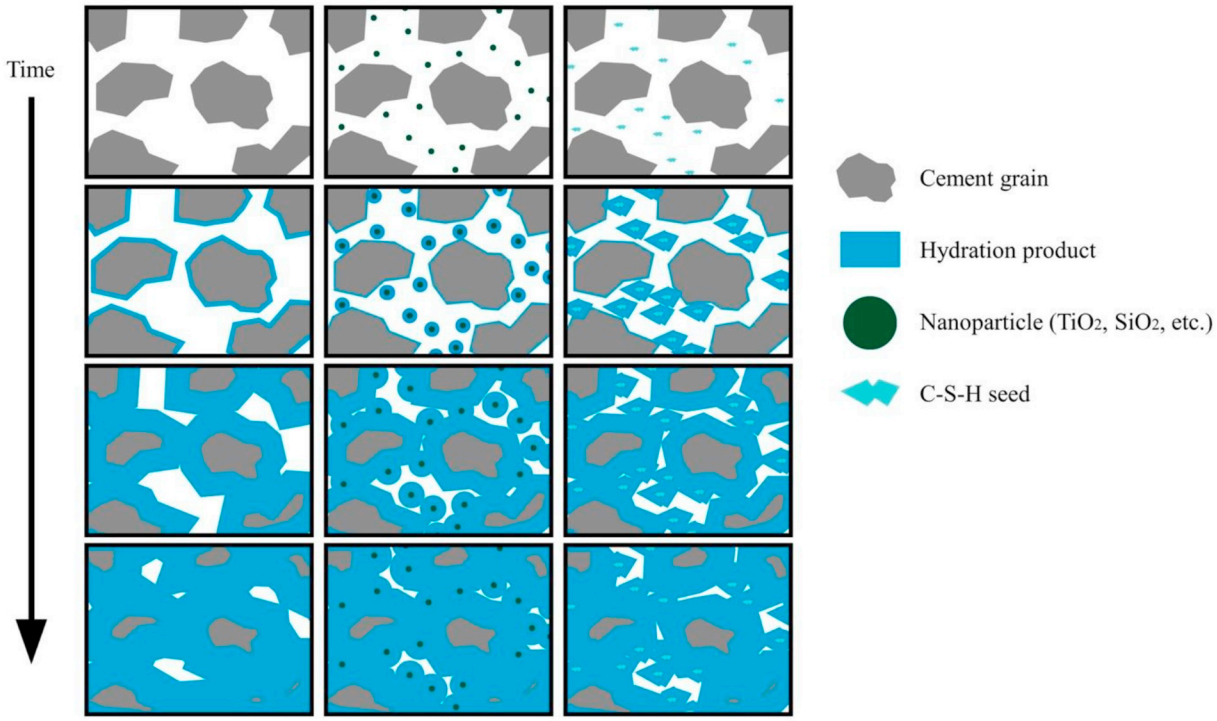

Fig. 20. Schematic diagrams of cement hydration and the influences of C-S-H seed and other nanoparticles. The acceleration effect of C-S-H seed on cement hydration is the strongest at an early age [220]. The long-term influence of C-S-H seed on hydration is still under debate.

found comparable strengths between seeded and unseeded cement. The deviating behaviors might be explained by different rates in microstructure evolution of pastes from fresh state to 28d. However, further comparison and investigation are difficult due to the lack of detailed information of the seeds. Schematic diagrams of cement hydration and the influences of C-S-H seed and other nanoparticles are shown in Fig. 20. Kanchanason and Plank have demonstrated that C-S-H/PCE nanocomposites had no adverse effect on the microstructure development of PC blended with 30 wt% fly ash, and the strengths of seeded mortars are higher than unseeded references from 6 h to 28d [225]. Owens et al. [223] found that the acceleration effect of seeds in the presence of 30 wt% GGBFS was weaker than OPC hydration system up to 24 h, and the reduction in 28d strength compared to unseeded PC-GGBFS system was also observed. Controversial results have been reported regarding the effects of semicrystalline C-S-H seed on the nucleation of alkali-activated GGBFS. Hubler et al. showed that sodium silicate activated GGBFS with 1.33% C-S-H seed exhibited 10 MPa higher strength from 1d to 14d compared to unseeded activated GGBFS when the pastes were cured under sealed conditions [226]; whereas SEM results from Suraneni et al. suggested that the addition of C-S-H into 0.1 M KOH activated GGBFS inhibited the activation of GGBFS and the microstructure of seeded alkali-activated GGBFS is significantly looser than an unseeded reference at 2d [227].

Despite rarely mentioned in the existing literature, solutions of hydrated portland cement and crystalline C-S-H phases with nano-size can also be used as C-S-H seeds. Land and Stephan's calorimetry study compared the acceleration effects of crystalline C-S-H phases (xonotlite and tobermorite) on cement hydration (w/s = 0.5) during the first 36 h [222]. In both cases, enhanced heat flow from dormant period to deceleration period was pronounced when C-S-H seed additions exceeded 1 wt%, while the acceleration effect of cement hydration with xonotlite addition is more intense, which was explained by a larger surface area of xonotlite. Horgnies et al. [228] investigated the acceleration effects of afwillite nano seed in hydrated C_3S. In the absence of PCE, afwillite-seeded C_3S pastes with w/s = 0.35 exhibited looser microstructure in SEM images than unseeded C_3S at 7d and 28d, with 20% higher total porosity. It is still not entirely understood what the dominating factors are (surface area of seeds, type of C-S-H phases, or water-to-solid ratio of pastes) of the deviating results in the influences of crystalline C-S-H phases on nucleation seeding. The influences of other crystalline C-S-H phases (e.g., jennite, hillebrandite, and reinhardbraunsite) on nucleation seeding and microstructure evolution of cement or C_3S pastes have not been examined yet. Unfortunately, most crystalline C-S-H phases are rare minerals, manufacturing crystalline C-S-H for seeds is expected instead of directly mining these minerals. However, massive production of crystalline C-S-H phases mainly requires hydrothermal synthesis, which is relatively energy-intense and time-consuming. Moreover, the synthesis methods for some crystalline C-S-H phases (e.g., suolunite, chegemite, and aklimaite) remain uninvestigated.

4.1. Nano-reinforcement

Instead of “inert” nano-reinforcement, such as nanoclay and carbon nanotubes (CNTs), which has been extensively studied before 2015, the community recently exhibited an increasing interest in modifying the microstructure with the use of graphene oxide (GO). Unlike nanoparticles, the low aspect ratio of which makes them difficult to arrest microcracks, two-dimensional nano-reinforcement, such as GO nanoplatelet, exhibits superior capacity of controlling crack initiation and propagation. With proper dispersion using sonication and/or surfactant (e.g., PCE), the length and thickness of GO nanoplatelets used in cementitious materials are typically hundreds of nanometers to microns and several to tens of nanometers, respectively. Research progress in the microstructure of cement with co-addition of GO and PCE is not reviewed here since the results from different sources are inconsistent, and there is a lack of information regarding the type and number of functional groups on GO nanoplatelets and PCE.

Many experimental studies have suggested that the typical optimal dosage of well-dispersed GO in cementitious materials is 0.01–0.1 wt%, which is about 1–2 orders of magnitude lower than that of conventional nanoparticles. Interestingly, such low dosage allows tens of percentages of increase in flexural and compressive strengths of cementitious

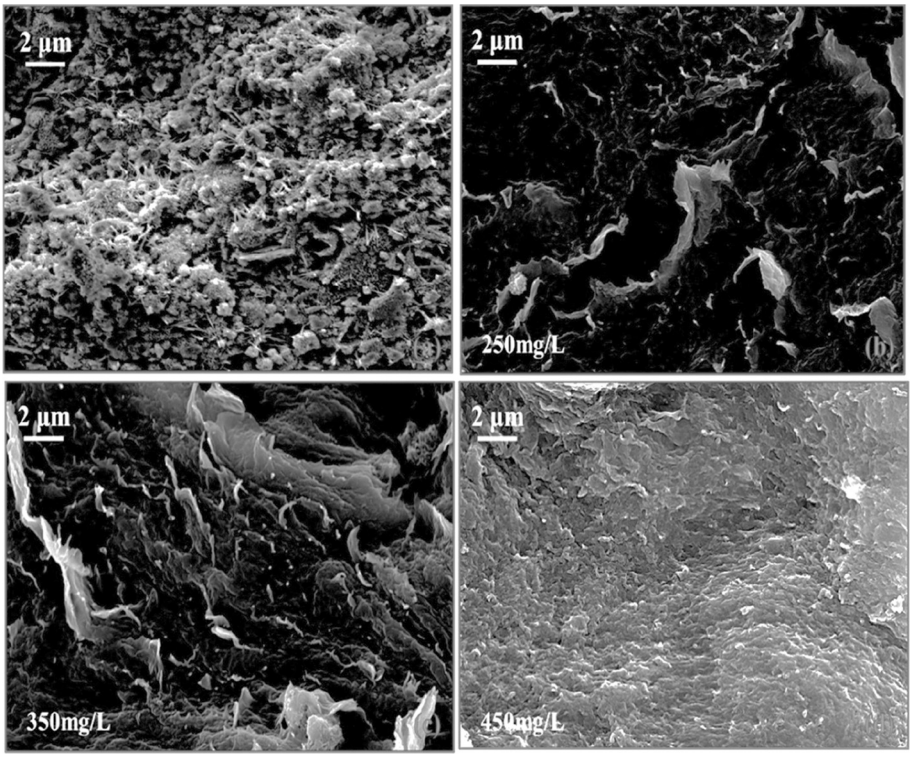

Fig. 21. SEM images of unreinforced cement and cement adsorption with GO nanoplatelets at different concentrations at 2 h (Wang et al., 2016).

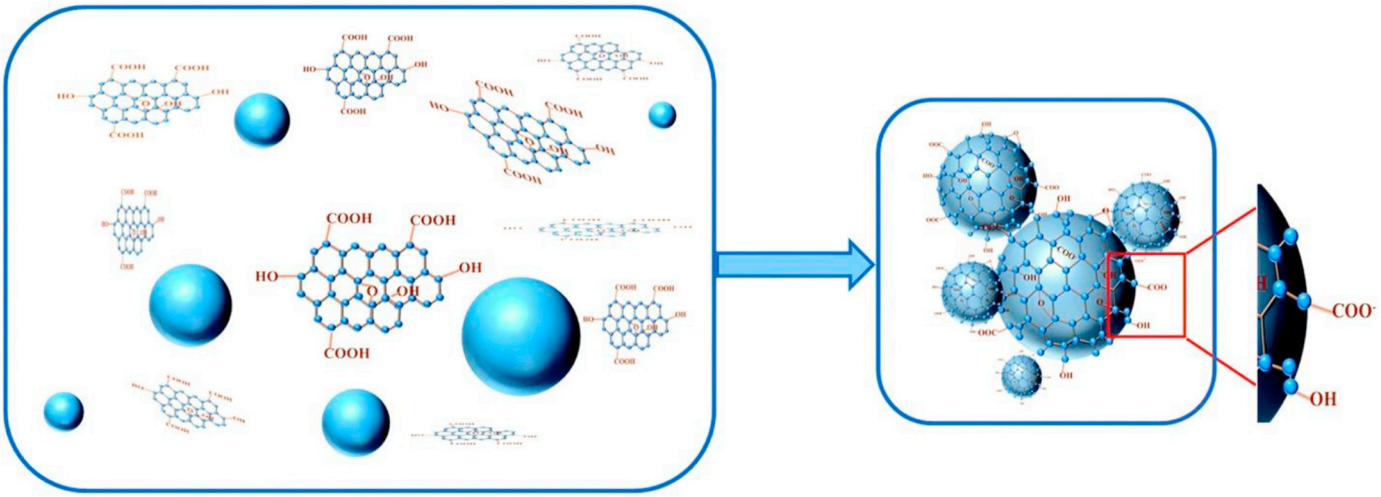

Fig. 22. Adsorption schematic of GO nanolayers on the cement surface. Left: before adsorption; right: after adsorption [233].

materials at all ages. The increased strengths with GO use have been explained by the accelerated early hydration, microstructure refinement of paste matrix, and crack-bridging of nano-reinforcement. Several studies have pointed out that the addition of GO slightly enhanced the heat flow during acceleration and deceleration periods of cement. The acceleration effects of GO on the reactivity of aluminate phases are stronger than silicate phases of cement in the first 24 h [229–232]. The acceleration of cement hydration was also demonstrated in an electrical resistivity study [229], where a dose of 0.01–0.06 wt% GO enhanced the resistivity during the initial 24 h. The authors proposed that the acceleration effect with GO use is either due to the nucleation seeding from GO, or the adsorption of cement grains to the functional groups of GO nanoplatelets and the further growth of hydration product from the adsorbed nanoplatelets. The latter hypothesis seems implausible since the size of GO nanoplatelets typically is much smaller than cement grains. The adsorption of GO on cement grains has been carefully studied using total organic carbon, XPS, FTIR, SEM [233]. The layer thickness of adsorbed GO on cement was measured to be ~10 nm, and SEM images (Fig. 21) showed the GO-covered cement surface at 2 h. The authors proposed that van der Waals force between GO layers shortened the distances among cement grains (Fig. 22), which can explain the generally observed loss of workability of fresh cementitious materials due to GO addition.

Note that the early acceleration effect of GO on C_3S was not observed in a calorimetry study. Moreover, retardation of GO on the hydration of clinker in the initial 30 h was reported, as the cumulative heat of clinker was higher than GO-modified clinker. The authors proposed that the retardation was due to the interaction of GO with the hydrous surface of clinker grains, which hindered the nucleation of hydration product [234]. However, no experimental evidence has been

provided to validate this hypothesis, and the acceleration of clinker hydration by GO after 30 h has not been not clearly explained. An XPS study proposed that, instead of portlandite precipitation, the consumption of Ca^{2+} in pore solution by –COOH of GO generates Ca $(HCOO)_2$ complexes, which accelerate the cement hydration [235]. However, a reduction in the quantity of portlandite has not been observed in many publications.

A MIP work presented a reduction in the amount of capillary pore of mortars in the presence of GO (0.01–0.06 wt%) at 28d, but with an increased total porosity by 0.5–2%. A clear trend of pore structure as a function of GO dosage in the mortars was not shown. On the contrary, another MIP study of GO-reinforced paste reported a reduction in total porosity by 4% and a reduced critical pore size by 8 nm at 28d [236,237]. In addition, a recent MIP study recorded a relatively unchanged total porosity at around 20%, but also reported a slight reduced critical pore size by 1–2 nm [232]. The deviating results regarding total porosity of pastes and mortars might be related to the agglomeration of GO in pore solution, which is often observed with an overdose of nanoparticles. By coupling MIP and X-ray tomography, Long et al. found a reduced volume fraction of pores at 6–20 μm and 0.05–0.23 μm by 0.1 wt% addition of GO, which also supported the pore-refinement concept of GO use [238]. The pore-refinement concept was reinforced by studies using nitrogen isotherm adsorption. Compared to unreinforced paste, the surface area of paste reinforced by 0.05 wt% GO is increased by 2.5% at 28d, the author assigned the increase to a higher degree of cement hydration with GO use [239]. Reduced size of gel pore and increased amount of gel pore in GO-modified mortars were also observed in another nitrogen isotherm adsorption test [240]. Many SEM studies presented a greater number of nuclei on the surface of GO-modified cement at early ages and a denser microstructure with fewer and finer microcracks at 28d. Since a typical dosage of GO in cement is below 0.1 wt%, it is challenging to locate the GO nanoplatelets at late ages if GO has been well dispersed [229,231,232]. Several nanoindentation studies have reported a decreased volume fraction of pores and an increased volume fraction of high-density C-S-H with a negligible change in volume fraction of low-density C-S-H, suggesting a denser microstructure of pastes with the addition of GO [238,241]. AFM-nanoindentation studies provided similar results compared to conventional nanoindentation- Horszczaruk et al. found that the elastic modulus of paste with 3 wt% GO ranged from 5 to 20 GPa, while the elastic modulus of unreinforced paste was 1–10 GPa [242]. Tong et al. revealed that the area of C-S-H in mortars with 0.1 wt% GO at 28d was larger than that in an nonreinforced mortar, and no apparent interfacial zone was found between C-S-H and GO nanoplatelets [241]. The trend in enhanced elastic moduli of GO modified pastes measured by AFM and nanoindentation are in a good agreement with the elastic moduli obtained from bulk strength measurements. The phase assignment in AFM-nanoindentation studies has been supported by the modification of C-S-H nanostructure by functional groups of GO, as suggested by a computational study and XPS results by Hou et al. [235].

5. Cement matrix at the mesoscale: experimental evidence and model

5.1. Structure of C-S-H at the mesoscale

The structure of C-S-H at the mesoscale has been the subject of experimental studies, which interpret the mesotexture either in terms of the pore structure or its dual solid matrix. Aside from microscopic air pockets, the C-S-H gel created from the hydration of portland cement contains capillary ($d_p > 10\,nm$) and gel pores ($d_p < 10$ nm) [243]. The nanoscale porosity exhibits a bimodal size distribution in small-angle neutron scattering (SANS) measurements [244,245]. As for the solid constituents, independent experimental techniques point to the formation of two C-S-H morphologies during OPC hydration. Although qualitative, transmission electron microscopy (TEM) images indicate the presence of a fine-textured inner product along with a fibrillar/foil-like outer product [48,49]. From mechanistic point of view, statistical nanoindentation experiments identify two distinct C-S-H phases, low-density (LD) and high-density (HD), with identical composition but mechanically distinct signatures [27,246,247]. Similarly, time-resolved SANS [248] and nitrogen adsorption isotherms [249] separately capture the formation of two morphologies with different surface areas. The observed duality is routinely explained by the free volume theory, i.e. interparticle vs. intraparticle space available for C-S-H's nucleation and growth [250,251]. It is intriguing to note that a more detailed analysis of SANS [245], nanoindentation [252] and adsorption [253] experiments independently suggest a unique nanogranular origins for C-S-H's seemingly two different morphologies. In particular, SANS data are interpreted using a self-similar fractal structure as produced by the diffusion-controlled single-particle aggregation of polydisperse non-spherical C-S-H nanoparticles with the average size of 5 nm [245]. Similar conclusions on the particle size have been recently reported through peak broadening analysis of X-ray diffraction (XRD) data [254,255]. Despite these efforts, several questions regarding the nature of C-S-H gel at the mesoscales remain to be answered. For instance, the relations between the size/shape of C-S-H nanoparticles and their chemical compositions remain elusive [52]. The thermodynamics routes to modulate the mesoscale texture of C-S-H are still unclear, and the impact of such modifications on concrete's macroscopic properties remains yet to be studied. The mesoscale simulations intend to systematically address these questions by combining the notions of intermolecular and surface forces with coarse-grained colloidal soft matter simulation approaches, which are discussed in following sections.

5.2. Effective interactions between C-S-H layers

Effective interactions between precipitating C-S-H particles govern the textural attributes of the C-S-H gel as it controls the local packing density during the mesoscale agglomeration process. These effective interactions are conventionally studied within the framework of the so-called potential-of-mean-force (PMF). The PMF is a thermodynamic state function, Helmholtz free energy, between two interacting objects, colloidal particles or surfaces, at a specified thermodynamic state, i.e. pressure, temperature, ionic concentration, etc. PMFs have been the subject of intensive research in condense matter physics, physical chemistry, and colloidal science in the past century and have shaped the notion of cohesion and setting in the cement and concrete community in modern times. Within the realm of intermolecular and surface forces, PMFs can be studied using theoretical, simulation and experimental approaches. In what follows, we will discuss these techniques in terms of the chemo-physical insight they provide to understand the effective interactions between C-S-H layers, their foundational assumptions, limitations and difficulties in utilizing these techniques to measure these thermodynamic state functions as well as possible future research opportunities.

From the theoretical perspective, PMFs have been studied within the context of mean-field theories [256–260]. Charged colloids in electrolytes, e.g. C-S-H layers formed in the compositionally time-varying electrolyte created in the clinker dissolution process, are subjected to a complex combination of repulsive, attractive and oscillatory forces. Based on the solution of the Poisson–Boltzmann (PB) equation, the electric double layer theory of Gouy and Chapman, describes the formation of electric double layer when two homogenously charged surfaces are submerged in an electrolyte solution [256]. Within this framework, one finds that the electrostatic pressure P, i.e. the derivative of the PMF with respect to the interparticle distance (D) divided by the surface, between two charged surfaces is given by $P(D) = k_B T[C_{ion}(D/2) - C(\infty)]$, where k_B, T, and $C_{ion}(D/2)$ are respectively the Boltzmann constant, temperature and cation concentration at the mid-separation. It appears that the pressure depends only on the midplane ionic

concentration, and, therefore, the double layer force is entropic in nature. Following the work of Gouy and Chapman, the Derjaguin-Landau-Verwey-Overbeek (DLVO) theory was established to address the cohesion and stability of charged layers separated by an electrolyte solution [261,262]. In DLVO theory, the overall interaction between charged colloids is decomposed into the double-layer repulsive and van der Waals attractive forces. This theory is designed for point charges, it is, therefore, a mean-field approach that ignores correlations in ionic fluctuations due to thermal agitations. Furthermore, it assumes that thermodynamic properties of electrolyte solutions around particles are akin to those of bulk, and the ion distribution in the slit pore follow the Maxwell-Boltzmann distribution. These constraints limit the application of DLVO theory to large separation distances (much greater than the size of a water molecule or cations), dilute electrolyte systems and surfaces with low surface charge densities. The actual charge of C-S-H layers depend strongly on the calcium-to-silicon ratio (C/S), the pH level of the solution as well as the ionic strength, and varies between 2.8 and 5.5 ($\bar{e}$/nm^2) depending on these conditions [263–266]. C-S-H's high surface charge induces cation condensation, which deviates the charge distribution from Maxwell-Boltzmann distribution. This condition is enough to undermine the application of DLVO theory to investigate the cohesion and surface forces in the cement paste.

To provide a more effective tool to study highly charged colloids, physicists have developed the so-called primitive model in the 80s [267,268]. In this approach, the charged layers and the solvated cations are represented respectively by uniformly charged infinite surfaces and point charges, while the solvent is implicitly described via the dielectric continuum approach. Within framework of primitive models, Kjellander et al. [267,269] and Valleau et al. [270] demonstrated that a system of charged plates and counter-ions can generate strong attractive electrostatic interactions. They argued that ion-ion correlated density fluctuations give rise to an attractive force, known as ionic correlation forces (ICFs), that are akin to correlations between instantaneous electronic dipoles in London dispersion forces. Subsequently, Pellenq and coworkers [271,272] studied the phase diagram of the attracto-replusive forces as function of the surface charge and interlayer distance. They showed the competition between ICFs, entropic and contact repulsive forces. At low surface charges and small separation distances, the entropic repulsive forces dominate leading to interlayer swelling and low cohesion as observed in sodium Montmorillonite clay systems. However, at high surface charges, counterions condensate on the charged surface entailing the reduction of entropic forces and ICFs dominance that result in strong cohesion and setting in cementitious materials. Focusing on the cement chemistry, Jönnson et al. [273,274] demonstrated that the electrostatic forces are sufficient to explain the charge inversion (reversal) phenomenon occurring in C-S-H at pH∼11.7, while varying $Ca(OH)_2$ concentration in the solution. As suggested by the change in the sign of the zeta potential in electrophoresis experiments [265,275], the apparent charge of C-S-H layers, i.e. the total charge of the C-S-H layer and adsorbed cations, switches from negative to positive values by increasing the solution pH or equivalently the surface charge. The charge overcompensation at high surface charges causes swelling of the overcrowded interlayer spacing by surpassing ICFs. Unequivocally, these primitive model studies confirm that the cohesion in cementitious materials is higher in the case of multivalent ions, which explain the high fluidity of alkali sulfate cement systems [272,273,276].

Primitive Models have obviously their own limitations. The surfaces of the slit pore are assumed to be fee of structural asperities [277] with uniform charge distributions, ions are considered to be fully hydrated and mobile and more importantly the solvent is considered to follow the dielectric continuum description, the dielectric constant of which is that of bulk water. These assumptions make the Primitive Model questionable, in particular at small interlayer separations in the order of a few nanometers. Full atomistic simulations have shown that the dielectric constant of the confined water between C-S-H layer at different C/S ratios diverge exponentially from that of bulk [263]. The dielectric constant converged to bulk values at a characteristic length scale of 5 nm. These results are in line with observation of interfacial liquid ordering at hydrophilic surfaces [278–280] that are at the origins of oscillatory solvation forces [279,281]. To address the discrepancy in dielectric constant, Carrier [282] developed an explicit solvent primitive model with point dipoles representing water molecules. The model was subsequently used to explore the role of cation valency in the swelling of Montmorillonites. These models are currently undergoing further refinement to investigate surface forces in cementitious materials. An accurate alternative approach to calculate PMFs is the full atomistic simulation. These simulations employ perturbative statistical physics-based approaches, known as free energy perturbation (FEP), to precisely measure incremental changes in the free energy profile along a prespecified reaction coordinate, e.g. the distance between C-S-H layers. While umbrella sampling technique [283] measures free energy difference by applying a bias potential, usually a harmonic potential, between two adjacent states, the weighted histogram analysis method [284] streamlines free energy calculations along a series of consecutive steps. Metadynamics [285,286] approach, on the other hand, measures the free energy by imposing gaussian bias functions along collective variables. Unlike previous approaches, simple overlap sampling [287] method does not require a bias potential and measures the free energy difference using a large number of half state perturbations. Regardless of the selected method, the free energy approaches are computationally expensive as they need long molecular dynamics (MD) trajectories or large number of Monte Carlo (MC) steps to properly sample the overlapping of energy levels between neighboring states.

A number of full atomistic works have already used FEP approaches to study for the interlamellar swelling of smectite clays [289] or cohesion between C-S-H layers [263,277,281,290]. Using grand canonical Monte Carlo (GCMC) approach, Bonnaud et al. [290] calculated the grand interaction potential between C-S-H layers at C/S = 1.7 and demonstrated the short-range attraction followed by a repulsive shoulder at 10% relative humidity and room temperature. Later, Masoumi et al. [281] calculated the PMF between Tobermorite layers at the ambient conditions and 100% saturation and observed a single attractive well with no entropic repulsive shoulder. Furthermore, they observed that the surface forces between Tobermorite layers exhibits an oscillatory force that originates from entropic solvation forces arising from ordering of water layers on the surface, see Fig. 23. More recently, Masoumi et al. [263] have systematically investigated the change in PMF between C-S-H layers as a function of stoichiometry, demonstrating a transition from single well to multiple well PMF by increasing C/S ratio. They argue that the surface charge of C-S-H layers decreases with increasing C/S ratio, leading to an increase in entropic repulsive forces and emergence of the repulsive shoulder. These simulations portray a unique picture of the total interaction between C-S-H layers, A_{CSH}, that can be decomposed in to the following contributions:

$$A_{CSH} = A_{contact} + A_{attractive} + A_{double\ layer} + A_{solvation} \quad (1)$$

where $A_{contact}$, $A_{attractive}$, $A_{double\ layer}$ and $A_{solvation}$ are respectively short range repulsive contact interactions, combined attractive interactions originating from van der Walls and ionic correlation forces, entropic repulsive double layer contributions and oscillatory solvation interactions. A detailed discussion on the form and coefficients of each of these terms as function of C/S ratio can be found in Masoumi's work [263]. We note that the full atomistic simulations are always subjected to the uncertainties arising from the transferability of interatomic force fields. The interested readers are referred to a recent review paper by Mishra et al. [291] for discussions about transferability of different force field to cementitious materials. Furthermore, the structure of C-S-H, especially at high C/S ratios, still remains the subject of intensive research [24,29,30,292–294]. Investigating the impact of uncertainties arising from the choice of the force field and molecular structures remain the subject of future research.

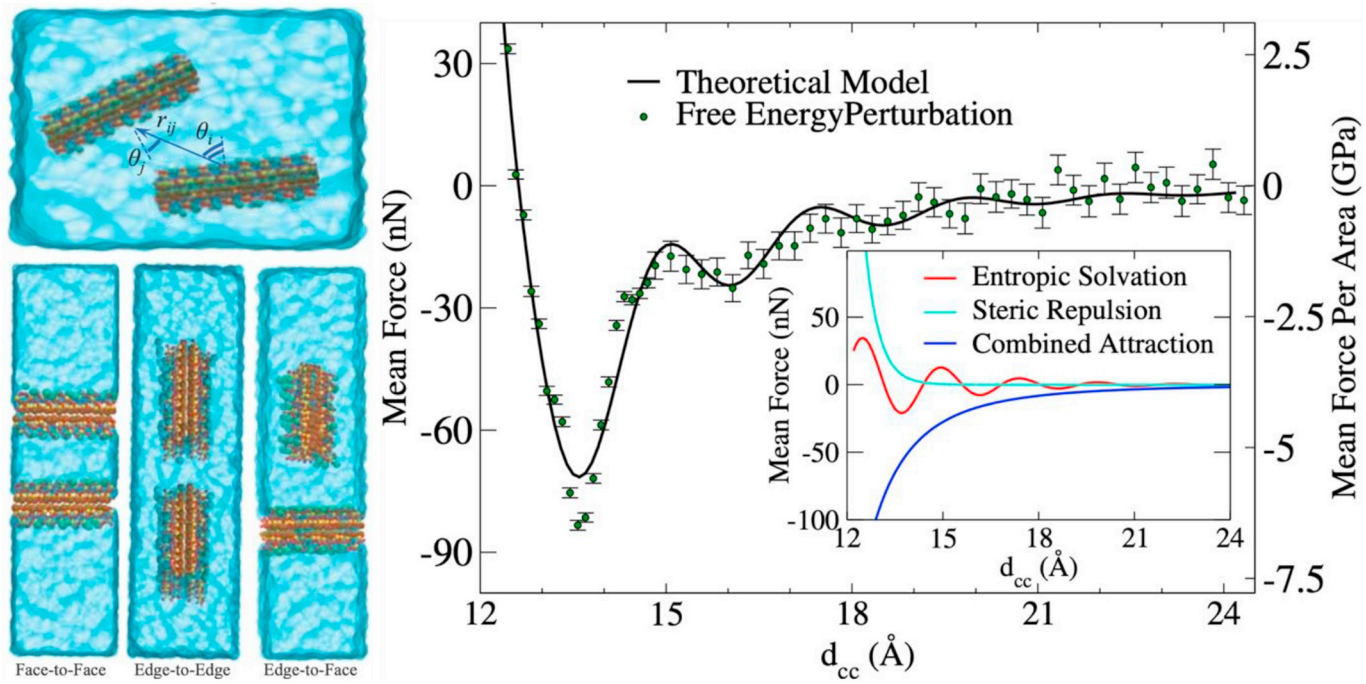

Fig. 23. Construction of the potential-of-mean-force between C-S-H layers via the full atomistic simulations. In this approach, the interaction in a general configuration between two finite-sized layers in an electrolyte solution, as depicted on the top left, is approximately realized by interactions in face-to-face, edge-to-edge and edge-to-face interactions. The graph on the right, shows the interaction free energy in face-to-face direction between two tobermorite layers, see Masoumi et al. [288] for details.

From an experimental point of view, the ideal setup to measure surface forces is the surface force apparatus (SFA). Developed by Winterton in 1960s, the instrument measures the surface force between two cylindrical objects in crossed geometry [295]. Later, Israelachvili and co-workers extended the original design to operate in liquid and electrolyte medium that enabled the measurement of solvation and double layer forces [296,297]. The technique requires the two mica cylinders to be uniformly coated by the material of interest, making applications to cementitious materials rather complicated. Recognizing this difficulty, Lesko et al. [298] explored the possibility of using atomic force microscope (AFM) to measure forces between a flat C-S-H surface and a C-S-H covered AFM cantilever tip. Later, Plassaerd et al. [299] refined the experiments and investigated the impact of solution parameters on C-S-H surface forces and confirmed that the calcium counterion concentration controls the attraction to repulsion ratio. They showed a transition from purely repulsive to purely attractive forces with increasing pH in the solution. More notably, they showed that C-S-H exhibits a repulsive shoulder and an attractive well at pH = 11.7, the charge reversal pH level [265,275]. Although they do not offer the full picture of surface forces, electrophoresis experiments provide a direct measurement of the electrokinetic potential at the slipping plane in the double layer. The zeta potential is found to be a key factor in superplasticizer adsorption on the surface of hydration products [300,301], adsorption of chloride ion on the surface of C-S-H [302], and understanding the mechanisms of hydration inhibition in tricalcium aluminate [303].

5.3. Composition-texture-property relations

As discussed in the previous section, the PMF is the key information piece allowing to coarse-grain physical chemistry information within a mesoscale model formulation. These interactions can serve as a thermodynamically consistent link between the molecular scale and the scale of colloidal C-S-H particles, see Fig. 24. Having such interactions at hand, one can use quite a few approaches to construct realistic mesostructure of nanogranular materials, namely grand canonical Monte Carlo (GCMC) [304], hybrid reverse Monte Carlo [305,306] and advanced molecular dynamics packing schemes such as incremental stress marching approach [307] as well as a wide-range of learning-based methods [308,309]. Masoero et al. [310] used the GCMC approach to simulate the mesotexture of C-S-H gel as an agglomeration of coarse-grained poly-disperse spherical particles. The mechanical stiffness in their models were similar to those measured in nanoindentation experiments. Later on, Ioannidou et al. [311] refined this model and demonstrated its capability in reproducing a wide range of available experimental data including nanoindentation, SANS, pore size, packing fraction and chord length distributions. In both studies, the authors intended to study the hardened cement paste and therefore they neglected entropic double layer and hydration forces. To this end, they used a simplified Lennard-Jones potential, whose parameters were calibrated using the notion of Hertz contact and nanoindentation data [310,311]. Otherwise stated, experimental measurements serve as the connecting link between the nanoscale chemical composition and mesotextural attributes. Furthermore, the coarse-graining of intraglobular features limits their application to study physical phenomena that involves disjoining, sliding and agglomeration of individual C-S-H layers. These issues necessitate the development of mesoscale models with intermediate resolutions that can seamlessly connect the scale of molecular chemistry to mesoscale morphology. To this end, more recently, Masoumi et al. calculated the PMF between C-S-H layers in full atomistic simulations and applied these interactions between coarse-grained descriptions of ellipsoidal C-S-H layers using Ga-Berne potential [277,312]. They showed that such description of interatomic interactions reproduces the indentation modulus as a function of the C-S-H layers' packing fraction. This confirms that the shape of C-S-H globules does not matter in determining the homogenized elastic response of the C-S-H at the microscale [313]. However, the shape of C-S-H globules might be important in controlling the strength and fracture properties. Furthermore, they showed that C-S-H layers form nanoscale clusters whose average size is roughly 5 nm in close agreement with SANS measurements. The rigidity threshold packing density in these cohesive models were shown to be significantly lower than those of hard contact

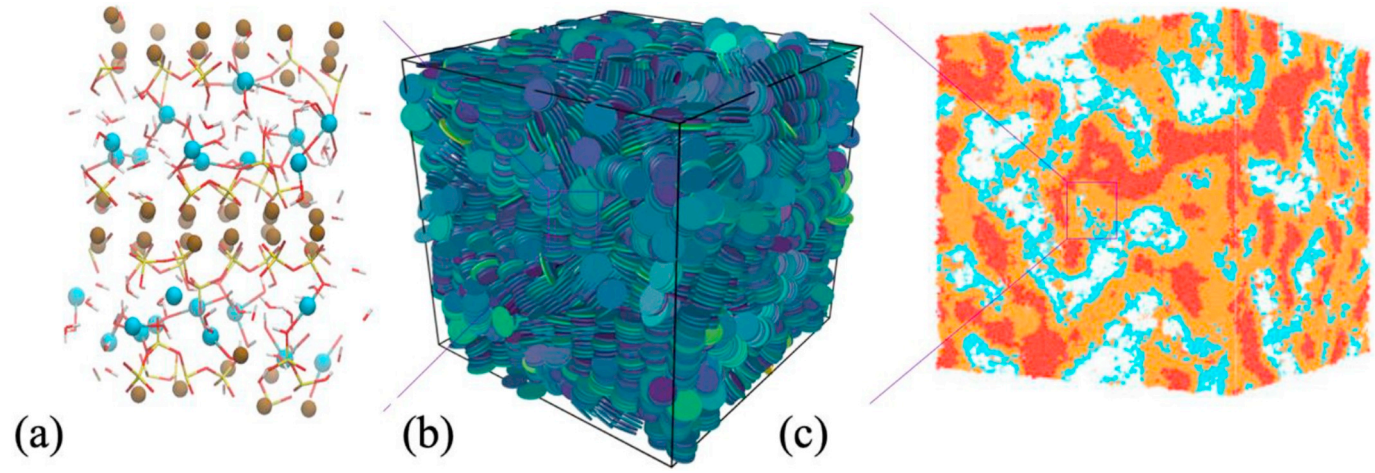

Fig. 24. A systematic hierarchical modeling of C-S-H gel across scales. a) full atomistic simulations of C-S-H structure. See references [24, 29, 30, 292–294] for more details. The simulation domains are typically only a few nanometers long. b) Mesoscale structures of C-S-H gel with coarse-grained oblate C-S-H models. The interaction between C-S-H platelets are calculated via the PMF approach. The layers form stacks of C-S-H layers with characteristic length scale of about 5 nm [318]. The length of the simulation domains is usually in the order of 50–100 nm. C) The coarse-grained structure of C-S-H gel with capillary and gel pores. The simulation domains are in the order of 500 nm [311].

oblate descriptions [313–316], and rather close to the case of overlapping ellipsoids of Garboczi and coworkers [317].

Combining MC and MD approaches with more realistic PMFs that include Yukawa-type double layer interactions in addition to the Lennard-Jones terms, Ioannidou et al. [319,320] investigated cement precipitation and settings at the mesoscale. Their study investigates C-S-H gels under out-of-equilibrium conditions. They observed hydrate precipitation curves akin to those experimentally observed in the acceleration and deceleration regimes and predicted the heat of hydration curve without pre-assumed kinetic models that always contain ill-defined and/or un-measurable parameters [321]. Later, Shvab et al. proposed an off-lattice kinetic Monte Carlo (KMC) framework to study the precipitation of mesoporous C-S-H gel upon aggregation of coarse-grained C-S-H nanoparticles [322]. The rate expressions for nanoparticle precipitation/dissolution in their KMC approach accounted for both the solution chemistry and mechanical interactions. They demonstrated how particle–particle and particle–substrate interactions determine various mechanisms such as layer-by-layer precipitation, islands formation, Cahn and Avrami nucleation and growth, and gel-like precipitation. To study the impact of superplasticizers of the hydration products, Turesson and coworkers developed a coarse-grained mesoscale model of C-S-H layers and coupled it with the coarse-grained description of either comb copolymers composed of anionic backbones with attached neutral side chains or anionic-neutral linear block copolymers [323]. In agreement with experimental studies, they showed that unlike comb copolymers which only adsorb on the external surfaces of C-S-H globules, block copolymers are found to intercalate between the platelets.

6. Concluding remarks

Understanding and modeling the microstructure of concrete remain critical for the development of advanced concrete science and technology. The present work reviews existing microscale experimental probes for the characterization of hydrated cementitious materials, giving emphasis to emerging methods and their pioneering applications. Aside from the improvement of the well-established methods, e.g. SEM/TEM, micro-CT and (in-situ) XRD, significant progress in this area has been achieved with high-resolution X-ray microscopy, particularly when coupled with ptychography imaging. This technique has the added benefit that it is possible to obtained valuable X-ray scattering information which can also be integrated with X-ray spectroscopy and provide unique integration of high-resolution imaging with chemical information. ^{1}H NMR has given new insights in the characterization of the hierarchical porous structure in the cementitious matrix, and it has been well-tuned for routinely lab-use. DHM is another technique that has provided nanoscale vision of surface dissolution process. In terms of new microstructural insights gained after the last International Congress on the Chemistry of Cement (ICCC) in 2015, the experimental observation that C-A-S-H can develop preferred orientation even under small deviatoric stresses is significant because it can provide fresh perspectives for creep and shrinkage of cementitious systems.

The use of ideal systems or model cements to study the behavior of chemical admixtures allows the identification of the origin of incompatibilities and the understanding of the mechanism at the molecular scale. Determination of the admixture behavior based on its molecular structures in such simplified systems is the first critical step to control the properties and side effects existing in current admixtures and to develop new types of molecules. Note that progress in machine learning has the potential to facilitate design in more complex systems [324]. The next step is to apply this knowledge in practice, which nowadays faces more challenging conditions due to the increase in complexity of the concrete mixture proportions, the use of alternative binders, and the combination of various admixtures. This fundamental approach will allow improvements not only in production rates, mechanical properties, durability but, equally importantly, also in sustainability.

Advances in the understanding the microstructure of concrete should be integrated with atomistic and mesoscale modeling to create a realistic and practical concrete nanoengineering, capable of developing predictive models and of creating new materials based on fundamental foundations. The challenge is great because it is necessary to provide solid relationships between the chemical composition and textural attributes of cement hydrates at the mesoscale and create efficient mesoscale simulations. Great progress has been achieved with use of potential-of-mean-force to simulate the effective interactions between precipitating C-S-H particles, an important step to fully grasp the mechanism of local packing density during the mesoscale agglomeration process.

Acknowledgments

Paulo J.M. Monteiro acknowledges the financial support given by the National Research Foundation-Prime Minister's office, Republic of

Singapore through a grant to the Berkeley Education Alliance for Research in Singapore (BEARS) for the Singapore-Berkeley Building Efficiency and Sustainability in the Tropics (SinBerBEST) Program. G. Geng acknowledges the European Union's Horizon 2020 research and innovation programme under the Marie Skłodowska-Curie grant agreement number 701647 and also the insightful discussion with Barbara Lothenbach and Jeffrey Bullard. Financial support for Delphine Marchon was provided by the Swiss National Science Foundation (Early Postdoc.Mobility grant no. P2EZP2-172177). MJAQ acknowledges the financial support by the National Science Foundation under Award No. CMMI-1826122 is awarded in United States. Wenxin Zhang is thanked for the design and drawing of Fig. 20. Kurtis and Alapati acknowledge support by the Federal Highway Administration (FHWA) through an Exploratory Advanced Research Project (Project ID FHWA-PROJ-14-0134). Any opinions, findings, and conclusions expressed in this document are those of the authors and do not necessarily reflect those of the sponsors.

References

[1] K.L. Scrivener, R.J. Kirkpatrick, Innovation in use and research on cementitious material, Cem. Concr. Res. 38 (2008) 128–136, https://doi.org/10.1016/j.cemconres.2007.09.025.
[2] F. Sanchez, K. Sobolev, Nanotechnology in concrete - a review, Constr. Build. Mater. 24 (2010) 2060–2071, https://doi.org/10.1016/j.conbuildmat.2010.03.014.
[3] J. Stark, Recent advances in the field of cement hydration and microstructure analysis, Cem. Concr. Res. 41 (2011) 666–678, https://doi.org/10.1016/j.cemconres.2011.03.028.
[4] K.L. Scrivener, A. Nonat, Hydration of cementitious materials, present and future, Cem. Concr. Res. 41 (2011) 651–665, https://doi.org/10.1016/j.cemconres.2011.03.026.
[5] K.L. Scrivener, P. Juilland, P.J.M. Monteiro, Advances in understanding hydration of Portland cement, Cem. Concr. Res. 78 (Part A) (2015) 38–56, https://doi.org/10.1016/j.cemconres.2015.05.025.
[6] K.L. Scrivener, R. Snellings, B. Lothenbach, A Practical Guide to Microstructural Analysis of Cementitious Materials, CRC Press, Taylor & Francis Group, 2016.
[7] K.K. Aligizaki, Pore Structure of Cement-Based Materials: Testing, Interpretation and Requirements, CRC Press, 2005, https://doi.org/10.1201/9781482271959.
[8] J. Cheung, A. Jeknavorian, L. Roberts, D. Silva, Impact of admixtures on the hydration kinetics of Portland cement, Cem. Concr. Res. 41 (2011) 1289–1309, https://doi.org/10.1016/j.cemconres.2011.03.005.
[9] S. Mann, G.A. Ozin, Synthesis of inorganic materials with complex form, Nature 382 (1996) 313–318.
[10] S.R. Qiu, A. Wierzbicki, C.A. Orme, A.M. Cody, J.R. Hoyer, G.H. Nancollas, S. Zepeda, J.J.D. Yoreo, Molecular modulation of calcium oxalate crystallization by osteopontin and citrate, PNAS 101 (2004) 1811–1815, https://doi.org/10.1073/pnas.0307900100.
[11] J.D. Rimer, Z. An, Z. Zhu, M.H. Lee, D.S. Goldfarb, J.A. Wesson, M.D. Ward, Crystal growth inhibitors for the prevention of l-Cystine kidney stones through molecular design, Science 330 (2010) 337–341, https://doi.org/10.1126/science.1191968.
[12] E. Berodier, L.R. Gibson, E. Burns, L. Roberts, J. Cheung, Robust production of sustainable concrete through the use of admixtures and in-transit concrete management systems, Cem. Concr. Compos. (2018), https://doi.org/10.1016/j.cemconcomp.2018.01.008.
[13] J.L. Provis, Alkali-activated materials, Cem. Concr. Res. 114 (2018) 40–48, https://doi.org/10.1016/j.cemconres.2017.02.009.
[14] K.L. Scrivener, V.M. John, E.M. Gartner, Eco-Efficient Cements: Potential, Economically Viable Solutions for a Low-CO2, Cement-based Materials Industry, UNEP, 2016.
[15] D. Marchon, U. Sulser, A. Eberhardt, R.J. Flatt, Molecular design of comb-shaped polycarboxylate dispersants for environmentally friendly concrete, Soft Matter 9 (2013) 10719–10728, https://doi.org/10.1039/C3SM51030A.
[16] R.J. Flatt, N. Roussel, C.R. Cheeseman, Concrete: An eco material that needs to be improved, J. Eur. Ceram. Soc. 32 (2012) 2787–2798, https://doi.org/10.1016/j.jeurceramsoc.2011.11.012.
[17] T. Wangler, E. Lloret, L. Reiter, N. Hack, F. Gramazio, M. Kohler, M. Bernhard, B. Dillenburger, J. Buchli, N. Roussel, R. Flatt, Digital concrete: opportunities and challenges, RILEM Technical Letters 1 (2016) 67–75, https://doi.org/10.21809/rilemtechlett.2016.16.
[18] L. Reiter, T. Wangler, N. Roussel, R.J. Flatt, The role of early age structural build-up in digital fabrication with concrete, Cem. Concr. Res. 112 (2018) 86–95, https://doi.org/10.1016/j.cemconres.2018.05.011.
[19] D. Marchon, S. Kawashima, H. Bessaies-Bey, S. Mantellato, S. Ng, Hydration and rheology control of concrete for digital fabrication: potential admixtures and cement chemistry, Cem. Concr. Res. 112 (2018) 96–110, https://doi.org/10.1016/j.cemconres.2018.05.014.
[20] J.J. Biernacki, J.W. Bullard, G. Sant, K. Brown, F.P. Glasser, S. Jones, T. Ley, R. Livingston, L. Nicoleau, J. Olek, F. Sanchez, R. Shahsavari, P.E. Stutzman, K. Sobolev, T. Prater, Cements in the 21st century: challenges, perspectives, and opportunities, J. Am. Ceram. Soc. 100 (2017) 2746–2773, https://doi.org/10.1111/jace.14948.
[21] ACI 241R-17, Report on Application of Nanotechnology and Nanomaterials in Concrete, (2017).
[22] V.C. Li, From micromechanics to structural engineering-the design of cementitious composites for civil engineering applications, J. Struct. Mech. Earthq. Eng. 10 (1993) 37–48.
[23] M. Li, V.C. Li, Rheology, fiber dispersion, and robust properties of engineered cementitious composites, Mater. Struct. 46 (2013) 405–420, https://doi.org/10.1617/s11527-012-9909-z.
[24] R.J.-M. Pellenq, A. Kushima, R. Shahsavari, K.J.V. Vliet, M.J. Buehler, S. Yip, F.-J. Ulm, A realistic molecular model of cement hydrates, Proc. Natl. Acad. Sci. 106 (2009) 16102–16107, https://doi.org/10.1073/pnas.0902180106.
[25] R. Alizadeh, L. Raki, J.M. Makar, J.J. Beaudoin, I. Moudrakovski, Hydration of tricalcium silicate in the presence of synthetic calcium–silicate–hydrate, J. Mater. Chem. 19 (2009) 7937, https://doi.org/10.1039/b910216g.
[26] A. Nonat, The structure and stoichiometry of C-S-H, Cem. Concr. Res. 34 (2004) 1521–1528, https://doi.org/10.1016/j.cemconres.2004.04.035.
[27] G. Constantinides, F.-J. Ulm, The nanogranular nature of C–S–H, Journal of the Mechanics and Physics of Solids 55 (2007) 64–90, https://doi.org/10.1016/j.jmps.2006.06.003.
[28] L.B. Skinner, S.R. Chae, C.J. Benmore, H.R. Wenk, P.J.M. Monteiro, Nanostructure of calcium silicate hydrates in cements, Phys. Rev. Lett. 104 (2010) 195502, , https://doi.org/10.1103/PhysRevLett.104.195502.
[29] M.J. Abdolhosseini Qomi, K.J. Krakowiak, M. Bauchy, K.L. Stewart, R. Shahsavari, D. Jagannathan, D.B. Brommer, A. Baronnet, M.J. Buehler, S. Yip, F.-J. Ulm, K.J. Van Vliet, R.J.-M. Pellenq, Combinatorial molecular optimization of cement hydrates, Nat. Commun. 5 (2014) 4960, https://doi.org/10.1038/ncomms5960 http://www.nature.com/ncomms/2014/140924/ncomms5960/full/ncomms5960.html (accessed September 24, 2014).
[30] G. Geng, R.J. Myers, M.J.A. Qomi, P.J.M. Monteiro, Densification of the interlayer spacing governs the nanomechanical properties of calcium-silicate-hydrate, Sci. Rep. 7 (2017) 10986, , https://doi.org/10.1038/s41598-017-11146-8.
[31] M. Bauchy, M.J. Abdolhosseini Qomi, C. Bichara, F.-J. Ulm, R.J.-M. Pellenq, Nanoscale structure of cement: viewpoint of rigidity theory, J. Phys. Chem. C 118 (2014) 12485–12493, https://doi.org/10.1021/jp502550z.
[32] M. Bauchy, M.J.A. Qomi, C. Bichara, F.-J. Ulm, R.J.-M. Pellenq, Rigidity transition in materials: hardness is driven by weak atomic constraints, Phys. Rev. Lett. 114 (2015) 125502, , https://doi.org/10.1103/PhysRevLett.114.125502.
[33] S.R. Chae, J. Moon, S. Yoon, S. Bae, P. Levitz, R. Winarski, P.J.M. Monteiro, Advanced nanoscale characterization of cement based materials using X-ray synchrotron radiation: a review, Int J Concr Struct Mater 7 (2013) 95–110, https://doi.org/10.1007/s40069-013-0036-1.
[34] S. Brisard, P. Levitz, Small-angle scattering of dense, polydisperse granular porous media: computation free of size effects, Phys. Rev. E 87 (2013) 013305, , https://doi.org/10.1103/PhysRevE.87.013305.
[35] A. Bazzoni, M. Suhua, Q. Wang, X. Shen, M. Cantoni, K.L. Scrivener, The effect of magnesium and zinc ions on the hydration kinetics of C3S, J. Am. Ceram. Soc. 97 (2014) 3684–3693, https://doi.org/10.1111/jace.13156.
[36] F. Bellmann, G.W. Scherer, Analysis of C-S-H growth rates in supersaturated conditions, Cem. Concr. Res. 103 (2018) 236–244, https://doi.org/10.1016/j.cemconres.2017.05.007.
[37] G.W. Scherer, F. Bellmann, Kinetic analysis of C-S-H growth on calcite, Cem. Concr. Res. 103 (2018) 226–235, https://doi.org/10.1016/j.cemconres.2016.07.017.
[38] K.L. Scrivener, Backscattered electron imaging of cementitious microstructures: understanding and quantification, Cem. Concr. Compos. 26 (2004) 935–945, https://doi.org/10.1016/j.cemconcomp.2004.02.029.
[39] V. Kocaba, E. Gallucci, K.L. Scrivener, Cement and concrete research methods for determination of degree of reaction of slag in blended cement pastes, Cem. Concr. Res. 42 (2012) 511–525, https://doi.org/10.1016/j.cemconres.2011.11.010.
[40] P.T. Durdziński, C.F. Dunant, M. Ben Haha, K.L. Scrivener, A new quantification method based on SEM-EDS to assess fly ash composition and study the reaction of its individual components in hydrating cement paste, Cem. Concr. Res. 73 (2015) 111–122, https://doi.org/10.1016/j.cemconres.2015.02.008.
[41] P.T. Durdziński, R. Snellings, C.F. Dunant, M.B. Haha, K.L. Scrivener, Fly ash as an assemblage of model Ca–Mg–Na-aluminosilicate glasses, Cem. Concr. Res. 78 (2015) 263–272, https://doi.org/10.1016/j.cemconres.2015.08.005.
[42] E. Berodier, K. Scrivener, Understanding the filler effect on the nucleation and growth of C-S-H, J. Am. Ceram. Soc. 97 (2014) 3764–3773, https://doi.org/10.1111/jace.13177.
[43] Z. Zhang, G.W. Scherer, A. Bauer, Morphology of cementitious material during early hydration, Cem. Concr. Res. 107 (2018) 85–100, https://doi.org/10.1016/j.cemconres.2018.02.004.
[44] S. Hemes, G. Desbois, J.L. Urai, B. Schröppel, J.-O. Schwarz, Multi-scale characterization of porosity in Boom Clay (HADES-level, Mol, Belgium) using a combination of X-ray μ-CT, 2D BIB-SEM and FIB-SEM tomography, Microporous Mesoporous Mater. 208 (2015) 1–20, https://doi.org/10.1016/j.micromeso.2015.01.022.
[45] Y. Song, C.A. Davy, D. Troadec, X. Bourbon, Pore network of cement hydrates in a high performance concrete by 3D FIB/SEM — implications for macroscopic fluid transport, Cem. Concr. Res. 115 (2019) 308–326, https://doi.org/10.1016/j.cemconres.2018.08.004.
[46] Z. Zhang, G.W. Scherer, Supercritical drying of cementitious materials, Cem. Concr. Res. 99 (2017) 137–154, https://doi.org/10.1016/j.cemconres.2017.05.

005.
[47] J.E. Rossen, K.L. Scrivener, Optimization of SEM-EDS to determine the C–A–S–H composition in matured cement paste samples, Mater. Charact. 123 (2017) 294–306, https://doi.org/10.1016/j.matchar.2016.11.041.
[48] I.G. Richardson, The nature of the hydration products in hardened cement pastes, Cem. Concr. Compos. 22 (2000) 97–113, https://doi.org/10.1016/S0958-9465(99)00036-0.
[49] I.G. Richardson, Tobermorite/jennite- and tobermorite/calcium hydroxide-based models for the structure of C-S-H: applicability to hardened pastes of tricalcium silicate, β-dicalcium silicate, Portland cement, and blends of Portland cement with blast-furnace slag, metakaolin, or silica fume, Cem. Concr. Res. 34 (2004) 1733–1777, https://doi.org/10.1016/j.cemconres.2004.05.034.
[50] I.G. Richardson, J. Skibsted, L. Black, R.J. Kirkpatrick, Characterisation of cement hydrate phases by TEM, NMR and Raman spectroscopy, Adv. Cem. Res. 22 (2010) 233–248, https://doi.org/10.1680/adcr.2010.22.4.233.
[51] A. Kumar, B.J. Walder, A. Kunhi Mohamed, A. Hofstetter, B. Srinivasan, A.J. Rossini, K. Scrivener, L. Emsley, P. Bowen, The atomic-level structure of cementitious calcium silicate hydrate, J. Phys. Chem. C 121 (2017) 17188–17196, https://doi.org/10.1021/acs.jpcc.7b02439.
[52] E.T. Rodriguez, I.G. Richardson, L. Black, E. Boehm-Courjault, A. Nonat, J. Skibsted, Composition, silicate anion structure and morphology of calcium silicate hydrates (C-S-H) synthesised by silica-lime reaction and by controlled hydration of tricalcium silicate (C3S), Adv. Appl. Ceram. 114 (2015) 362–371, https://doi.org/10.1179/1743676115Y.0000000038.
[53] A.V. Girão, I.G. Richardson, R. Taylor, R.M.D. Brydson, Cement and concrete research composition, morphology and nanostructure of C – S – H in 70% fl y ash blends hydrated at 55 °C, Cem. Concr. Res. 40 (2010) 1350–1359, https://doi.org/10.1016/j.cemconres.2010.03.012.
[54] A. Fernández-Jiménez, A. Palomo, M. Criado, Microstructure development of alkali-activated fly ash cement: a descriptive model, Cem. Concr. Res. 35 (2005) 1204–1209, https://doi.org/10.1016/j.cemconres.2004.08.021.
[55] I.G. Richardson, A.V. Girão, R. Taylor, S. Jia, Cement and concrete research hydration of water- and alkali-activated white Portland cement pastes and blends with low-calcium pulverized fuel ash, Cem. Concr. Res. 83 (2016) 1–18, https://doi.org/10.1016/j.cemconres.2016.01.008.
[56] S. Jia, I.G. Richardson, Cement and Concrete Research Micro- and nano-structural evolutions in white Portland cement/pulverized fuel ash cement pastes due to deionized-water leaching, Cem. Concr. Res. 103 (2018) 191–203, https://doi.org/10.1016/j.cemconres.2017.10.014.
[57] I.G. Richardson, S. Li, Composition and structure of an 18-year-old 5M KOH-activated ground granulated blast-furnace slag paste, 168 (2018) 404–411, https://doi.org/10.1016/j.conbuildmat.2018.02.034.
[58] R. Taylor, I.G. Richardson, R.M.D. Brydson, Composition and microstructure of 20-year-old ordinary Portland cement–ground granulated blast-furnace slag blends containing 0 to 100% slag, Cem. Concr. Res. > 40 (2010) 971–983, https://doi.org/10.1016/j.cemconres.2010.02.012.
[59] J.E. Rossen, B. Lothenbach, K.L. Scrivener, Cement and concrete research composition of C – S – H in pastes with increasing levels of silica fume addition, Cem. Concr. Res. 75 (2015) 14–22, https://doi.org/10.1016/j.cemconres.2015.04.016.
[60] A. Bazzoni, M. Cantoni, K.L. Scrivener, Impact of annealing on the early hydration of tricalcium silicate, J. Am. Ceram. Soc. 97 (2014) 584–591, https://doi.org/10.1111/jace.12691.
[61] R. Taylor, A. Sakdinawat, S.R. Chae, H.R. Wenk, P. Levitz, R. Sougrat, P.J.M. Monteiro, Developments in TEM Nanotomography of calcium silicate hydrate, J. Am. Ceram. Soc. 98 (2015) 2307–2312, https://doi.org/10.1111/jace.13585.
[62] S. Bae, R. Taylor, D. Shapiro, P. Denes, J. Joseph, R. Celestre, S. Marchesini, H. Padmore, T. Tyliszczak, T. Warwick, D. Kilcoyne, P. Levitz, P.J. M Monteiro, Soft X-ray ptychographic imaging and morphological quantification of calcium silicate hydrates (C-S-H), J. Am. Ceram. Soc. 98 (2015) 4090–4095, https://doi.org/10.1111/jace.13808.
[63] P. Levitz, D. Tchoubar, Disordered porous solids: from chord distributions to small angle scattering, Journal de Physique I 2 (1992) 771–790.
[64] G. Geng, R. Taylor, S. Bae, D. Hernández-Cruz, D.A. Kilcoyne, A.-H. Emwas, P.J.M. Monteiro, Atomic and nano-scale characterization of a 50-year-old hydrated C3S paste, Cem. Concr. Res. 77 (2015) 36–46, https://doi.org/10.1016/j.cemconres.2015.06.010.
[65] K.Y. Kim, T.S. Yun, K.P. Park, Evaluation of pore structures and cracking in cement paste exposed to elevated temperatures by X-ray computed tomography, Cem. Concr. Res. 50 (2013) 34–40, https://doi.org/10.1016/j.cemconres.2013.03.020.
[66] N. Bossa, P. Chaurand, J. Vicente, D. Borschneck, C. Levard, O. Aguerre-Chariol, J. Rose, Micro-and nano-X-ray computed-tomography: a step forward in the characterization of the pore network of a leached cement paste, Cem. Concr. Compos. 67 (2015) 138–147.
[67] D. Hernández-Cruz, C.W. Hargis, J. Dominowski, M.J. Radler, P.J.M. Monteiro, Fiber reinforced mortar affected by alkali-silica reaction: A study by synchrotron microtomography, Cem. Concr. Compos. 68 (2016) 123–130, https://doi.org/10.1016/j.cemconcomp.2016.02.003.
[68] P.A. Itty, M. Serdar, C. Meral, D. Parkinson, A.A. MacDowell, D. Bjegović, P.J.M. Monteiro, In situ 3D monitoring of corrosion on carbon steel and ferritic stainless steel embedded in cement paste, Corros. Sci. 83 (2014) 409–418, https://doi.org/10.1016/j.corsci.2014.03.010.
[69] S.Y. Chung, M.A. Elrahman, D. Stephan, P.H. Kamm, Investigation of characteristics and responses of insulating cement paste specimens with Aer solids using X-ray micro-computed tomography, Constr. Build. Mater. 118 (2016) 204–215, https://doi.org/10.1016/j.conbuildmat.2016.04.159.
[70] K.Y. Kim, T.S. Yun, J. Choo, D.H. Kang, H.S. Shin, Determination of air-void parameters of hardened cement-based materials using X-ray computed tomography, Constr. Build. Mater. 37 (2012) 93–101, https://doi.org/10.1016/j.conbuildmat.2012.07.012.
[71] M.B. Leite, P.J.M. Monteiro, Microstructural analysis of recycled concrete using X-ray microtomography, Cem. Concr. Res. 81 (2016) 38–48, https://doi.org/10.1016/j.cemconres.2015.11.010.
[72] S. Das, P. Yang, S.S. Singh, J.C.E. Mertens, X. Xiao, N. Chawla, N. Neithalath, Effective properties of a fly ash geopolymer: synergistic application of X-ray synchrotron tomography, nanoindentation, and homogenization models, Cem. Concr. Res. 78 (2015) 252–262, https://doi.org/10.1016/j.cemconres.2015.08.004.
[73] T. Ponikiewski, J. Gołaszewski, M. Rudzki, M. Bugdol, Determination of steel fibres distribution in self-compacting concrete beams using X-ray computed tomography, Archives of Civil and Mechanical Engineering 15 (2015) 558–568, https://doi.org/10.1016/j.acme.2014.08.008.
[74] Z. Yang, W. Ren, R. Sharma, S. McDonald, M. Mostafavi, Y. Vertyagina, T.J. Marrow, In-situ X-ray computed tomography characterisation of 3D fracture evolution and image-based numerical homogenisation of concrete, Cem. Concr. Compos. 75 (2017) 74–83, https://doi.org/10.1016/j.cemconcomp.2016.10.001.
[75] L. Yang, Y. Zhang, Z. Liu, P. Zhao, C. Liu, In-situ tracking of water transport in cement paste using X-ray computed tomography combined with CsCl enhancing, Mater. Lett. 160 (2015) 381–383, https://doi.org/10.1016/j.matlet.2015.08.011.
[76] G. Geng, R.J. Myers, Y.S. Yu, D.A. Shapiro, R. Winarski, P.E. Levitz, D.A.L. Kilcoyne, P.J.M. Monteiro, Synchrotron X-ray nanotomographic and spectromicroscopic study of the tricalcium aluminate hydration in the presence of gypsum, Cem. Concr. Res. 111 (2018) 130–137, https://doi.org/10.1016/j.cemconres.2018.06.002.
[77] Q. Hu, M. Aboustait, M.T. Ley, J.C. Hanan, V. Rose, R. Winarski, Combined three-dimensional structure and chemistry imaging with nanoscale resolution, Acta Mater. 77 (2014) 173–182, https://doi.org/10.1016/j.actamat.2014.05.050.
[78] Q. Hu, M. Aboustait, T. Kim, M.T. Ley, J.W. Bullard, G. Scherer, J.C. Hanan, V. Rose, R. Winarski, J. Gelb, Direct measurements of 3d structure, chemistry and mass density during the induction period of C3s hydration, Cem. Concr. Res. 89 (2016) 14–26, https://doi.org/10.1016/j.cemconres.2016.07.008.
[79] S. Brisard, R.S. Chae, I. Bihannic, L. Michot, P. Guttmann, J. Thieme, G. Schneider, P.J.M. Monteiro, P. Levitz, Morphological quantification of hierarchical geomaterials by X-ray nano-CT bridges the gap from nano to micro length scales, Am. Mineral. 97 (2012) 480–483, https://doi.org/10.2138/am.2012.3985.
[80] M.D. Jackson, J. Moon, E. Gotti, R. Taylor, S.R. Chae, M. Kunz, A.-H. Emwas, C. Meral, P. Guttmann, P. Levitz, H.-R. Wenk, P.J.M. Monteiro, Material and elastic properties of Al-tobermorite in ancient Roman seawater concrete, J. Am. Ceram. Soc. 96 (2013) 2598–2606, https://doi.org/10.1111/jace.12407.
[81] F. Yang, F. Prade, M. Griffa, I. Jerjen, C. Di Bella, J. Herzen, A. Sarapata, F. Pfeiffer, P. Lura, Dark-field X-ray imaging of unsaturated water transport in porous materials, Appl. Phys. Lett. 105 (2014), https://doi.org/10.1063/1.4898783.
[82] F. Yang, F. Prade, M. Griffa, R. Kaufmann, J. Herzen, F. Pfeiffer, P. Lura, X-ray dark-field contrast imaging of water transport during hydration and drying of early-age cement-based materials, Mater. Charact. 142 (2018) 560–576, https://doi.org/10.1016/j.matchar.2018.06.021.
[83] F. Prade, K. Fischer, D. Heinz, P. Meyer, J. Mohr, F. Pfeiffer, Time resolved X-ray dark-field tomography revealing water transport in a fresh cement sample, Sci. Rep. 6 (2016) 1–7, https://doi.org/10.1038/srep29108.
[84] G. Geng, J. Li, Y.S. Yu, D.A. Shapiro, D.A.L. Kilcoyne, P.J.M. Monteiro, Nanometer-resolved spectroscopic study reveals the conversion mechanism of CaO·Al2O3·10H2O to 2CaO·Al2O3·8H2O and 3CaO·Al2O3·6H2O at an elevated temperature, Crystal Growth and Design. 17 (2017) 4246–4253, https://doi.org/10.1021/acs.cgd.7b00553.
[85] A. Cuesta, A.G. De La Torre, I. Santacruz, P. Trtik, J.C. Da Silva, A. Diaz, M. Holler, M.A.G. Aranda, Chemistry and mass density of aluminum hydroxide gel in eco-cements by ptychographic X-ray computed tomography, J. Phys. Chem. C 121 (2017) 3044–3054, https://doi.org/10.1021/acs.jpcc.6b10048.
[86] J.C. Da Silva, P. Trtik, A. Diaz, M. Holler, M. Guizar-Sicairos, J. Raabe, O. Bunk, A. Menzel, Mass density and water content of saturated never-dried calcium silicate hydrates, Langmuir 31 (2015) 3779–3783, https://doi.org/10.1021/la504478j.
[87] P. Trtik, A. Diaz, M. Guizar-Sicairos, A. Menzel, O. Bunk, Density mapping of hardened cement paste using ptychographic X-ray computed tomography, Cem. Concr. Compos. 36 (2013) 71–77, https://doi.org/10.1016/j.cemconcomp.2012.06.001.
[88] D.A. Shapiro, Y.S. Yu, T. Tyliszczak, J. Cabana, R. Celestre, W. Chao, K. Kaznatcheev, A.L.D. Kilcoyne, F. Maia, S. Marchesini, Y.S. Meng, T. Warwick, L.L. Yang, H.A. Padmore, Chemical composition mapping with nanometre resolution by soft X-ray microscopy, Nat. Photonics 8 (2014) 765–769, https://doi.org/10.1038/nphoton.2014.207.
[89] M.R. McCartney, D.J. Smith, Electron holography: phase imaging with nanometer resolution, Annu. Rev. Mater. Res. 37 (2007) 729–767, https://doi.org/10.1146/annurev.matsci.37.052506.084219.
[90] A.S. Brand, J.W. Bullard, Dissolution kinetics of cubic Tricalcium aluminate measured by digital holographic microscopy, Langmuir 33 (2017) 9645–9656, https://doi.org/10.1021/acs.langmuir.7b02400.
[91] A.S. Brand, P. Feng, J.W. Bullard, Calcite dissolution rate spectra measured by in situ digital holographic microscopy, Geochim. Cosmochim. Acta 213 (2017) 317–329, https://doi.org/10.1016/j.gca.2017.07.001.
[92] P. Feng, A.S. Brand, L. Chen, J.W. Bullard, In situ nanoscale observations of

gypsum dissolution by digital holographic microscopy, Chem. Geol. 460 (2017) 25–36, https://doi.org/10.1016/j.chemgeo.2017.04.008.
[93] E. Perfect, C.L. Cheng, M. Kang, H.Z. Bilheux, J.M. Lamanna, M.J. Gragg, D.M. Wright, Neutron imaging of hydrogen-rich fluids in geomaterials and engineered porous media: a review, Earth Sci. Rev. 129 (2014) 120–135, https://doi.org/10.1016/j.earscirev.2013.11.012.
[94] M. Wyrzykowski, P. Trtik, B. Münch, J. Weiss, P. Vontobel, P. Lura, Plastic shrinkage of mortars with shrinkage reducing admixture and lightweight aggregates studied by neutron tomography, Cem. Concr. Res. 73 (2015) 238–245.
[95] N. Toropovs, F. Lo Monte, M. Wyrzykowski, B. Weber, G. Sahmenko, P. Vontobel, R. Felicetti, P. Lura, Real-time measurements of temperature, pressure and moisture profiles in high-performance concrete exposed to high temperatures during neutron radiography imaging, Cem. Concr. Res. 68 (2015) 166–173, https://doi.org/10.1016/j.cemconres.2014.11.003.
[96] D. Snoeck, S. Steuperaert, K. Van Tittelboom, P. Dubruel, N. De Belie, Visualization of water penetration in cementitious materials with superabsorbent polymers by means of neutron radiography, Cem. Concr. Res. 42 (2012) 1113–1121, https://doi.org/10.1016/j.cemconres.2012.05.005.
[97] D. Jansen, F. Goetz-Neunhoeffer, C. Stabler, J. Neubauer, A remastered external standard method applied to the quantification of early OPC hydration, Cem. Concr. Res. 41 (2011) 602–608, https://doi.org/10.1016/j.cemconres.2011.03.004.
[98] D. Jansen, C. Naber, D. Ectors, Z. Lu, X.-M. Kong, F. Goetz-Neunhoeffer, J. Neubauer, The early hydration of OPC investigated by in-situ XRD, heat flow calorimetry, pore water analysis and 1H NMR: learning about adsorbed ions from a complete mass balance approach, Cem. Concr. Res. 109 (2018) 230–242, https://doi.org/10.1016/j.cemconres.2018.04.017.
[99] A. Quennoz, K.L. Scrivener, Interactions between alite and C3A-gypsum hydrations in model cements, Cem. Concr. Res. 44 (2013) 46–54, https://doi.org/10.1016/j.cemconres.2012.10.018.
[100] C. Hesse, F. Goetz-Neunhoeffer, J. Neubauer, A new approach in quantitative in-situ XRD of cement pastes: correlation of heat flow curves with early hydration reactions, Cem. Concr. Res. 41 (2011) 123–128, https://doi.org/10.1016/j.cemconres.2010.09.014.
[101] C. Hesse, F. Goetz-Neunhoeffer, J. Neubauer, M. Braeu, P. Gaeberlein, Quantitative in situ X-ray diffraction analysis of early hydration of Portland cement at defined temperatures, Powder Diffract. 24 (2009) 112–115, https://doi.org/10.1154/1.3120603.
[102] D. Jansen, S.T. Bergold, F. Goetz-Neunhoeffer, The hydration of alite: a time resolved quantitative X-ray diffraction approach using G-factor method compared with heat release, J. Appl. Crystallogr. 44 (5) (2011) 895–901.
[103] D. Jansen, J. Neubauer, F. Goetz-Neunhoeffer, R. Haerzschel, W.-D. Hergeth, Change in reaction kinetics of a Portland cement caused by a superplasticizer — calculation of heat flow curves from XRD data, Cem. Concr. Res. 42 (2012) 327–332, https://doi.org/10.1016/j.cemconres.2011.10.005.
[104] L.E. Burris, K.E. Kurtis, Influence of set retarding admixtures on calcium sulfoaluminate cement hydration and property development, Cem. Concr. Res. 104 (2018) 105–113, https://doi.org/10.1016/j.cemconres.2017.11.005.
[105] A. Quennoz, Hydration of C3A with Calcium Sulfate Alone and in the Presence of Calcium Silicate, http://infoscience.epfl.ch/record/164029, (2011) , Accessed date: 25 March 2016.
[106] T. Li, A.J. Senesi, B. Lee, Small angle X-ray scattering for nanoparticle research, Chem. Rev. 116 (2016) 11128–11180, https://doi.org/10.1021/acs.chemrev.5b00690.
[107] A.J. Allen, J.J. Thomas, Analysis of C-S-H gel and cement paste by small-angle neutron scattering, Cem. Concr. Res. 37 (2007) 319–324, https://doi.org/10.1016/j.cemconres.2006.09.002.
[108] J.J. Thomas, A.J. Allen, H.M. Jennings, Structural changes to the calcium-silicate-hydrate gel phase of hydrated cement with age, drying, and resaturation, J. Am. Ceram. Soc. 91 (2008) 3362–3369, https://doi.org/10.1111/j.1551-2916.2008.02636.x.
[109] W.S. Chiang, E. Fratini, F. Ridi, S.H. Lim, Y.Q. Yeh, P. Baglioni, S.M. Choi, U.S. Jeng, S.H. Chen, Microstructural changes of globules in calcium-silicate-hydrate gels with and without additives determined by small-angle neutron and X-ray scattering, J. Colloid Interface Sci. 398 (2013) 67–73, https://doi.org/10.1016/j.jcis.2013.01.065.
[110] W.S. Chiang, E. Fratini, P. Baglioni, D. Liu, S.H. Chen, Microstructure determination of calcium-silicate-hydrate globules by small-angle neutron scattering, J. Phys. Chem. C 116 (2012) 5055–5061, https://doi.org/10.1021/jp300745g.
[111] W.S. Chiang, G. Ferraro, E. Fratini, F. Ridi, Y.Q. Yeh, U.S. Jeng, S.H. Chen, P. Baglioni, Multiscale structure of calcium- and magnesium-silicate-hydrate gels, J. Mater. Chem. A 2 (2014) 12991–12998, https://doi.org/10.1039/c4ta02479f.
[112] A.C.A. Muller, K.L. Scrivener, A.M. Gajewicz, P.J. McDonald, Densification of C-S-H measured by 1H NMR relaxometry, J. Phys. Chem. C 117 (2013) 403–412, https://doi.org/10.1021/jp3102964.
[113] A. Valori, P.J. McDonald, K.L. Scrivener, The morphology of C-S-H: lessons from 1H nuclear magnetic resonance relaxometry, Cem. Concr. Res. 49 (2013) 65–81, https://doi.org/10.1016/j.cemconres.2013.03.011.
[114] A.C.A. Muller, K.L. Scrivener, J. Skibsted, A.M. Gajewicz, P.J. McDonald, Influence of silica fume on the microstructure of cement pastes: new insights from ^{1}H NMR relaxometry, Cem. Concr. Res. 74 (2015) 116–125, https://doi.org/10.1016/j.cemconres.2015.04.005.
[115] D. Ectors, F. Goetz-Neunhoeffer, W.D. Hergeth, U. Dietrich, J. Neubauer, In situ ^{1}H-TD-NMR: quantification and microstructure development during the early hydration of alite and OPC, Cem. Concr. Res. 79 (2016) 366–372, https://doi.org/10.1016/j.cemconres.2015.10.011.
[116] P. Jongvisuttisun, J. Leisen, K.E. Kurtis, Key mechanisms controlling internal curing performance of natural fibers, Cem. Concr. Res. 107 (2018) 206–220, https://doi.org/10.1016/j.cemconres.2018.02.007.
[117] M. Wyrzykowski, P.J. McDonald, K.L. Scrivener, P. Lura, Water redistribution within the microstructure of cementitious materials due to temperature changes studied with ^{1}H NMR, J. Phys. Chem. C 121 (2017) 27950–27962, https://doi.org/10.1021/acs.jpcc.7b08141.
[118] A.M. Gajewicz, E. Gartner, K. Kang, P.J. McDonald, V. Yermakou, A1H NMR relaxometry investigation of gel-pore drying shrinkage in cement pastes, Cem. Concr. Res. 86 (2016) 12–19, https://doi.org/10.1016/j.cemconres.2016.04.013.
[119] Z. Hu, M. Wyrzykowski, K. Scrivener, P. Lura, A novel method to predict internal relative humidity in cementitious materials by 1H NMR, Cem. Concr. Res. 104 (2018) 80–93, https://doi.org/10.1016/j.cemconres.2017.11.001.
[120] A.C.A. Muller, K.L. Scrivener, A reassessment of mercury intrusion porosimetry by comparison with1H NMR relaxometry, Cem. Concr. Res. 100 (2017) 350–360, https://doi.org/10.1016/j.cemconres.2017.05.024.
[121] U.F. Kocks, C.N. Tomé, H.R. Wenk, A.J. Beaudoin, Texture and Anisotropy: Preferred Orientations in Polycrystals and Their Effect on Materials Properties, Cambridge university press, 2000.
[122] H.R. Wenk, P. Van Houtte, Texture and anisotropy, Rep. Prog. Phys. 67 (2004) 1367–1428, https://doi.org/10.1088/0034-4885/67/8/R02.
[123] R.J. Detwiler, P.J.M. Monteiro, H.R. Wenk, Z. Zhong, Texture of calcium hydroxide near the cement paste-aggregate interface, Cem. Concr. Res. 18 (1988) 823–829, https://doi.org/10.1016/0008-8846(88)90109-3.
[124] P.J.M. Monteiro, J.C. Maso, J.P. Ollivier, The aggregate-mortar interface, Cem. Concr. Res. 15 (1985) 953–958, https://doi.org/10.1016/0008-8846(85)90084-5.
[125] H.R. Wenk, P.J.M. Monteiro, M. Kunz, K. Chen, N. Tamura, L. Lutterotti, J. Del Arroz, Preferred orientation of ettringite in concrete fractures, J. Appl. Crystallogr. 42 (2009) 429–432, https://doi.org/10.1107/S0021889809015349.
[126] G. Gelardi, S. Mantellato, D. Marchon, M. Palacios, A.B. Eberhardt, R.J. Flatt, 9 - chemistry of chemical admixtures, in: P.-C. Aïtcin, R.J. Flatt (Eds.), Science and Technology of Concrete Admixtures, Woodhead Publishing, 2016, pp. 149–218 http://www.sciencedirect.com/science/article/pii/B9780081006931000096 , Accessed date: 15 December 2015.
[127] R. Flatt, I. Schober, 7 - superplasticizers and the rheology of concrete, in: N. Roussel (Ed.), Understanding the Rheology of Concrete, Woodhead Publishing, 2012, pp. 144–208 http://www.sciencedirect.com/science/article/pii/B9780857090287500078 , Accessed date: 28 December 2015.
[128] J. Plank, E. Sakai, C.W. Miao, C. Yu, J.X. Hong, Chemical admixtures — chemistry, applications and their impact on concrete microstructure and durability, Cem. Concr. Res. 78 (Part A) (2015) 81–99, https://doi.org/10.1016/j.cemconres.2015.05.016.
[129] F. Winnefeld, S. Becker, J. Pakusch, T. Götz, Effects of the molecular architecture of comb-shaped superplasticizers on their performance in cementitious systems, Cem. Concr. Compos. 29 (2007) 251–262, https://doi.org/10.1016/j.cemconcomp.2006.12.006.
[130] D. Marchon, S. Mantellato, A.B. Eberhardt, R.J. Flatt, 10 - adsorption of chemical admixtures, in: P.-C. Aïtcin, R.J. Flatt (Eds.), Science and Technology of Concrete Admixtures, Woodhead Publishing, 2016, pp. 219–256 http://www.sciencedirect.com/science/article/pii/B9780081006931000102 , Accessed date: 15 December 2015.
[131] D. Marchon, R.J. Flatt, 12 - impact of chemical admixtures on cement hydration, in: P.-C. Aïtcin, R.J. Flatt (Eds.), Science and Technology of Concrete Admixtures, Woodhead Publishing, 2016, pp. 279–304 http://www.sciencedirect.com/science/article/pii/B9780081006931000126 , Accessed date: 28 December 2015.
[132] D. Marchon, P. Juilland, E. Gallucci, L. Frunz, R.J. Flatt, Molecular and submolecular scale effects of comb-copolymers on tri-calcium silicate reactivity: toward molecular design, J. Am. Ceram. Soc. 100 (2017) 817–841, https://doi.org/10.1111/jace.14695.
[133] R.J. Flatt, Y.F. Houst, A simplified view on chemical effects perturbing the action of superplasticizers, Cem. Concr. Res. 31 (2001) 1169–1176, https://doi.org/10.1016/S0008-8846(01)00534-8.
[134] P. Suraneni, R.J. Flatt, Use of micro-reactors to obtain new insights into the factors influencing tricalcium silicate dissolution, Cem. Concr. Res. 78 (2015) 208–215, https://doi.org/10.1016/j.cemconres.2015.07.011.
[135] G. Gelardi, R.J. Flatt, 11 - working mechanisms of water reducers and superplasticizers, in: P.-C. Aïtcin, R.J. Flatt (Eds.), Science and Technology of Concrete Admixtures, Woodhead Publishing, 2016, pp. 257–278 http://www.sciencedirect.com/science/article/pii/B9780081006931000114 , Accessed date: 28 December 2015.
[136] A. Zingg, F. Winnefeld, L. Holzer, J. Pakusch, S. Becker, R. Figi, L. Gauckler, Interaction of polycarboxylate-based superplasticizers with cements containing different C3A amounts, Cem. Concr. Compos. 31 (2009) 153–162, https://doi.org/10.1016/j.cemconcomp.2009.01.005.
[137] F. Dalas, S. Pourchet, A. Nonat, D. Rinaldi, S. Sabio, M. Mosquet, Fluidizing efficiency of comb-like superplasticizers: the effect of the anionic function, the side chain length and the grafting degree, Cem. Concr. Res. 71 (2015) 115–123, https://doi.org/10.1016/j.cemconres.2015.02.001.
[138] W. Fan, F. Stoffelbach, J. Rieger, L. Regnaud, A. Vichot, B. Bresson, N. Lequeux, A new class of organosilane-modified polycarboxylate superplasticizers with low sulfate sensitivity, Cem. Concr. Res. 42 (2012) 166–172, https://doi.org/10.1016/j.cemconres.2011.09.006.
[139] J. Witt, J. Plank, A Novel Type of PCE Possessing Silyl Functionalities, SP, vol. 288, (2012), pp. 1–14.
[140] C. Miao, Q. Ran, J. Liu, Y. Mao, Y. Shang, J. Sha, New generation amphoteric comb-like copolymer superplasticizer and its properties, Polymers & Polymer

Composites 19 (2011) 1–8.
[141] W. Guo, N. Sun, J. Qin, J. Zhang, M. Pei, Y. Wang, S. Wang, Synthesis and properties of an amphoteric polycarboxylic acid-based superplasticizer used in sulfoaluminate cement, J. Appl. Polym. Sci. 125 (2012) 283–290, https://doi.org/10.1002/app.35565.
[142] R.J. Flatt, I. Schober, E. Raphael, C. Plassard, E. Lesniewska, Conformation of adsorbed comb copolymer dispersants, Langmuir 25 (2009) 845–855, https://doi.org/10.1021/la801410e.
[143] J.J. Thomas, H.M. Jennings, J.J. Chen, Influence of nucleation seeding on the hydration mechanisms of tricalcium silicate and cement, J. Phys. Chem. C 113 (2009) 4327–4334, https://doi.org/10.1021/jp809811w.
[144] L. Nicoleau, G. Albrecht, K. Lorenz, E. Jetzlsperger, D. Fridrich, T. Wohlhaupter, R. Dorfner, H. Leitner, M. Vierle, D. Schmitt, M. Braeu, C. Hesse, S.M. Pancera, S. Zuern, M. Kutschera, Plasticizer-Containing Hardening Accelerator Composition, US20110269875A1, https://patents.google.com/patent/US20110269875/en, (2011) , Accessed date: 23 January 2019.
[145] L. Nicoleau, T. Gädt, L. Chitu, G. Maier, O. Paris, Oriented aggregation of calcium silicate hydrate platelets by the use of comb-like copolymers, Soft Matter 9 (2013) 4864, https://doi.org/10.1039/c3sm00022b.
[146] E. John, T. Matschei, D. Stephan, Nucleation seeding with calcium silicate hydrate – a review, Cem. Concr. Res. 113 (2018) 74–85, https://doi.org/10.1016/j.cemconres.2018.07.003.
[147] V. Kanchanason, J. Plank, Role of pH on the structure, composition and morphology of C-S-H–PCE nanocomposites and their effect on early strength development of Portland cement, Cem. Concr. Res. 102 (2017) 90–98, https://doi.org/10.1016/j.cemconres.2017.09.002.
[148] E. Bonaccorsi, S. Merlino, A.R. Kampf, The crystal structure of tobermorite 14 Å (plombierite), a C–S–H phase, J. Am. Ceram. Soc. 88 (2005) 505–512, https://doi.org/10.1111/j.1551-2916.2005.00116.x.
[149] E. Bonaccorsi, S. Merlino, H.F.W. Taylor, The crystal structure of jennite, Ca9Si6O18(OH)6·8H2O, Cem. Concr. Res. 34 (2004) 1481–1488, https://doi.org/10.1016/j.cemconres.2003.12.033.
[150] H.M. Jennings, A model for the microstructure of calcium silicate hydrate in cement paste, Cem. Concr. Res. 30 (2000) 101–116, https://doi.org/10.1016/S0008-8846(99)00209-4.
[151] A.J. Allen, J.J. Thomas, H.M. Jennings, Composition and density of nanoscale calcium–silicate–hydrate in cement, Nat. Mater. 6 (2007) 311–316, https://doi.org/10.1038/nmat1871.
[152] E.M. Gartner, K.E. Kurtis, P.J.M. Monteiro, Proposed mechanism of C-S-H growth tested by soft X-ray microscopy, Cem. Concr. Res. 30 (2000) 817–822, https://doi.org/10.1016/S0008-8846(00)00235-0.
[153] A. Cuesta, J.D. Zea-Garcia, D. Londono-Zuluaga, A.G. De La Torre, I. Santacruz, O. Vallcorba, M. Dapiaggi, S.G. Sanfélix, M.A.G. Aranda, Multiscale understanding of tricalcium silicate hydration reactions, Sci. Rep. 8 (2018), https://doi.org/10.1038/s41598-018-26943-y.
[154] N. Krautwurst, L. Nicoleau, M. Dietzsch, I. Lieberwirth, C. Labbez, A. Fernandez-Martinez, A.E.S. Van Driessche, B. Barton, S. Leukel, W. Tremel, Two-step nucleation process of calcium silicate hydrate, the nanobrick of cement, Chem. Mater. 30 (2018) 2895–2904, https://doi.org/10.1021/acs.chemmater.7b04245.
[155] M. Schönlein, J. Plank, A TEM study on the very early crystallization of C-S-H in the presence of polycarboxylate superplasticizers: transformation from initial C-S-H globules to nanofoils, Cem. Concr. Res. 106 (2018) 33–39, https://doi.org/10.1016/j.cemconres.2018.01.017.
[156] J. Rieger, J. Thieme, C. Schmidt, Study of precipitation reactions by X-ray microscopy: CaCO3 precipitation and the effect of polycarboxylates, Langmuir 16 (2000) 8300–8305, https://doi.org/10.1021/la0004193.
[157] G. Falini, S. Manara, S. Fermani, N. Roveri, M. Goisis, G. Manganelli, L. Cassar, Polymeric admixtures effects on calcium carbonate crystallization: relevance to cement industries and biomineralization, CrystEngComm 9 (2007) 1162, https://doi.org/10.1039/b707492a.
[158] H. Keller, J. Plank, Mineralisation of CaCO3 in the presence of polycarboxylate comb polymers, Cem. Concr. Res. 54 (2013) 1–11, https://doi.org/10.1016/j.cemconres.2013.06.017.
[159] C.A. Orozco, B.W. Chun, G. Geng, A.H. Emwas, P.J.M. Monteiro, Characterization of the bonds developed between calcium silicate hydrate and polycarboxylate-based superplasticizers with silyl functionalities, Langmuir 33 (2017) 3404–3412, https://doi.org/10.1021/acs.langmuir.6b04368.
[160] A. Picker, L. Nicoleau, A. Nonat, C. Labbez, H. Cölfen, Identification of binding peptides on calcium silicate hydrate: a novel view on cement additives, Adv. Mater. 26 (2014) 1135–1140, https://doi.org/10.1002/adma.201303345.
[161] A. Picker, L. Nicoleau, Z. Burghard, J. Bill, I. Zlotnikov, C. Labbez, A. Nonat, H. Cölfen, Mesocrystalline calcium silicate hydrate: A bioinspired route toward elastic concrete materials, Sci. Adv. 3 (2017) e1701216, , https://doi.org/10.1126/sciadv.1701216.
[162] Y. He, X. Zhang, R.D. Hooton, Effects of organosilane-modified polycarboxylate superplasticizer on the fluidity and hydration properties of cement paste, Constr. Build. Mater. 132 (2017) 112–123, https://doi.org/10.1016/j.conbuildmat.2016.11.122.
[163] Z. Lu, X. Kong, H. Liu, Z. Wang, Y. Zhang, B. Dong, F. Xing, Interaction of silylated superplasticizers with cementitious materials, J. Appl. Polym. Sci. 133 (2016), https://doi.org/10.1002/app.44161.
[164] A. Franceschini, S. Abramson, V. Mancini, B. Bresson, C. Chassenieux, N. Lequeux, New covalent bonded polymer–calcium silicate hydrate composites, J. Mater. Chem. 17 (2007) 913–922, https://doi.org/10.1039/B613077A.
[165] E. Cappelletto, S. Borsacchi, M. Geppi, F. Ridi, E. Fratini, P. Baglioni, Comb-shaped polymers as nanostructure modifiers of calcium silicate hydrate: a 29Si solid-state NMR investigation, J. Phys. Chem. C 117 (2013) 22947–22953, https://doi.org/10.1021/jp407740t.
[166] M. Liu, J. Lei, L. Guo, X. Du, J. Li, The application of thermal analysis, XRD and SEM to study the hydration behavior of tricalcium silicate in the presence of a polycarboxylate superplasticizer, Thermochim. Acta 613 (2015) 54–60, https://doi.org/10.1016/j.tca.2015.05.020.
[167] P. Juilland, E. Gallucci, Impact of sucrose on dissolution and nucleation, Proceedings ICCC 2015, Beijing, 2015.
[168] L. Reiter, M. Palacios, T. Wangler, R.J. Flatt, Putting Concrete to Sleep and Waking It Up with Chemical Admixtures, SP, vol. 302, (2015), pp. 145–154.
[169] J.W. Bullard, R.J. Flatt, New insights into the effect of calcium hydroxide precipitation on the kinetics of Tricalcium silicate hydration, J. Am. Ceram. Soc. 93 (2010) 1894–1903, https://doi.org/10.1111/j.1551-2916.2010.03656.x.
[170] C. Taviot-Guého, V. Prévot, C. Forano, G. Renaudin, C. Mousty, F. Leroux, Tailoring hybrid layered double hydroxides for the development of innovative applications, Adv. Funct. Mater. 28 (2018) 1703868, , https://doi.org/10.1002/adfm.201703868.
[171] C. Giraudeau, J.-B. D'Espinose De Lacaillerie, Z. Souguir, A. Nonat, R.J. Flatt, Surface and intercalation chemistry of polycarboxylate copolymers in cementitious systems, J. Am. Ceram. Soc. 92 (2009) 2471–2488, https://doi.org/10.1111/j.1551-2916.2009.03413.x.
[172] J. Plank, Z. Dai, P.R. Andres, Preparation and characterization of new Ca–Al–polycarboxylate layered double hydroxides, Mater. Lett. 60 (2006) 3614–3617, https://doi.org/10.1016/j.matlet.2006.03.070.
[173] S. Ng, E. Metwalli, P. Müller-Buschbaum, J. Plank, Occurrence of intercalation of PCE superplasticizers in calcium aluminate cement under actual application conditions, as evidenced by SAXS analysis, Cem. Concr. Res. 54 (2013) 191–198, https://doi.org/10.1016/j.cemconres.2013.09.002.
[174] J. Plank, H. Keller, P.R. Andres, Z. Dai, Novel organo-mineral phases obtained by intercalation of maleic anhydride–allyl ether copolymers into layered calcium aluminum hydrates, Inorg. Chim. Acta 359 (2006) 4901–4908, https://doi.org/10.1016/j.ica.2006.08.038.
[175] J. Plank, D. Zhimin, H. Keller, F.v. Hössle, W. Seidl, Fundamental mechanisms for polycarboxylate intercalation into C3A hydrate phases and the role of sulfate present in cement, Cem. Concr. Res. 40 (2010) 45–57, https://doi.org/10.1016/j.cemconres.2009.08.013.
[176] C. Shi, G. Zhang, T. He, Y. Li, Effects of superplasticizers on the stability and morphology of ettringite, Constr. Build. Mater. 112 (2016) 261–266, https://doi.org/10.1016/j.conbuildmat.2016.02.198.
[177] A.M. Cody, H. Lee, R.D. Cody, P.G. Spry, The effects of chemical environment on the nucleation, growth, and stability of ettringite [Ca3Al(OH)6]2(SO4)3·26H2O, Cem. Concr. Res. 34 (2004) 869–881, https://doi.org/10.1016/j.cemconres.2003.10.023.
[178] M.R. Meier, J. Plank, Crystal growth of [Ca3Al(OH)6·12H2O]2·(SO4)3·2H2O (ettringite) under microgravity: on the impact of anionicity of polycarboxylate comb polymers, J. Cryst. Growth 446 (2016) 92–102, https://doi.org/10.1016/j.jcrysgro.2016.04.049.
[179] M.R. Meier, A. Rinkenburger, J. Plank, Impact of different types of polycarboxylate superplasticisers on spontaneous crystallisation of ettringite, Adv. Cem. Res. 28 (2016) 310–319, https://doi.org/10.1680/jadcr.15.00114.
[180] W. Prince, M. Edwards-Lajnef, P.-C. Aïtcin, Interaction between ettringite and a polynaphthalene sulfonate superplasticizer in a cementitious paste, Cem. Concr. Res. 32 (2002) 79–85, https://doi.org/10.1016/S0008-8846(01)00632-9.
[181] W. Prince, M. Espagne, P.-C. Aïtcin, Ettringite formation: a crucial step in cement superplasticizer compatibility, Cem. Concr. Res.. 33 (2003) 635–641. doi:https://doi.org/10.1016/S0008-8846(02)01042-6.
[182] G. Ferrari, L. Valentini, V. Russo, M.C. Dalconi, M. Favero, G. Artioli, Improving the performance of PCE superplasticizers in early stiffening Portland cement, Constr. Build. Mater. 130 (2017) 83–91, https://doi.org/10.1016/j.conbuildmat.2016.11.015.
[183] A. Picker, Influence of Polymers on Nucleation and Assembly of Calcium Silicate Hydrates, Einfluss von Polymeren auf die Nukleation und Aggregation von Calciumsilikathydraten, https://kops.uni-konstanz.de/handle/123456789/23156, (2013) , Accessed date: 29 December 2015.
[184] C. Nalet, A. Nonat, Ionic complexation and adsorption of small organic molecules on calcium silicate hydrate: relation with their retarding effect on the hydration of C3S, Cem. Concr. Res. 89 (2016) 97–108, https://doi.org/10.1016/j.cemconres.2016.08.012.
[185] C. Nalet, A. Nonat, Effects of hexitols on the hydration of tricalcium silicate, Cem. Concr. Res. 91 (2017) 87–96, https://doi.org/10.1016/j.cemconres.2016.11.004.
[186] C. Nalet, A. Nonat, Effects of functionality and stereochemistry of small organic molecules on the hydration of tricalcium silicate, Cem. Concr. Res. 87 (2016) 97–104, https://doi.org/10.1016/j.cemconres.2016.06.002.
[187] T. Sowoidnich, T. Rachowski, C. Rößler, A. Völkel, H.-M. Ludwig, Calcium complexation and cluster formation as principal modes of action of polymers used as superplasticizer in cement systems, Cem. Concr. Res. 73 (2015) 42–50, https://doi.org/10.1016/j.cemconres.2015.01.016.
[188] D. Marchon, P. Juilland, L. Frunz, R.J. Flatt, Hydration of pure tricalcium silicate in presence of a polycarboxylate ether superplasticizer, Cem. Concr. Res.. (under review).
[189] D. Marchon, Controlling Cement Hydration Through the Molecular Structure of Comb Copolymer Superplasticizers, PhD thesis ETH Zürich, 2016.
[190] R.P. Sangodkar, B.J. Smith, D. Gajan, A.J. Rossini, L.R. Roberts, G.P. Funkhouser, A. Lesage, L. Emsley, B.F. Chmelka, Influences of dilute organic adsorbates on the hydration of low-surface-area silicates, J. Am. Chem. Soc. 137 (2015) 8096–8112, https://doi.org/10.1021/jacs.5b00622.

[191] B.J. Smith, A. Rawal, G.P. Funkhouser, L.R. Roberts, V. Gupta, J.N. Israelachvili, B.F. Chmelka, Origins of saccharide-dependent hydration at aluminate, silicate, and aluminosilicate surfaces, PNAS 108 (2011) 8949–8954, https://doi.org/10.1073/pnas.1104526108.

[192] F. Ridi, E. Fratini, P. Luciani, F. Winnefeld, P. Baglioni, Tricalcium silicate hydration reaction in the presence of comb-shaped superplasticizers: boundary nucleation and growth model applied to polymer-modified pastes, J. Phys. Chem. C 116 (2012) 10887–10895, https://doi.org/10.1021/jp209156n.

[193] P. Juilland, L. Nicoleau, R.S. Arvidson, E. Gallucci, Advances in dissolution understanding and their implications for cement hydration, RILEM Technical Letters 2 (2017) 90–98, https://doi.org/10.21809/rilemtechlett.2017.47.

[194] L. Valentini, M. Favero, M.C. Dalconi, V. Russo, G. Ferrari, G. Artioli, Kinetic model of calcium-silicate hydrate nucleation and growth in the presence of PCE superplasticizers, Cryst. Growth Des. 16 (2016) 646–654, https://doi.org/10.1021/acs.cgd.5b01127.

[195] G. Artioli, L. Valentini, M. Voltolini, M.C. Dalconi, G. Ferrari, V. Russo, Direct imaging of nucleation mechanisms by synchrotron diffraction micro-tomography: superplasticizer-induced change of C–S–H nucleation in cement, Cryst. Growth Des. 15 (2015) 20–23, https://doi.org/10.1021/cg501466z.

[196] H. Heinz, C. Pramanik, O. Heinz, Y. Ding, R.K. Mishra, D. Marchon, R.J. Flatt, I. Estrela-Lopis, J. Llop, S. Moya, R.F. Ziolo, Nanoparticle decoration with surfactants: molecular interactions, assembly, and applications, Surf. Sci. Rep. 72 (2017) 1–58, https://doi.org/10.1016/j.surfrep.2017.02.001.

[197] F. Dalas, S. Pourchet, D. Rinaldi, A. Nonat, S. Sabio, M. Mosquet, Modification of the rate of formation and surface area of ettringite by polycarboxylate ether superplasticizers during early C3A–CaSO4 hydration, Cem. Concr. Res. 69 (2015) 105–113, https://doi.org/10.1016/j.cemconres.2014.12.007.

[198] C. Rössler, B. Möser, J. Stark, Influence of Superplasticizers on C3A Hydration and Ettringite Growth in Cement Paste, Finger Institute for Building Materials Science, Bauhaus-University Weimar, 2007.

[199] A. Zingg, L. Holzer, A. Kaech, F. Winnefeld, J. Pakusch, S. Becker, L. Gauckler, The microstructure of dispersed and non-dispersed fresh cement pastes — new insight by cryo-microscopy, Cem. Concr. Res. 38 (2008) 522–529, https://doi.org/10.1016/j.cemconres.2007.11.007.

[200] S. Mantellato, M. Palacios, R.J. Flatt, Reliable specific surface area measurements on anhydrous cements, Cem. Concr. Res. 67 (2015) 286–291, https://doi.org/10.1016/j.cemconres.2014.10.009.

[201] S. Mantellato, M. Palacios, R.J. Flatt, Impact of sample preparation on the specific surface area of synthetic ettringite, Cem. Concr. Res. 86 (2016) 20–28, https://doi.org/10.1016/j.cemconres.2016.04.005.

[202] J. Zhang, G.W. Scherer, Comparison of methods for arresting hydration of cement, Cem. Concr. Res. 41 (2011) 1024–1036, https://doi.org/10.1016/j.cemconres.2011.06.003.

[203] S. Kawashima, J.W.T. Seo, D. Corr, M.C. Hersam, S.P. Shah, Dispersion of CaCO3 nanoparticles by sonication and surfactant treatment for application in fly ash-cement systems, Mater. Struct. 47 (2014) 1011–1023, https://doi.org/10.1617/s11527-013-0110-9.

[204] A.H. Korayem, N. Tourani, M. Zakertabrizi, A.M. Sabziparvar, W.H. Duan, A review of dispersion of nanoparticles in cementitious matrices: nanoparticle geometry perspective, Constr. Build. Mater. 153 (2017) 346–357, https://doi.org/10.1016/j.conbuildmat.2017.06.164.

[205] E. Berodier, K. Scrivener, Understanding the filler effect on the nucleation and growth of C-S-H, J. Am. Ceram. Soc. 97 (2014) 3764–3773, https://doi.org/10.1111/jace.13177.

[206] A. Hakamy, F.U.A. Shaikh, I.M. Low, Characteristics of nanoclay and calcined nanoclay-cement nanocomposites, Compos Part B-Eng 78 (2015) 174–184, https://doi.org/10.1016/j.compositesb.2015.03.074.

[207] P. Hosseini, R. Hosseinpourpia, A. Pajum, M.M. Khodavirdi, H. Izadi, A. Vaezi, Effect of nano-particles and aminosilane interaction on the performances of cement-based composites: An experimental study, Constr. Build. Mater. 66 (2014) 113–124, https://doi.org/10.1016/j.conbuildmat.2014.05.047.

[208] M.S.M. Norhasri, M.S. Hamidah, A.M. Fadzil, Applications of using nano material in concrete: A review, Constr. Build. Mater. 133 (2017) 91–97, https://doi.org/10.1016/j.conbuildmat.2016.12.005.

[209] M. Oltulu, R. Sahin, Single and combined effects of nano-SiO2, nano-Al2O3 and nano-Fe2O3 powders on compressive strength and capillary permeability of cement mortar containing silica fume, Mat Sci Eng A-Struct 528 (2011) 7012–7019, https://doi.org/10.1016/j.msea.2011.05.054.

[210] B.J. Zhan, D.X. Xuan, C.S. Poon, The effect of nanoalumina on early hydration and mechanical properties of cement pastes, Constr. Build. Mater. 202 (2019) 169–176.

[211] S. Barbhuiya, S. Mukherjee, H. Nikraz, Effects of nano-Al2O3 on early-age microstructural properties of cement paste, Constr. Build. Mater. 52 (2014) 189–193, https://doi.org/10.1016/j.conbuildmat.2013.11.010.

[212] G. Land, D. Stephan, Controlling cement hydration with nanoparticles, Cement Concrete Comp 57 (2015) 64–67, https://doi.org/10.1016/j.cemconcomp.2014.12.003.

[213] M. Zajac, A. Rossberg, G. Le Saout, B. Lothenbach, Influence of limestone and anhydrite on the hydration of Portland cements, Cement Concrete Comp 46 (2014) 99–108, https://doi.org/10.1016/j.cemconcomp.2013.11.007.

[214] T. Meng, Y. Yu, Z.J. Wang, Effect of nano-CaCO3 slurry on the mechanical properties and micro-structure of concrete with and without fly ash, Compos Part B-Eng 117 (2017) 124–129, https://doi.org/10.1016/j.compositesb.2017.02.030.

[215] T. Sato, J.J. Beaudoin, Effect of nano-CaCO3 on hydration of cement containing supplementary cementitious materials, Adv. Cem. Res. 23 (2011) 33–43, https://doi.org/10.1680/adcr.9.00016.

[216] S. W.M. Supit, F. U.A. Shaikh, Effect of Nano-CaCO3 on compressive strength development of high volume fly ash mortars and concretes, J. Adv. Concr. Technol. 12 (2014) 178–186, https://doi.org/10.3151/jact.12.178.

[217] R. Roychand, S. De Silva, S. Setunge, D. Law, A quantitative study on the effect of nano SiO2, nano Al2O3 and nano CaCO3 on the physicochemical properties of very high volume fly ash cement composite, Eur. J. Environ. Civ. Eng. (2017) 1–16.

[218] G. Artioli, L. Valentini, M.C. Dalconi, M. Parisatto, M. Voltolini, V. Russo, G. Ferrari, Imaging of nano-seeded nucleation in cement pastes by X-ray diffraction tomography, Int. J. Mater. Res. 105 (2014) 628–631, https://doi.org/10.3139/146.111049.

[219] J.F. Sun, H. Shi, B.B. Qian, Z.Q. Xu, W.F. Li, X.D. Shen, Effects of synthetic C-S-H/PCE nanocomposites on early cement hydration, Constr. Build. Mater. 140 (2017) 282–292, https://doi.org/10.1016/j.conbuildmat.2017.02.075.

[220] P. Bost, M. Regnier, M. Horgnies, Comparison of the accelerating effect of various additions on the early hydration of Portland cement, Constr. Build. Mater. 113 (2016) 290–296, https://doi.org/10.1016/j.conbuildmat.2016.03.052.

[221] V. Kanchanason, J. Plank, Role of pH on the structure, composition and morphology of C-S-H–PCE nanocomposites and their effect on early strength development of Portland cement, Cem. Concr. Res. 102 (2017) 90–98, https://doi.org/10.1016/j.cemconres.2017.09.002.

[222] G. Land, D. Stephan, The effect of synthesis conditions on the efficiency of C-S-H seeds to accelerate cement hydration, Cement Concrete Comp 87 (2018) 73–78, https://doi.org/10.1016/j.cemconcomp.2017.12.006.

[223] K. Owens, M.I. Russell, G. Donnelly, A. Kirk, P.A.M. Basheer, Use of nanocrystal seeding chemical admixture in improving Portland cement strength development: application for precast concrete industry, Adv. Appl. Ceram. 113 (2014) 478–484, https://doi.org/10.1179/1743676114y.0000000176.

[224] L. Jiang, X. Kong, Influence of nano-sized CSH particles on cement hydration of OPC in the presence of fly ash or polycarboxylate superplasticizer, Proceedings of the 15th International Conference on the Chemistry of Cement, 2015.

[225] V. Kanchanason, J. Plank, Effectiveness of a calcium silicate hydrate - Polycarboxylate ether (C-S-H-PCE) nanocomposite on early strength development of fly ash cement, Constr. Build. Mater. 169 (2018) 20–27, https://doi.org/10.1016/j.conbuildmat.2018.01.053.

[226] M.H. Hubler, J.J. Thomas, H.M. Jennings, Influence of nucleation seeding on the hydration kinetics and compressive strength of alkali activated slag paste, Cement Concrete Res 41 (2011) 842–846, https://doi.org/10.1016/j.cemconres.2011.04.002.

[227] P. Suraneni, M. Palacios, R.J. Flatt, New insights into the hydration of slag in alkaline media using a micro-reactor approach, Cement Concrete Res 79 (2016) 209–216, https://doi.org/10.1016/j.cemconres.2015.09.015.

[228] M. Horgnies, L.J. Fei, R. Arroyo, J.J. Chen, E.M. Gartner, The effects of seeding C3S pastes with afwillite, Cement Concrete Res 89 (2016) 145–157, https://doi.org/10.1016/j.cemconres.2016.08.015.

[229] W.G. Li, X.Y. Li, S.J. Chen, Y.M. Liu, W.H. Duan, S.P. Shah, Effects of graphene oxide on early-age hydration and electrical resistivity of Portland cement paste, Constr. Build. Mater. 136 (2017) 506–514, https://doi.org/10.1016/j.conbuildmat.2017.01.066.

[230] L. Zhao, X.L. Guo, Y.Y. Liu, Y.H. Zhao, Z.T. Chen, Y.S. Zhang, L.P. Guo, X. Shu, J.P. Liu, Hydration kinetics, pore structure, 3D network calcium silicate hydrate, and mechanical behavior of graphene oxide reinforced cement composites, Constr. Build. Mater. 190 (2018) 150–163, https://doi.org/10.1016/j.conbuildmat.2018.09.105.

[231] Z.Y. Lu, X.Y. Li, A. Hanif, B.M. Chen, P. Parthasarathy, J.G. Yu, Z.J. Li, Early-age interaction mechanism between the graphene oxide and cement hydrates, Constr. Build. Mater. 152 (2017) 232–239, https://doi.org/10.1016/j.conbuildmat.2017.06.176.

[232] X.Y. Li, Y.M. Liu, W.G. Li, C.Y. Li, J.G. Sanjayan, W.H. Duan, Z.J. Li, Effects of graphene oxide agglomerates on workability, hydration, microstructure and compressive strength of cement paste (vol 145, pg 402, 2017), Constr. Build. Mater. 179 (2018) 537–538, https://doi.org/10.1016/j.conbuildmat.2018.05.265.

[233] M. Wang, R. Wang, H. Yao, Z. Wang, S. Zheng, Adsorption characteristics of graphene oxide nanosheets on cement, RSC Adv. 6 (2016) 63365–63372, https://doi.org/10.1039/C6RA10902K.

[234] S. Ghazizadeh, P. Duffour, N.T. Skipper, Y. Bai, Understanding the behaviour of graphene oxide in Portland cement paste, Cement Concrete Res 111 (2018) 169–182, https://doi.org/10.1016/j.cemconres.2018.05.016.

[235] D.S. Hou, Z.Y. Lu, X.Y. Li, H.Y. Ma, Z.J. Li, Reactive molecular dynamics and experimental study of graphene-cement composites: structure, dynamics and reinforcement mechanisms, Carbon 115 (2017) 188–208, https://doi.org/10.1016/j.carbon.2017.01.013.

[236] A. Mohammed, J.G. Sanjayan, W.H. Duan, A. Nazari, Incorporating graphene oxide in cement composites: A study of transport properties, Constr. Build. Mater. 84 (2015) 341–347, https://doi.org/10.1016/j.conbuildmat.2015.01.083.

[237] K. Gong, Z. Pan, A.H. Korayem, L. Qiu, D. Li, F. Collins, C.M. Wang, W.H. Duan, Reinforcing effects of graphene oxide on Portland cement paste, J Mater Civil Eng. 27 (2015) (doi:Artn A4014010 10.1061/(Asce)Mt.1943-5533.0001125).

[238] W.J. Long, Y.C. Gu, B.X. Xiao, Q.M. Zhang, F. Xing, Micro-mechanical properties and multi-scaled pore structure of graphene oxide cement paste: synergistic application of nanoindentation, X-ray computed tomography, and SEM-EDS analysis, Constr. Build. Mater. 179 (2018) 661–674, https://doi.org/10.1016/j.conbuildmat.2018.05.229.

[239] Z. Pan, L. He, L. Qiu, A.H. Korayem, G. Li, J.W. Zhu, F. Collins, D. Li, W.H. Duan, M.C. Wang, Mechanical properties and microstructure of a graphene oxide-cement

composite, Cement Concrete Comp 58 (2015) 140–147, https://doi.org/10.1016/j.cemconcomp.2015.02.001.
[240] A. Mohammed, J.G. Sanjayan, W.H. Duan, A. Nazari, Graphene oxide impact on hardened cement expressed in enhanced freeze-thaw resistance, J Mater Civil Eng. 28 (2016). doi:Artn 04016072 https://doi.org/10.1061/(Asce)Mt.1943-5533.0001586.
[241] T. Tong, Z. Fan, Q. Liu, S. Wang, S.S. Tan, Q. Yu, Investigation of the effects of graphene and graphene oxide nanoplatelets on the micro- and macro-properties of cementitious materials, Constr. Build. Mater. 106 (2016) 102–114, https://doi.org/10.1016/j.conbuildmat.2015.12.092.
[242] E. Horszczaruk, E. Mijowska, R.J. Kalenczuk, M. Aleksandrzak, S. Mijowska, Nanocomposite of cement/graphene oxide - impact on hydration kinetics and Young's modulus, Constr. Build. Mater. 78 (2015) 234–242, https://doi.org/10.1016/j.conbuildmat.2014.12.009.
[243] J.J. Thomas, H.M. Jennings, The surface area of hardened cement paste as measured by various techniques, Concr. Sci. Eng. 1 (1999) 45–64.
[244] A.J. Allen, C.G. Windsor, V. Rainey, D. Pearson, D.D. Double, N.M. Alford, A small-angle neutron scattering study of cement porosities, J. Phys. D. Appl. Phys. 15 (1982) 1817, https://doi.org/10.1088/0022-3727/15/9/027.
[245] A.J. Allen, R.C. Oberthur, D. Pearson, P. Schofield, C.R. Wilding, Development of the fine porosity and gel structure of hydrating cement systems, Philos. Mag. B 56 (1987) 263–288, https://doi.org/10.1080/13642818708221317.
[246] G. Constantinides, F.J. Ulm, The effect of two types of C-S-H on the elasticity of cement-based materials: results from nanoindentation and micromechanical modeling, Cem. Concr. Res. 34 (2004) 67–80, https://doi.org/10.1016/S0008-8846(03)00230-8.
[247] K. J. Krakowiak, W. Wilson, S. James, S. Musso, F.-J. Ulm, Inference of the phase-to-mechanical property link via coupled X-ray spectrometry and indentation analysis: application to cement-based materials, Cem. Concr. Res. 67 (2015) 271–285, https://doi.org/10.1016/j.cemconres.2014.09.001.
[248] J.J. Thomas, H.M. Jennings, A.J. Allen, The surface area of cement paste as measured by neutron scattering: evidence for two C-S-H morphologies, Cem. Concr. Res. 28 (1998) 897–905, https://doi.org/10.1016/S0008-8846(98)00049-0.
[249] P.D. Tennis, H.M. Jennings, A model for two types of calcium silicate hydrate in the microstructure of Portland cement pastes, Cem. Concr. Res. 30 (2000) 855–863, https://doi.org/10.1016/S0008-8846(00)00257-X.
[250] J.W. Bullard, H.M. Jennings, R.A. Livingston, A. Nonat, G.W. Scherer, J.S. Schweitzer, K.L. Scrivener, J.J. Thomas, Mechanisms of cement hydration, Cem. Concr. Res. 41 (2011) 1208–1223, https://doi.org/10.1016/j.cemconres.2010.09.011.
[251] S. Rahimi-Aghdam, Z.P. Bazant, M.J. Abdolhosseini Qomi, Cement hydration from hours to centuries controlled by diffusion through barrier shells of C-S-H, Journal of the Mechanics and Physics of Solids 99 (2017) 211–224, https://doi.org/10.1016/j.jmps.2016.10.010.
[252] F.-J. Ulm, M. Vandamme, C. Bobko, J.A. Ortega, Statistical indentation techniques for hydrated nanocomposites: concrete, bone, and shale, J. Am. Ceram. Soc. 90 (2007) 2677–2692, https://doi.org/10.1111/j.1551-2916.2007.02012.x.
[253] H.M. Jennings, Refinements to colloid model of C-S-H in cement: CM-II, Cem. Concr. Res. 38 (2008) 275–289, https://doi.org/10.1016/j.cemconres.2007.10.006.
[254] K.J. Krakowiak, J.J. Thomas, S. James, M. Abuhaikal, F.-J. Ulm, Development of silica-enriched cement-based materials with improved aging resistance for application in high-temperature environments, Cem. Concr. Res. 105 (2018) 91–110, https://doi.org/10.1016/j.cemconres.2018.01.004.
[255] S. Grangeon, F. Claret, C. Roosz, T. Sato, S. Gaboreau, Y. Linard, Structure of nanocrystalline calcium silicate hydrates: insights from X-ray diffraction, synchrotron X-ray absorption and nuclear magnetic resonance, J. Appl. Crystallogr. 49 (2016) 771–783, https://doi.org/10.1107/S1600576716003885.
[256] J.N. Israelachvili, Intermolecular and Surface Forces: Revised Third Edition, Academic Press, Cambridge, MA, 2011.
[257] G.N. Patey, The interaction of two spherical colloidal particles in electrolyte solution. An application of the hypernetted-chain approximation, J. Chem. Phys. 72 (1980) 5763–5771, https://doi.org/10.1063/1.438997.
[258] F.W. Tavares, D. Bratko, H.W. Blanch, J.M. Prausnitz, Ion-specific effects in the colloid − colloid or protein − protein potential of mean force: role of salt − - macroion van der Waals interactions, J. Phys. Chem. B 108 (2004) 9228–9235, https://doi.org/10.1021/jp037809t.
[259] S. Bhattacharjee, C.-H. Ko, M. Elimelech, DLVO interaction between rough surfaces, Langmuir 14 (1998) 3365–3375, https://doi.org/10.1021/la971360b.
[260] H.K. Christenson, Non-Dlvo forces between surfaces -solvation, hydration and capillary effects, J. Dispers. Sci. Technol. 9 (1988) 171–206, https://doi.org/10.1080/01932698808943983.
[261] B. Derjaguin, L. Landau, Theory of the stability of strongly charged lyophobic sols and of the adhesion of strongly charged particles in solutions of electrolytes, Acta Physico Chemica URSS 14 (1941) 633–662.
[262] E.J.W. Verwey, J.T.G. Overbeek, Theory of the Stability of Lyophobic Colloids, Courier Corporation, New York, 1999.
[263] S. Masoumi, S. Zare, H. Valipour, M.J. Abdolhosseini Qomi, Effective interactions between calcium-silicate-hydrate nanolayers, J. Phys. Chem. C (2019), https://doi.org/10.1021/acs.jpcc.8b08146.
[264] M.J. Abdolhosseine Qomi, M. Bauchy, R.J.-M. Pellenq, Nanoscale composition-texture-property-relation in calcium-silicate-hydrates, Handbook of Materials Modeling: Applications: Current and Emerging Materials, 2018, pp. 1–32.
[265] H. Viallis-Terrisse, A. Nonat, J.-C. Petit, Zeta-potential study of calcium silicate hydrates interacting with alkaline cations, J. Colloid Interface Sci. 244 (2001) 58–65, https://doi.org/10.1006/jcis.2001.7897.
[266] C. Labbez, B. Jönsson, I. Pochard, A. Nonat, B. Cabane, Surface charge density and electrokinetic potential of highly charged minerals: experiments and Monte Carlo simulations on calcium silicate hydrate, J. Phys. Chem. B 110 (2006) 9219–9230, https://doi.org/10.1021/jp057096+.
[267] R. Kjellander, S. Marcelja, R.M. Pashley, J.P. Quirk, Double-layer ion correlation forces restrict calcium-clay swelling, J. Phys. Chem. 92 (1988) 6489–6492, https://doi.org/10.1021/j100334a005.
[268] L. Guldbrand, B. Jönsson, H. Wennerström, P. Linse, Electrical double layer forces. A Monte Carlo study, J. Chem. Phys. 80 (1984) 2221–2228, https://doi.org/10.1063/1.446912.
[269] R. Kjellander, T. Åkesson, B. Jönsson, S. Marčelja, Double layer interactions in mono- and divalent electrolytes: A comparison of the anisotropic HNC theory and Monte Carlo simulations, J. Chem. Phys. 97 (1992) 1424–1431, https://doi.org/10.1063/1.463218.
[270] J.P. Valleau, R. Ivkov, G.M. Torrie, Colloid stability: the forces between charged surfaces in an electrolyte, J. Chem. Phys. 95 (1991) 520–532, https://doi.org/10.1063/1.461452.
[271] A. Delville, R.J.-M. Pellenq, J.M. Caillol, A Monte Carlo (N,V,T) study of the stability of charged interfaces: A simulation on a hypersphere, J. Chem. Phys. 106 (1997) 7275–7285, https://doi.org/10.1063/1.473689.
[272] R.J.-M. Pellenq, J.M. Caillol, A. Delville, Electrostatic attraction between two charged surfaces: A (N,V,T) Monte Carlo simulation, J. Phys. Chem. B 101 (1997) 8584–8594, https://doi.org/10.1021/jp971273s.
[273] B. Jönsson, A. Nonat, C. Labbez, B. Cabane, H. Wennerström, Controlling the cohesion of cement paste, Langmuir 21 (2005) 9211–9221, https://doi.org/10.1021/la051048z.
[274] B. Jönsson, H. Wennerström, A. Nonat, B. Cabane, Onset of cohesion in cement paste, Langmuir 20 (2004) 6702–6709, https://doi.org/10.1021/la0498760.
[275] L. Nachbaur, P.-C. Nkinamubanzi, A. Nonat, J.-C. Mutin, Electrokinetic properties which control the coagulation of silicate cement suspensions during early age hydration, J. Colloid Interface Sci. 202 (1998) 261–268, https://doi.org/10.1006/jcis.1998.5445.
[276] R.J.-M. Pellenq, N. Lequeux, H. van Damme, Engineering the bonding scheme in C–S–H: the iono-covalent framework, Cem. Concr. Res. 38 (2008) 159–174, https://doi.org/10.1016/j.cemconres.2007.09.026.
[277] S. Masoumi, H. Valipour, M.J. Abdolhosseini Qomi, Interparticle interactions in colloidal systems: toward a comprehensive mesoscale model, ACS Appl. Mater. Interfaces 9 (2017) 27338–27349, https://doi.org/10.1021/acsami.7b08465.
[278] D. Ebrahimi, R.J.-M. Pellenq, A.J. Whittle, Nanoscale elastic properties of montmorillonite upon water adsorption, Langmuir 28 (2012) 16855–16863, https://doi.org/10.1021/la302997g.
[279] A.G. Kalinichev, J. Wang, R.J. Kirkpatrick, Molecular dynamics modeling of the structure, dynamics and energetics of mineral–water interfaces: application to cement materials, Cem. Concr. Res. 37 (2007) 337–347, https://doi.org/10.1016/j.cemconres.2006.07.004.
[280] P.A. Bonnaud, B. Coasne, R.J.-M. Pellenq, Molecular simulation of water confined in nanoporous silica, J. Phys. Condens. Matter 22 (2010) 284110, , https://doi.org/10.1088/0953-8984/22/28/284110.
[281] Tulio Honorio, Monte Carlo Molecular Modeling of Temperature and Pressure Effects on the Interactions between Crystalline Calcium Silicate Hydrate Layers, Langmuir 35 (11) (2019) 3907–3916.
[282] B. Carrier, Influence of Water on the Short-Term and Long-term Mechanical Properties of Swelling Clays: Experiments on Self-Supporting Films and Molecular Simulations, phdthesis Université Paris-Est, 2013, https://pastel.archives-ouvertes.fr/pastel-00960833/document , Accessed date: 14 March 2018.
[283] G.M. Torrie, J.P. Valleau, Nonphysical sampling distributions in Monte Carlo free-energy estimation: umbrella sampling, J. Comput. Phys. 23 (1977) 187–199, https://doi.org/10.1016/0021-9991(77)90121-8.
[284] S. Kumar, J.M. Rosenberg, D. Bouzida, R.H. Swendsen, P.A. Kollman, THE weighted histogram analysis method for free-energy calculations on biomolecules. I. The method, J. Comput. Chem. 13 (1992) 1011–1021, https://doi.org/10.1002/jcc.540130812.
[285] A. Barducci, M. Bonomi, M. Parrinello, Metadynamics, WIREs Comput Mol Sci 1 (2011) 826–843, https://doi.org/10.1002/wcms.31.
[286] A. Barducci, G. Bussi, M. Parrinello, Well-tempered metadynamics: A smoothly converging and tunable free-energy method, Phys. Rev. Lett. 100 (2008) 020603, , https://doi.org/10.1103/PhysRevLett.100.020603.
[287] C. Chipot, A. Pohorille, Free Energy Calculations, Springer-Verlag, Berlin Heidelberg, 2007http://link.springer.com/content/pdf/10.1007/978-3-540-38448-9.pdf , Accessed date: 19 September 2016.
[288] S. Masoumi, H. Valipour, M.J. Abdolhosseini Qomi, Intermolecular forces between nanolayers of crystalline calcium-silicate-hydrates in aqueous medium, J. Phys. Chem. C 121 (2017) 5565–5572, https://doi.org/10.1021/acs.jpcc.6b10735.
[289] D. Ebrahimi, A.J. Whittle, R.J.-M. Pellenq, Mesoscale properties of clay aggregates from potential of mean force representation of interactions between nanoplatelets, J. Chem. Phys. 140 (2014) 154309, , https://doi.org/10.1063/1.4870932.
[290] P.A. Bonnaud, C. Labbez, R. Miura, A. Suzuki, N. Miyamoto, N. Hatakeyama, A. Miyamoto, K.J.V. Vliet, Interaction grand potential between calcium–silicate–hydrate nanoparticles at the molecular level, Nanoscale 8 (2016) 4160–4172, https://doi.org/10.1039/C5NR08142D.
[291] R.K. Mishra, A.K. Mohamed, D. Geissbühler, H. Manzano, T. Jamil, R. Shahsavari, A.G. Kalinichev, S. Galmarini, L. Tao, H. Heinz, R. Pellenq, A.C.T. van Duin, S.C. Parker, R.J. Flatt, P. Bowen, cemff: a force field database for cementitious materials including validations, applications and opportunities, Cem. Concr. Res. 102 (2017) 68–89, https://doi.org/10.1016/j.cemconres.2017.09.003.

[292] G. Kovačević, B. Persson, L. Nicoleau, A. Nonat, V. Veryazov, Atomistic modeling of crystal structure of Ca1.67SiHx, Cem. Concr. Res. 67 (2015) 197–203, https://doi.org/10.1016/j.cemconres.2014.09.003.
[293] E. Gartner, I. Maruyama, J. Chen, A new model for the C-S-H phase formed during the hydration of Portland cements, Cem. Concr. Res. 97 (2017) 95–106, https://doi.org/10.1016/j.cemconres.2017.03.001.
[294] A. Kumar, B.J. Walder, A. Kunhi Mohamed, A. Hofstetter, B. Srinivasan, A.J. Rossini, K. Scrivener, L. Emsley, P. Bowen, The atomic-level structure of cementitious calcium silicate hydrate, J. Phys. Chem. C 121 (2017) 17188–17196, https://doi.org/10.1021/acs.jpcc.7b02439.
[295] Tabor David, R.H.S. Winterton, The direct measurement of normal and retarded van der Waals forces, Proceedings of the Royal Society of London. A. Mathematical and Physical Sciences. 312 (1969) 435–450, https://doi.org/10.1098/rspa.1969.0169.
[296] J.N. Israelachvili, G.E. Adams, Direct measurement of long range forces between two mica surfaces in aqueous KNO3 solutions, Nature 262 (1976) 774–776, https://doi.org/10.1038/262774a0.
[297] J.N. Israelachvili, G.E. Adams, Measurement of forces between two mica surfaces in aqueous electrolyte solutions in the range 0–100 nm, Journal of the Chemical Society, Faraday Transactions 1: Physical Chemistry in Condensed Phases 74 (1978) 975–1001, https://doi.org/10.1039/F19787400975.
[298] S. Lesko, E. Lesniewska, A. Nonat, J.-C. Mutin, J.-P. Goudonnet, Investigation by atomic force microscopy of forces at the origin of cement cohesion, Ultramicroscopy 86 (2001) 11–21, https://doi.org/10.1016/S0304-3991(00)00091-7.
[299] C. Plassard, E. Lesniewska, I. Pochard, A. Nonat, Nanoscale experimental investigation of particle interactions at the origin of the cohesion of cement, Langmuir. 21 (2005) 7263–7270, https://doi.org/10.1021/la050440+.
[300] J. Plank, C. Hirsch, Impact of zeta potential of early cement hydration phases on superplasticizer adsorption, Cem. Concr. Res. 37 (2007) 537–542, https://doi.org/10.1016/j.cemconres.2007.01.007.
[301] A. Zingg, F. Winnefeld, L. Holzer, J. Pakusch, S. Becker, L. Gauckler, Adsorption of polyelectrolytes and its influence on the rheology, zeta potential, and microstructure of various cement and hydrate phases, J. Colloid Interface Sci. 323 (2008) 301–312, https://doi.org/10.1016/j.jcis.2008.04.052.
[302] Y. Elakneswaran, T. Nawa, K. Kurumisawa, Electrokinetic potential of hydrated cement in relation to adsorption of chlorides, Cem. Concr. Res. 39 (2009) 340–344, https://doi.org/10.1016/j.cemconres.2009.01.006.
[303] R.J. Myers, G. Geng, J. Li, E.D. Rodríguez, J. Ha, P. Kidkhunthod, G. Sposito, L.N. Lammers, A.P. Kirchheim, P.J.M. Monteiro, Role of adsorption phenomena in cubic tricalcium aluminate dissolution, Langmuir 33 (2017) 45–55, https://doi.org/10.1021/acs.langmuir.6b03474.
[304] D. Frenkel, B. Smit, Understanding Molecular Simulation: From Algorithms to Applications, Academic Press, 2001.
[305] R.L. McGreevy, Reverse Monte Carlo modelling, J. Phys. Condens. Matter 13 (2001) R877, https://doi.org/10.1088/0953-8984/13/46/201.
[306] J. Pikunic, C. Clinard, N. Cohaut, K.E. Gubbins, J.-M. Guet, R.J.-M. Pellenq, I. Rannou, J.-N. Rouzaud, Structural modeling of porous carbons: constrained reverse Monte Carlo method, Langmuir 19 (2003) 8565–8582, https://doi.org/10.1021/la034595y.
[307] A. Morshedifard, S. Masoumi, M.J.A. Qomi, Nanoscale origins of creep in calcium silicate hydrates, Nat. Commun. 9 (2018) 1785, https://doi.org/10.1038/s41467-018-04174-z.
[308] R. Bostanabad, A.T. Bui, W. Xie, D.W. Apley, W. Chen, Stochastic microstructure characterization and reconstruction via supervised learning, Acta Mater. 103 (2016) 89–102, https://doi.org/10.1016/j.actamat.2015.09.044.
[309] R. Bostanabad, Y. Zhang, X. Li, T. Kearney, L.C. Brinson, D.W. Apley, W.K. Liu, W. Chen, Computational microstructure characterization and reconstruction: review of the state-of-the-art techniques, Prog. Mater. Sci. 95 (2018) 1–41, https://doi.org/10.1016/j.pmatsci.2018.01.005.
[310] E. Masoero, E. Del Gado, R.J.-M. Pellenq, F.-J. Ulm, S. Yip, Nanostructure and nanomechanics of cement: polydisperse colloidal packing, Phys. Rev. Lett. 109 (2012) 155503, , https://doi.org/10.1103/PhysRevLett.109.155503.
[311] K. Ioannidou, K.J. Krakowiak, M. Bauchy, C.G. Hoover, E. Masoero, S. Yip, F.-J. Ulm, P. Levitz, R.J.-M. Pellenq, E.D. Gado, Mesoscale texture of cement hydrates, PNAS 113 (2016) 2029–2034, https://doi.org/10.1073/pnas.1520487113.
[312] Emanuela Del Gado, J. Roland, M. Pellenq, Modeling the Structural Development and the Mechanics of Complex Soft Materials: Overview, Springer Nature Switzerland AG, in: W. Andreoni, S. Yip (Eds.), Handbook of Materials Modeling (2019), https://doi.org/10.1007/978-3-319-50257-1 126-1.
[313] F.-J. Ulm, H.M. Jennings, Does C–S–H particle shape matter? A discussion of the paper 'modelling elasticity of a hydrating cement paste', by Julien Sanahuja, Luc Dormieux and Gilles Chanvillard. CCR 37 (2007) 1427–1439, Cem. Concr. Res. 38 (2008) 1126–1129, https://doi.org/10.1016/j.cemconres.2008.03.023.
[314] J. Sanahuja, L. Dormieux, G. Chanvillard, Modelling elasticity of a hydrating cement paste, Cem. Concr. Res. 37 (2007) 1427–1439, https://doi.org/10.1016/j.cemconres.2007.07.003.
[315] B.J. Buchalter, R.M. Bradley, Orientational order in amorphous packings of ellipsoids, EPL 26 (1994) 159, https://doi.org/10.1209/0295-5075/26/3/001.
[316] J.D. Sherwood, Packing of spheroids in three-dimensional space by random sequential addition, J. Phys. A Math. Gen. 30 (1997) L839, https://doi.org/10.1088/0305-4470/30/24/004.
[317] E.J. Garboczi, K.A. Snyder, J.F. Douglas, M.F. Thorpe, Geometrical percolation threshold of overlapping ellipsoids, Phys. Rev. E 52 (1995) 819–828, https://doi.org/10.1103/PhysRevE.52.819.
[318] S. Masoumi, D. Ebrahimi, H. Valipour, M.J. Abdolhosseine Qomi, Nanolayered attributes of calcium-silicate-hydrate gels, Journal of the Mechanics and Physics of Solids (2019) Under Review.
[319] K. Ioannidou, K.J. Krakowiak, M. Bauchy, C.G. Hoover, E. Masoero, S. Yip, F.-J. Ulm, P. Levitz, R.J.-M. Pellenq, E.D. Gado, Mesoscale texture of cement hydrates, PNAS 113 (2016) 2029–2034, https://doi.org/10.1073/pnas.1520487113.
[320] K. Ioannidou, R.J.-M. Pellenq, E.D. Gado, Controlling local packing and growth in calcium–silicate–hydrate gels, Soft Matter 10 (2014) 1121–1133, https://doi.org/10.1039/C3SM52232F.
[321] J.J. Thomas, J.J. Biernacki, J.W. Bullard, S. Bishnoi, J.S. Dolado, G.W. Scherer, A. Luttge, Modeling and simulation of cement hydration kinetics and microstructure development, Cem. Concr. Res. 41 (2011) 1257–1278, https://doi.org/10.1016/j.cemconres.2010.10.004.
[322] I. Shvab, L. Brochard, H. Manzano, E. Masoero, Precipitation mechanisms of mesoporous nanoparticle aggregates: off-lattice, coarse-grained, kinetic simulations, Cryst. Growth Des. 17 (2017) 1316–1327, https://doi.org/10.1021/acs.cgd.6b01712.
[323] M. Turesson, A. Nonat, C. Labbez, Stability of negatively charged platelets in calcium-rich anionic copolymer solutions, Langmuir 30 (2014) 6713–6720, https://doi.org/10.1021/la501228w.
[324] A. Menon, C.M. Childs, B. Poczós, N.R. Washburn, K.E. Kurtis, Molecular engineering of superplasticizers for Metakaolin-Portland cement blends with hierarchical machine learning, Advanced Theory and Simulations. 0 (n.d.) 1800164. doi:https://doi.org/10.1002/adts.201800164.